Editor-in-Chief
Dr. Kouroush Jenab

INTERNATIONAL JOURNAL OF ENGINEERING (IJE)

ISSN : 1985-2312

Volume 6 • Issue 1 • February 2012

Publication Frequency: 6 Issues / Year

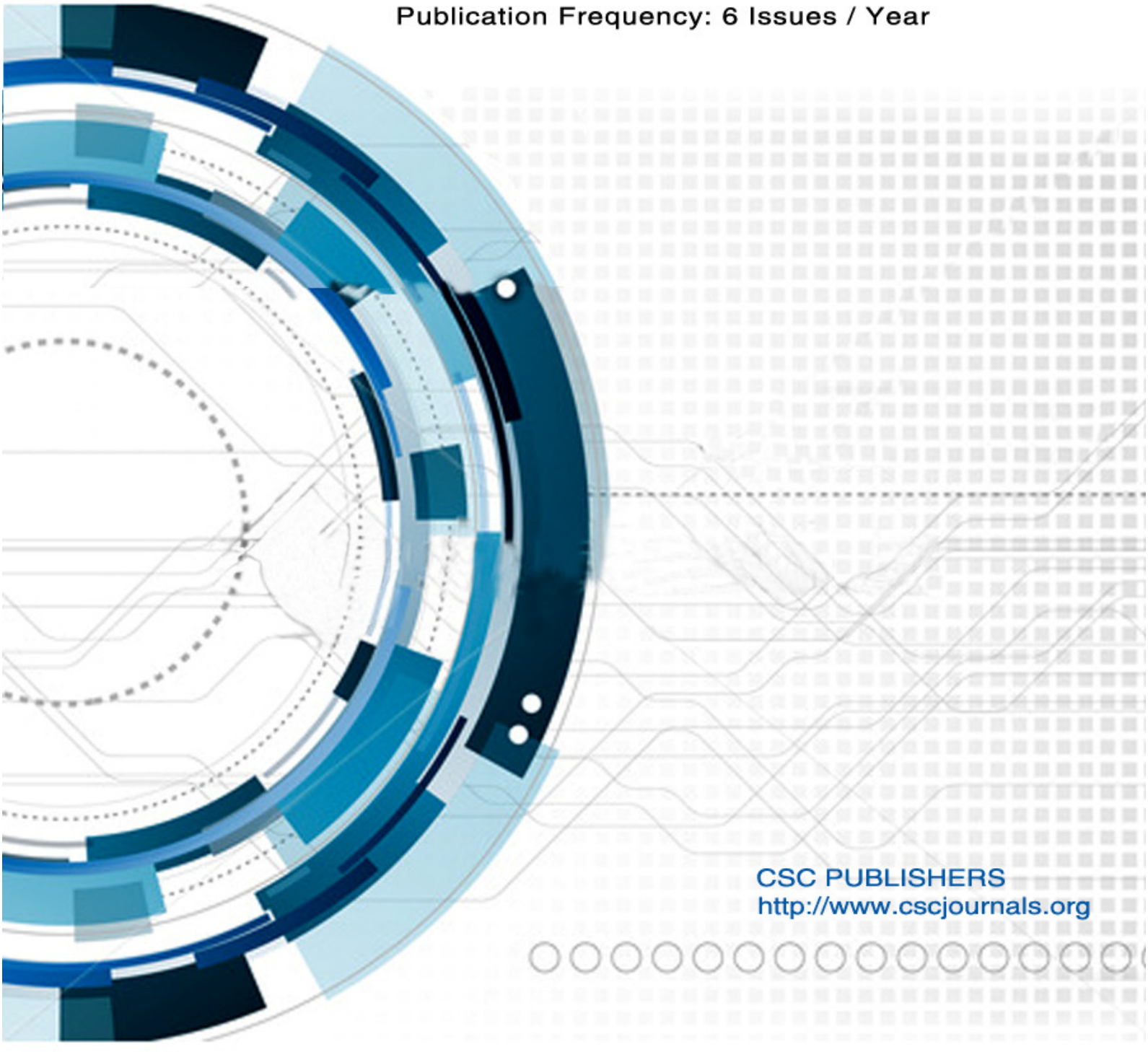

CSC PUBLISHERS
http://www.cscjournals.org

INTERNATIONAL JOURNAL OF ENGINEERING (IJE)

VOLUME 6, ISSUE 1 2012

EDITED BY
DR. NABEEL TAHIR

ISSN (Online): 1985-2312

International Journal of Engineering is published both in traditional paper form and in Internet. This journal is published at the website http://www.cscjournals.org, maintained by Computer Science Journals (CSC Journals), Malaysia.

IJE Journal is a part of CSC Publishers

Computer Science Journals

http://www.cscjournals.org

INTERNATIONAL JOURNAL OF ENGINEERING (IJE)

Book: Volume 6, Issue 1, February 2012
Publishing Date: 21-02-2012
ISSN (Online): 1985-2312

IJE Journal is a part of CSC Publishers
http://www.cscjournals.org

Published in Malaysia

Typesetting: Camera-ready by author, data conversation by CSC Publishing Services – CSC Journals, Malaysia

CSC Publishers, 2012

EDITORIAL PREFACE

This is the first issue of volume six of International Journal of Engineering (IJE). The Journal is published bi-monthly, with papers being peer reviewed to high international standards. The International Journal of Engineering is not limited to a specific aspect of engineering but it is devoted to the publication of high quality papers on all division of engineering in general. IJE intends to disseminate knowledge in the various disciplines of the engineering field from theoretical, practical and analytical research to physical implications and theoretical or quantitative discussion intended for academic and industrial progress. In order to position IJE as one of the good journal on engineering sciences, a group of highly valuable scholars are serving on the editorial board. The International Editorial Board ensures that significant developments in engineering from around the world are reflected in the Journal. Some important topics covers by journal are nuclear engineering, mechanical engineering, computer engineering, electrical engineering, civil & structural engineering etc.

The initial efforts helped to shape the editorial policy and to sharpen the focus of the journal. Starting with volume 6, 2012, IJE appears in more focused issues. Besides normal publications, IJE intend to organized special issues on more focused topics. Each special issue will have a designated editor (editors) – either member of the editorial board or another recognized specialist in the respective field.

The coverage of the journal includes all new theoretical and experimental findings in the fields of engineering which enhance the knowledge of scientist, industrials, researchers and all those persons who are coupled with engineering field. IJE objective is to publish articles that are not only technically proficient but also contains information and ideas of fresh interest for International readership. IJE aims to handle submissions courteously and promptly. IJE objectives are to promote and extend the use of all methods in the principal disciplines of Engineering.

IJE editors understand that how much it is important for authors and researchers to have their work published with a minimum delay after submission of their papers. They also strongly believe that the direct communication between the editors and authors are important for the welfare, quality and wellbeing of the Journal and its readers. Therefore, all activities from paper submission to paper publication are controlled through electronic systems that include electronic submission, editorial panel and review system that ensures rapid decision with least delays in the publication processes.

To build its international reputation, we are disseminating the publication information through Google Books, Google Scholar, Directory of Open Access Journals (DOAJ), Open J Gate, ScientificCommons, Docstoc and many more. Our International Editors are working on establishing ISI listing and a good impact factor for IJE. We would like to remind you that the success of our journal depends directly on the number of quality articles submitted for review. Accordingly, we would like to request your participation by submitting quality manuscripts for review and encouraging your colleagues to submit quality manuscripts for review. One of the great benefits we can provide to our prospective authors is the mentoring nature of our review process. IJE provides authors with high quality, helpful reviews that are shaped to assist authors in improving their manuscripts.

Editorial Board Members
International Journal of Engineering (IJE)

EDITORIAL BOARD

TABLE OF CONTENTS

Volume 6, Issue 1, February 2012

Pages

1 - 9 On Text Realization Image Steganography
Mohammed Nasser Hussein Al-Turfi

10- 24 Design of a Process Plant for the Production of Poundo Yam
Ayodeji Sesan Peter, Olabanji Olayinka Mohammed, Adeyeri Michael Kani

25 – 41 Design Novel Lookup Table Changed Auto Tuning FSMC: Applied to Robot Manipulator
Farzin Piltan, Mohammad Ali Dialame, Abbas Zare, Ali Badri

42 - 52 Heat Transfer in Porous Media With Slurry of Phase Change Materials
Manali Shukla, Fatemeh Hassanipour

53 – 69 A Study on the Effects of Tyre Vibration to the Noise in Passenger Car Cabin
Ahmad Kadri Junoh, Zulkifli Mohd Nopiah, Abdull Halim Abdul, Mohd. Jailani Mohd Nor, Ahmad Kamal Ariffin Mohd. Ihsan, Mohammad Hosseini Fouladi

Text Realization Image Steganography

Dr. Mohammed Nasser Hussein Al-Turfi *mohammed_alturfi@yahoo.com*
Department of Computer and Software Engineering
Al-Mustansiriyah University
Baghdad-Iraq

Abstract

In this paper the steganography strategy is going to be implemented but in a different way from a different scope since the important data will neither be hidden in an image nor transferred through the communication channel inside an image, but on the contrary, a well known image will be used exists on both sides of the channel and a text message contains important data will be transmitted. With the suitable operations, we can re-mix and re-make the source image.

MATLAB7 is the program where the algorithm implemented on it, where the algorithm shows high ability for achieving the task to different type and size of images. Perfect reconstruction was achieved on the receiving side. But the most interesting is that the algorithm that deals with secured image transmission transmits no images at all.

Key Words: Steganography, Text Stream, Secured Data

1. INTRODUCTION

The art of hiding information inside an image is called image steganography, where the ability of hiding information inside this image without noticeable distortion depends on the hiding algorithm and this decides the degree of successfulness [1]. The degree of successfulness may be specified by the amount of security and hardness that must be paid to extract features and important data. [9]

Steganography is a Greek word of two syllables, "stego" means "cover" while "grafia" means "writing" define it's a "cover writing" [10], therefore text file is the first impression about the meaning of the word. Hiding data in a text file is more difficult than hiding data in an image because it might change the text meaning or format or both [11]. Therefore two ways where followed either by not changing text meaning or by creating a rubbished, un-understandable, symbolic file keeping the file format. [12,14]

Early works depends upon using the Least Significant Bits (LSB) of the cover image for implementing data hiding since its effect is the minimum and the size effect is equi-probabile to other bits. Then certain operations are implemented on the source data in order to increase the rate of securing the data and then to be inserted inside the cover image and mostly in the LSB since the distortion rate will rise if the data inserted inside other bits. [2, 3]

DSP and convolutional techniques are used now a day for implementing image steganography to increase the rate of security and to reduce the rate of distortion but of course all these complications consume time, efforts, and processing powers. [2, 4]

Using some special functions that randomize the way of choosing the position was one of the alternatives where the processed data will be stored in. This will enlarge the plain of searching inside the cover image and reduces the rate of distortion since there is no linearity in the process especially if the image is RGB because at least this will triple the efforts. [3][5]

Some use the pixel-value differences in their researches inorder to increase the amount of embedded information where an Optimal Pixel Adjustment Process (OPAP) is used to enhance the stego-image quality. The confidential information can be extracted from the stego-image without the assistance of the original image [4].

Others search for certain places inside the image like a 2*2 block of pixels with high contrast where message bits can be embedded into these blocks. Mathematical functions like MOD-4 and a coding key is used to increase the amount of embedded data while maintaining the data fidelity and the process is as easy as possible since the process applied in the data hiding phase is the same as the one in the data extraction phase[10].

Some researches didn't apply the process from the computer point of view but from the communication point of view by applying Spread Spectrum Image Steganography (SSIS). SSIS conceals a message of substantial length with in digital imagery while maintaining the original image size and dynamic range. The hidden message can be recovered using the appropriate keys without any knowledge of the original image [13].

In this paper a new algorithm is proposed, the algorithm chooses the best cover image size exists on the system data base that matches the size of the source image. The difference between the cover and the source image is evaluated and transformed to text, then the text will be transferred as a text message, an E-Mail, or even as an SMS where this make the change as small as possible, hence reduce the need for a sophisticated channel and is more secured since the source image is not transferred at any way.

2. IMAGE VERSES TEXT

One of the most important principles that must be obeyed in image steganography is that the cover image must be larger in size than the source image so that we can hide the small inside the large where the larger cover the best secured data transmission and less distortion but this will be in need for larger, faster, and more powerful channel which means more cost and complex electronic circuitry, this will be insistence if the used images are colored. [4, 6]

Images may fall in different types depending upon their extensions, but in general they contains pixels, their representation starts from 8-bits of brightness in Black & White images (Gray Scale) where the brightness level may reaches up to 32-bits especially in true color image applications like Photoshop's and rendering (as in 3-D Max).[5]

Texts are quite different, they may fall in different type of files but the text itself inside these files is the same since the way of implementation (writing) is the same where here the ASCII code is the bible book and the representation is fixed given by 7-bits only and the variety is given by different re-arrangements but not by different types. [6, 7]

The important property that exists on text but not in images is that texts need no operational function for decoding while for images, there must be an operational de-coding and de-compression function depending upon the image extension "jpeg, tiff, gif, …etc" and the way of de-compression and operation "played with fox viewer or on media player, …etc" where this means that dealing with text is much easier than dealing with images. [6, 7]

In this paper we are going to use text to represent the difference between the source image and a pre-notified image stored and indexed in the system data-base exists on both sides of the channel where no noise will affect the images. The important useful data is delivered in different type and may be in different way " for example if the application is not urgent or channels are occupied or not secured then the difference may be sent in a message written ;where different types of watermarking and letter security algorithms may be applied; through the post office or by the person himself". [8]

3. PROPOSED ALGORITHM

One of the most important features of the proposed algorithm in this paper is that the cover image may be equal in size to the source image where data security and the hardness for extracting the important data maintained. Second, the algorithm doesn't transmit any image at all which is very important feature because the image stands for millions of words and any intrusion or system breaking may cause security alert.

Third, the easiness that stand for transporting the vital data from one end to the other by transmitting through the secured channel, or by mobile equipments like cellular mobiles or

PDA's as an SMS, or by letters either written and entered by hands or written and entered using OCR's.

Perfect reconstruction that appears at the receiving ends which is the fourth important property, since the system can stand strong and fight noise well in an easy ways and not in need for sophisticated equipments which rises the overall system cost.

4. ALGORITHM IMPLEMENTATION

The proposed algorithm may fall into two parts: - Forward (where the process applied at the transmitting end. The difference between source and cover image is generated), and Backward (Re-arrange the received text to extract the source image from the received text).

4.1 Forward Phase

The system must pass through the following steps to achieve data hiding where fig(1) shows the flow chart of the process explained as given:-

a) Image Comparative: - The cover image must be selected from the system data-base of images in such a way that the selected one must be as near as possible to the size of the source image so that we can maintain the channel resources. An important note must be taken in consideration is that it's not necessary they have the same extension or properties since both images are going to be changed to matrices but it's preferred that they are from the same color type (Both are RGB or Black & White).

b) Image Transforming: - In this step the algorithm will read the image using **imread(name)** function and transform each image into a matrix and each matrix into a vector where both vectors must be unified in length by adding zeros to the shorter one.

c) Difference Evaluation: -This step is performed by the ordinary mathematical subtraction. The difference is stored in a difference vector; its length equal to the larger one. An important tag is added for each operation performed which is very necessary at the receiving end to hold perfect reconstruction. If the operation output is positive then the tag of the operation is (0) and (1) if the output is negative.

d) Bit Traverse: - This part of the system is responsible for transforming the difference vector (which consists of 8-bits of brightness) from decimal to binary values in order to prepare these values to be changed into letters or texts (consists of 7-bits ASCII code).

e) Re-arranging: - This part of the algorithm is responsible for text generation where the system will begin to take seven bits at a time and transfer them into a letter (because the image pixels are represented in 8-bits) by applying the **char(number)** function. For example char (65) is "A" while char (97) is "a".

f) File Creation:- The file to be transferred is created and arranged as the following:-

1- The file is created for an open and append operations while the extension of the text file must be chosen (for example "txt", "doc" …etc).

2- The first part of contents of the file up to the first coma (,) represents the cover image index number (for example "173," this means the used cover image is numbered 173).

3- From the first to the second coma the data represents the image size (for example the image dimensions are 80*60*3).

4- From the second to the third coma the stream of (0's) and (1's) represents the status of the output of the subtraction operations where the number of bits in this stream is equal to the number of subtractions and is equal to the multiplication of the image dimensions (80*60*3=14400).

5- From the third coma to the EOF (End Of File) the text represents the difference between the pixels of the source and the cover images which is transformed to text.

At this point we can notify two things; the first is that the source image is not exchanged between the ends in any way or any how because the algorithm can extract the source image using the text file only and depending on the index value given which represents the cover image index. Second is that the text file and the source image are nearly of the same size which means no extra size is needed for the cover image as in the traditional steganography.

4.2 Backward Phase

At the receiving end the algorithm is in need for a text message contains the difference between the source and the cover images as a text, no matter how the letter is received

whether this letter may be an E-Mail, Secured encrypted message through secured channel, a letter entered by hand delivered by the post mail or even by a letter printed by a printer and entered using OCR scanner program, the letter must pass through the following steps:-

a) When the file is received the algorithm will start to read the data until it reaches the first coma (,) where this part represents the index number of the image used from the system images data base. At this point the stored vector (which represents the specified indexed image that is transformed from an image into a vector) is located and is ready to be used for comparison process.
b) The data stored between the 1st & 2nd coma represents the dimensions of the source image which is very important for image reassembling.
c) The data stored between the 2nd & 3rd coma (,) represents a stream of (0's) & (1's) which specifies the status of the difference operation where the number of bits is equal to the number of subtraction operations implemented and equal to the number of pixels in it.
d) Starting from the 3rd coma (,) to the EOF the text will be transferred to start processing which include:-

1- Reading the text and transfer it in a vector, letter by letter or symbol by symbol.
2- Apply the **abs('letter')** function to transfer the text in the vector to decimal values.
3- Transfer the decimal values in the text vector to binary values made of 7-bits.
4- Re-arrange the new train of bits into 8-bits values and convert it into new decimal values.

e) Applying the correspondence algebraic operations to re-create the source image from the cover image where if the status bit is (0) means the subtraction output is positive and the operation to be implemented now is subtraction to retrieve the original data. While if the status bit is (1) then the output is negative and the operation to be implemented is addition to retrieve original data.
f) The new decimal values obtained are arranged in a pre-defined matrix dimension where the function **imwrite(a,filename,fmt)** writes the matrix "a" of dimensions similar to the dimensions of the image to the file specified by "filename" in the format specified by "fmt". Matrix "a" can be an M-by-N (grayscale image) or M-by-N-by-3 (color image) array. If the format specified is "tiff" it can also accept an M-by-N-by-4 array containing color data that uses the CMYK color space.

5. RESULTS

Fig (2) clarifies parts of the file that will appear. The 1st line starts with the value 173 which represents the index code number of the cover image in the system image database that leads to the vector represents that cover image. In this vector the cover image is stored in a vector ready for subtraction to reduce the processing time and to increase the system speed.

Next value after the 1st coma represents the source image dimension which is important to prepare a matrix with these dimensions to store the results from the subtraction process between the received values and the stored one in the recieving side and to create the status vector, its size equal to the multiplication of the matrix dimension (as in our example 80*60*3=.14400) to store status bits.

After the 2nd coma the status bits will be stored in the status vector, each bit in a separate cell to decide whether the operation to be implemented between the received and the stored values are addition or subtraction.

The difference between the cover and the source image is stored as text after the 3rd coma. Part of the reconstruction process is demonstrated in fig (3). The demonstration shows how the real values are extracted from the received text applied on 20 characters as an example for the process flow.

The reconstruction was perfect; distortion rate was 0%, the process very fast because the algorithm is not complex especially at the receiving end where the cover images on both sides are transferred into vectors stored on the system data base ready to implement the subtraction process immediately.

From the brief shown in fig (2) it can be noticed that the status bits have high redundancy where a compression technique may be applied to reduce size, while a randomization

function may be added to randomize the sequence of data for mixing both status bits with difference texts to increase file security, on the same way data hiding or coding may be applied to cover the index, image size, …etc.

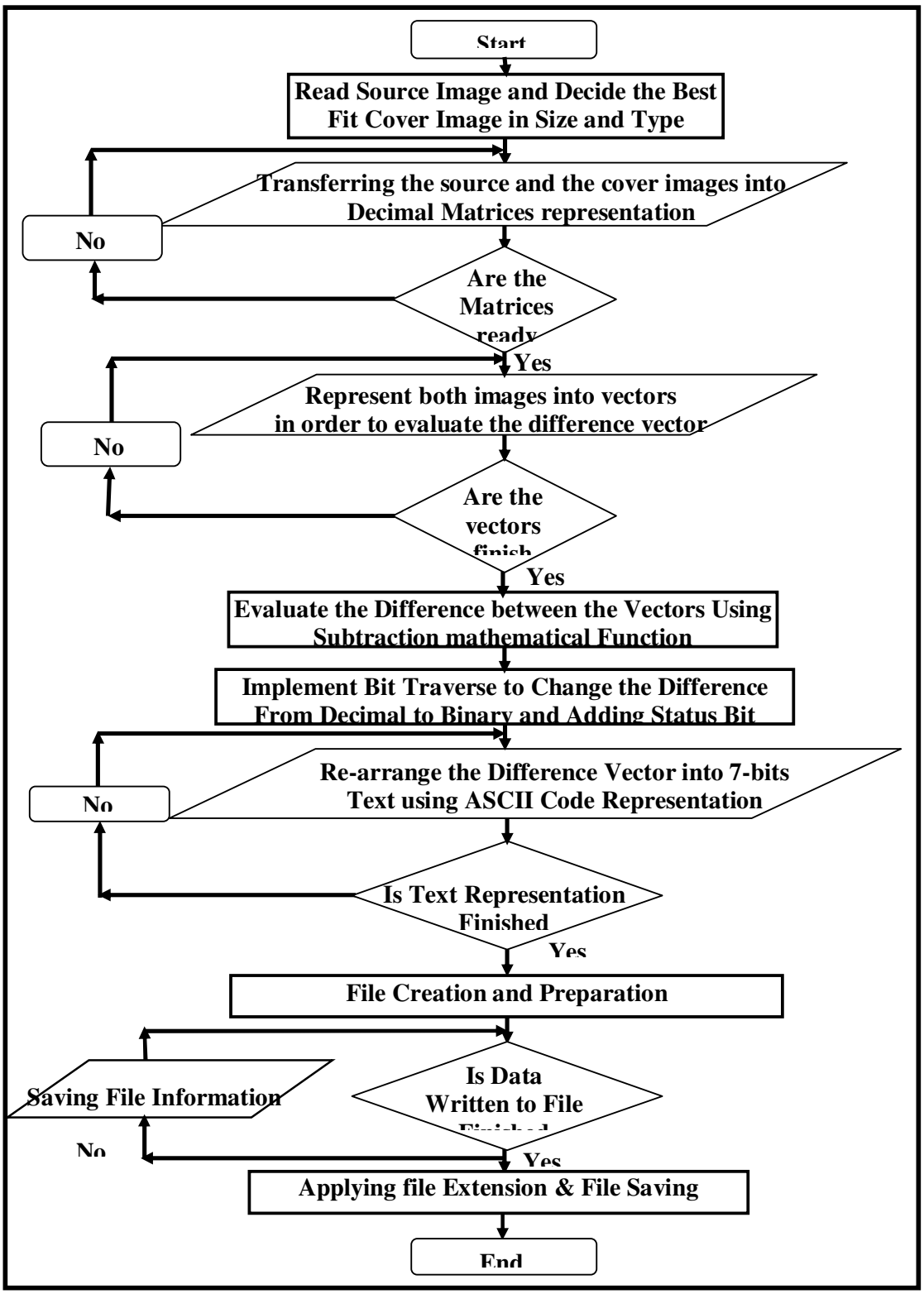

FIGURE 1: the flow chart of the forward phase

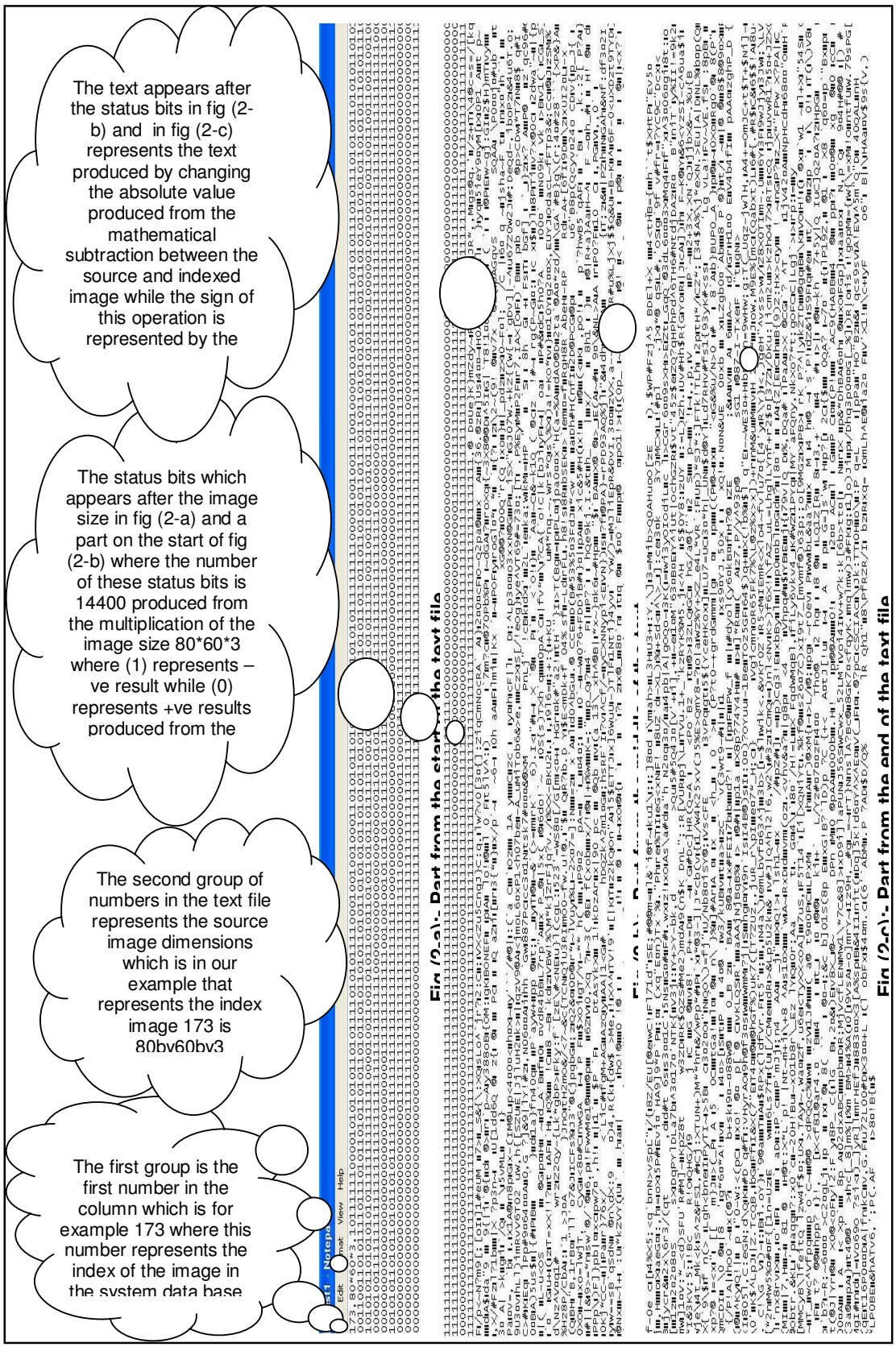

FIGURE 2: Part of the contents of the text file from Different places

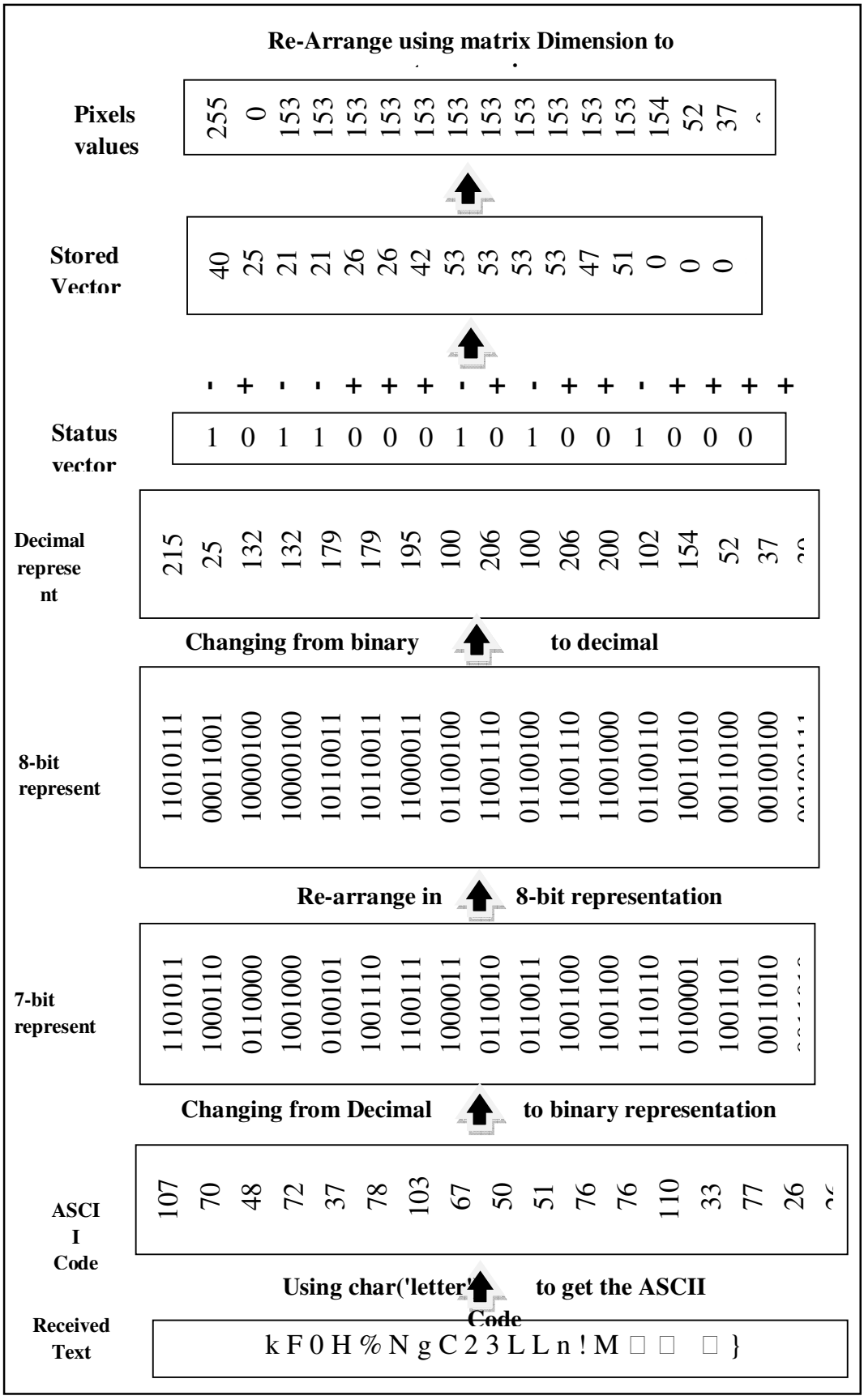

FIGURE 3: A demonstration for the process applied at the receiving end for 20 character

6. REFERENCES

[1] Juneja, M. --- Sandhu, P.S., "Designing of robust image steganography technique based on LSB insertion and encryption" International Conference on Advances in Recent Technologies in Communication and Computing Year: 2009 Pages: 302-305 Provider: IEEE Publisher: IEEE DOI: 10.1109/ARTCom.2009.228.

[2] Raja, K.B. --- Chowdary, C.R. --- Venugopal, K.R. --- Patnaik, L.M. "A secure image steganography using LSB, DCT and compression technique on raw image" Intelligent Sensing and Information Processing, 2005. ICISIP 2005. Third International Conference on ISBN: 0780395883 Year: 2005 Pages: 171-176 Provider: IEEE Publisher: IEEE.

[3] Neeta, D. --- Snehal, K. --- Jacobs, D., "Implementation of LSB steganography and its evaluation for various bits", 1st International Conference on Digital Information Management **ISBN**: 142440682X **Year**: 2007 **Pages**: 173-178 **Provider**: IEEE **Publisher**: IEEE **DOI**: 10.1109/ICDIM.2007.369349.

[4] Hanling Zhang --- Guangzhi Geng --- Caiqiong Xiong ,"Image steganography using pixel – value differencing" , Second International Symposium on Electronic Commerce and Security Year: 2009 Volume: 2 Pages: 109-112 Provider: IEEE Publisher: IEEE DOI: 10.1109/ISECS.2009.139.

[5] Nasser Hamad Faculty of Information Technology, Arab American University, Palestine, *Hiding Text Information in a Digital Image Based on Entropy Function* , The International Arab Journal of Information Technology, Vol. 7, No. 2, April 2010

[6] Muhalim Mohamed, Mohamed Amin, Subariah Ibrahim, Mazleen Salleh, Mohd Rozi Katmin. , "Information Hiding Using Steganography", Department of Computer System & Communication Faculty of Computer Science and Information system University Technology Malaysia, 2003.

[7] Sukhpreet Kaur , Department of Computer Science and Engineering Baba Farid College of Engineering and Technology Bathinda-India & Sumeet Kaur, Department of Computer Engineering Yadavindra College of Engineering Punjabi ,University Guru Kashi Campus Talwandi Sabo, *A Novel Approach for Hiding Text Using Image Steganography* , (IJCSIS) International Journal of Computer Science and Information Security ,Vol. 8, No. 7, Punjab, India October2010.

[8] H.B.Kekre, Archana Athawale, and Pallavi N.Halarnkar , *Increased Capacity of Information Hiding in LSB's Method for Text and Image,* International Journal of Electrical and Electronics Engineering 2:4:2008

[9] K Suresh Babu*, K B Raja*, Kiran Kumar K*, Manjula Devi T H*, Venugopal K R*, L M Patnaik** "Authentication of Secret Information in Image Steganography" , TENCON 2008 - 2008 IEEE Region 10 Conference Year: 2008 Pages: 1-6 Provider: IEEE Publisher: IEEE DOI: 10.1109/TENCON.2008.4766581

[10] *Department of Computer Science and Engineering University Visvesvaraya College of Engineering, Bangalore University, Bangalore 560 001

[11] ** Microprocessor Applications Laboratory, Indian Institute of Science, Bangalore ksureshbabu uvce@rediff.com

[12] K. Pramitha1, Dr. L.Padma Suresh2, K.L.Shunmuganathan3 " Image Steganography Using MOD-4 Embedding Algorithm Based on Image Contrast" TENCON 2008 - 2008 IEEE Region 10 Conference Year: 2008 Pages: 1-6 Provider: IEEE Publisher: IEEE DOI: 10.1109/TENCON.2008.4766581

[13] 1 Department of Electrical and Electronics Engineering, P.G. Scholar, NIU, Kumaracoil. E-mail:pramitha2007@gmail.com

[14] 2 Department of Electrical and Electronics Engineering, HOD, NIU, Kumaracoil. E-mail: suresh_lps@yahoo.co.in

[15] 3 Department of Computer Science Engineering, Professor, RMK Engineering College. E-mail:kls_nathan@yahoo.com

[16] Deshpande Neeta, Kamalapur Snehal Computer Science Dept. K.K.Wagh Institute of Engineering Education & Research, Nashik India , deshpande_neeta@yahoo.com, kamalapur_snehal@yahoo.com Daisy Jacobs School of Information Technology University of Pretoria, Pretoria 002 South Africa daisy.jacobs@up.ac.za, "Implementation of LSB Steganography and Its Evaluation for Various Bits", : 1st International Conference on Digital Information Management ISBN: 142440682X Year: 2007 Pages: 173-178 Provider: IEEE Publisher: IEEE DOI: 10.1109/ICDIM.2007.369349

[17] Hossein Malekmohamadi and Shahrokh Ghaemmaghami Sharif University of Technology, Tehran, Iran h_malekmohamadi@ee.sharif.ir, ghaemmag@sharif.edu "Steganalysis of LSB Based Image Steganography Using Spatial and Frequency Features", IEEE International Conference on Multimedia and Expo ISSN: 19457871 Year: 2009 Pages: 1744-1747 Provider: IEEE Publisher: IEEE DOI: 10.1109/ICME.2009.5202858

[18] Lisa M. Marvel and Charles T. Retter U.S. Army Research Laboratory Aberdeen Proving Ground, MD 21005 marvelQar1. Mil Charles G. Boncelet, Jr University of Delaware Newark, DE 19716 boncelet @ee.udel.edu, "Hiding Information in Images *" Image Processing, 1998. ICIP 98. Proceedings. 1998 International Conference on ISBN: 08186882 Year: 1998 Volume: 2 Pages: 396-398 vol.2 Provider: IEEE Publisher: IEEE Comput. Soc

[19] 14) Mohammad Shirali-Shahreza, Sajad Shirali- Shahreza. d Shirali-Shahreza"Steganography in TeX Documents", 3rd International Conference on Intelligent System and Knowledge Engineering Year: 2008 Volume: 1 Pages: 1363-1366 Provider: IEEE Publisher: IEEE DOI: 10.1109/ISKE.2008.4731144

[20] 1.Computer Science Department Sharif University of Technology Tehran, IRAN

[21] 2.Computer Engineering Department Sharif University of Technology Tehran, IRAN shirali@cs.sharif.edu, shirali@ce.sharif.edu

Design of a Process Plant for the Production of Poundo Yam

Ayodeji Sesan Peter *ayodejisesan@yahoo.com*
Engineering and Engineering Technology/
Department of Mechanical Engineering
The Federal University of Technology Akure,
P.M.B. 704, Akure Ondo State, Nigeria

Olabanji, Olayinka Mohammed *obayinclox@yahoo.com*
Engineering and Engineering Technology/
Department of Mechanical Engineering
The Federal University of Technology Akure,
P.M.B. 704, Akure Ondo State, Nigeria

Adeyeri Michael Kanisuru *sademike2003@yahoo.co.uk*
Engineering and Engineering Technology/
Department of Mechanical Engineering
The Federal University of Technology Akure,
P.M.B. 704, Akure Ondo State, Nigeria

Abstract

This paper explicitly gives the details of the design of an integrated process plant for poundo yam production. The paper covers the deign analysis of each machine involved in the production process of the process plant. Viz a viz peeling and slicing machine; parboiling machine; conveyor; sieving machine; drying machine and grinding machine. It explained the material required for the fabrication of each part of the machines used in the process plant and the cost analysis. A simulation was done to confirm the workability of the design for fabrication purpose. The plant has a capacity of converting 23tubers of yam(discorea alata) into 250Kg of poundo yam in 7hrs.

Keywords: Design , Process Plant, Manufacturing, Poundo Yam

1. INTRODUCTION

High post harvest food losses, arising largely from limited food preservation capacity are a major factor constraining food and nutrition security in the developing countries of West Africa, where seasonal food shortages and nutritional deficiency diseases are still a major concern [1]. It is estimated that about 50% of perishable food commodities including fruits, vegetables, roots and tubers and about 30% of the food grains including maize, sorghum, millet, rice, cowpeas are lost after harvest in west Africa. The factors responsible for post harvest food losses in West Africa are ineffective or inappropriate food processing technology, Careless harvesting and inefficient post harvest handling practice, Poor transportation media, Bad market practice and Lack of storage facilities. In essence to reduce post harvest food losses traditional foods have to be improved using technological food processing techniques. One of these techniques is processing of yam into instant yam flour.

The slow progress in upgrading traditional food processing and preservation techniques in the country, contributes to food and nutrition insecurity. Simple low cost traditional food processing techniques are the bedrock of small scale food processing enterprises that are crucial to rural development, employment opportunity, rural-urban migration and associated social problems. Regrettably, small scale food industries in the country are hampered by adoption of inefficient and inappropriate technologies, poor management, inadequate working capital, limited access to banks and other financial institutions, high interest rates and low profit margins.

Yam, Dioscorea (spp), a dicotyledonous perennial plant, is an important source of carbohydrate for many people of the sub-Saharan region especially in the yam zones of West Africa. Several

species of yam are grown in the in the tropics and temperate zones of the world since it grows easily, it has large yield and is little affected by disease and pests. It is the second most important root/tuber crop in West Africa after cassava, with production reaching just under one third the level of cassava. Some are grown for medicinal purposes and other for edible purposes. The most common of the edible species are *Dioscorea alata L*; (known as the greater yam), *Dioscorea cayenensis lam*; (the yellow yam) *Dioscorea rotundata poir*. *Dioscorea esculenta* (white yam) [2]. Yam has an energy content of about 30 billion kcal with a corresponding protein content of 0.66 million ton [3].

Yam is a source of carbohydrates in human diet being processed into pounded yam for human consumption. The tubers of yam cannot be stored much longer after harvest before decaying, and so processing follows immediately after harvesting. Poundo yam which is also referred to as instant pounded yam flour (IPYF) is a processed white powdery form of yam (dehydrated yam flour) which is produced desiccating machine. It is a fast means of making pounded yam which is done by pouring a measured quantity of the yam flour into boiling water, which is stirred continuously until the required texture and taste is achieved. Yam processing leading to size reduction includes peeling, slicing, parboiling, grating, drying, drying and sieving [4]

2. LITERATURE REVIEW

Yam can supply a substantial portion of the manganese and phosphorus requirement of adults and to a lesser extent the copper and magnesium. The tubers can grow up to 2.5 meters in length and weigh up to 70kg (150pounds) [3]. The vegetable has a rough skin which is difficult to peel but which softens after heating. The skin varies in color from dark brown to light pink. Nigeria has been adjudged as the top producer of yam with a value of 26.6million metric ton [3]. Table1shows the output of top yam producers in 2005.

S/n	Country	Production (million metric ton)
1	Nigeria	26.6
2	Ghana	3.9
3	Australia	3.2
4	Cote d' Ivoire	3.0
5	Benin	2.3
6	Togo	0.6
7	Colombia	0.3
	World total	39.9

TABLE1: Yam Output 2005 (Top Producers as at 2005) [2]

Design and Construction of a yam pounding machine has been developed in which the machine consists of a shaft, pulleys, belt, bearings, electric motor and yam beaters [5]. The existing design works have been on different separate entity of process. But the present research or design work has integrated all the processes into an entire production plant process.

The production process of instant pounded yam flour consist of simple operations which can be mechanized. These unit operations can be summarized as follows

***Yam Selection and Weighing*:** This involves the selection of suitable varieties of yam, considering the size and shape of the tubers. The wholesome tubers are then weighed.

Washing: The selected tubers are washed properly to remove adhering sand. The essence of the washing is to ensure that the peeling is done effectively.

Peeling and Slicing: The washed tubers are carefully loaded into a yam peeling and slicing machine for peeling the bark of the yam. The pilled tubers are then mechanically sliced to desirable thickness in a slicing machine made of stainless steel.

Parboiling: The yam slices are blanched in boiling water (parboiling) for some minutes, depending on the thickness of the slices

Drying: The parboiled yam slices are dried in a dryer at specified drying temperature for few hours. The dried yams chips are stored in air tight containers

Grinding: The dried yam chips are grinded directly into flour of uniform particle size distribution.

***Sieving and Packaging**:* The yam flour is sieved and packed into air tight, moisture proof packaging materials

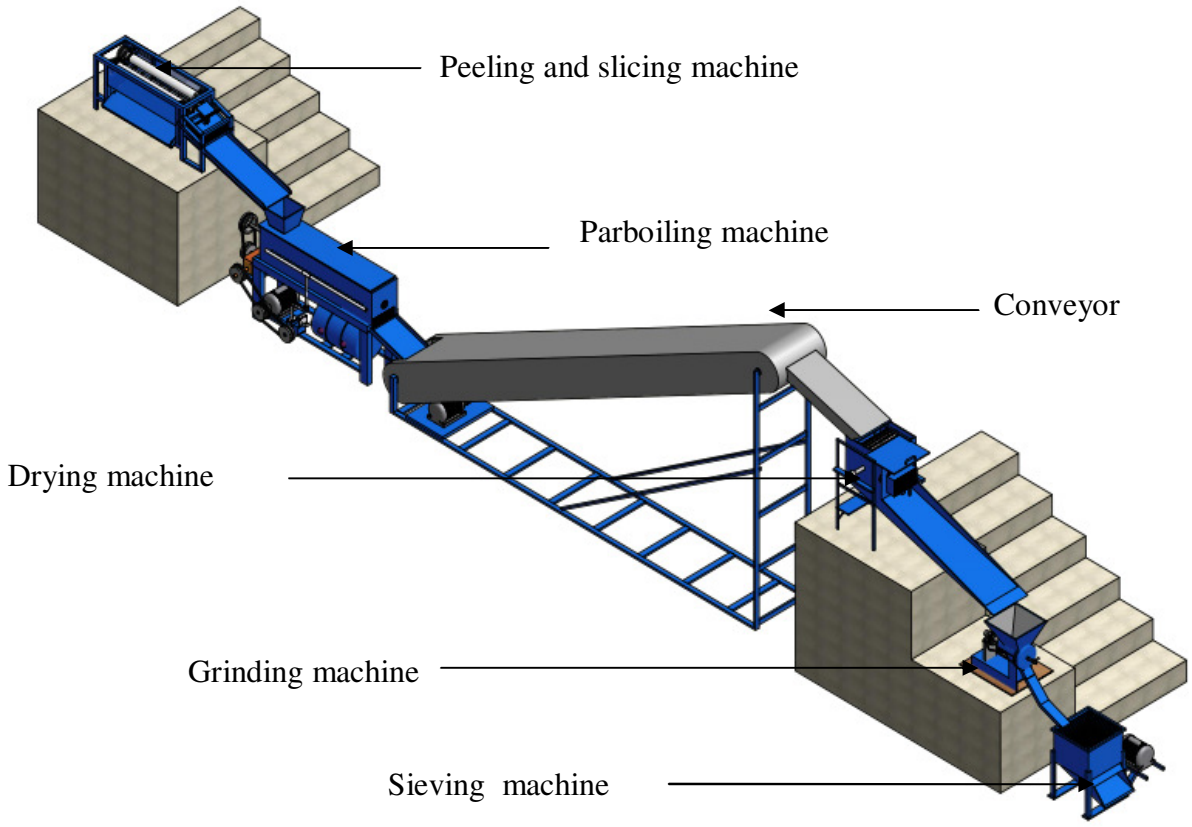

FIGURE 1 : The designed product plant for poundo yam production

3. MATERIALS AND METHODS

The production of poundo yam is a continuous process production. It involves the production of continuous stream of instant yam flour. The type of equipment layout suitable for plant is a process layout. In a process layout the equipments are arranged in such a way that they satisfy the production stages of the product. The plant is made up of various machines which the yam must pass through before getting to the final product. These machines are peeling and slicing machine, parboiling machine, drying machine, grating machine, sieving machine and the conveyor. These are as shown in figure 1.

The component part of each machine was designed. The arrangements of the plant at designed level is as shown in figure 2.

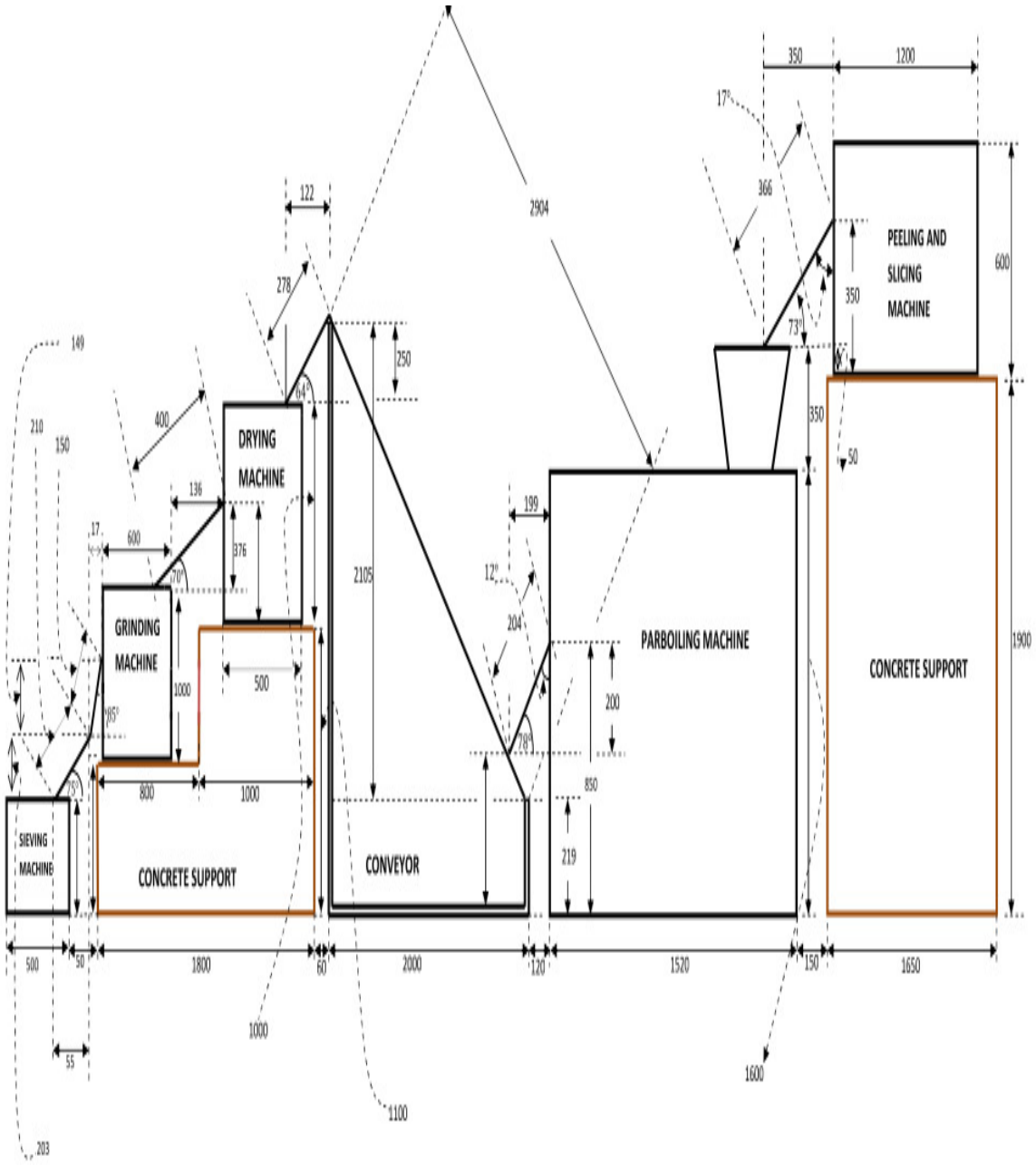

FIGURE 2: Schematic diagram of the process plant showing angle of repose of the delivery chutes and the distance separating the machines

The diameter of the peeling shaft and auger shaft was determined using the below empirical equation [4].

$$d^3 = \frac{16}{\pi S_s}\sqrt{\left\{(K_b M_b)^2 + (K_t M_t)^2\right\}} \qquad (1)$$

Where ;

d = diameter of the shaft (m); S_s = Allowable shear stress N/m^2

K_b = Combined shock and fatigue factor applied to bending moment

K_t = Combined shock and fatigue factor applied to torsional moment

M_b = Bending moment (Nm); M_t = Torsional moment (Nm)

The length of belt transmitting power between two pulleys of dissimilar diameters was derived [6].

Lenght of belt $L = \sqrt{4x^2 - (D_2 - D_1)} + \frac{1}{2}(D\theta_2 - D\theta_1)$ (2)

Where $D\theta_2 = \frac{\theta_2}{360} \times \pi D_2$

and $D\theta_1 = \frac{\theta_1}{360} \times \pi D_1$

Where:
D_1 and D_2 are the diameters of the pulleys
x = center distance between the two shafts
θ_1 and θ_2 are the angle of lap of the belts on the pulley
When the pulleys are of the same diameter the length of belt is obtained.

$$L = \pi\left\{\frac{D_4}{2} + \frac{D_3}{2}\right\} + 2C + \frac{(D_4 - D_3)^2}{2} \quad [8] \quad (3)$$

Where:
L = Length of the belt
D_4 and D_3 are the diameters of the two pulleys attached to the peeling and auger shaft respectively. C is the center distance between the two pulleys.
The volume of the hopper in the parboiling machine was obtained as stated below [9].

$$V_{hopper} = V_{wholepyramid} - V_{cutawaypyramid} \quad (4)$$

$$V_{hopper} = \{0.5 \times L_{b1} \times L_{b2} \times H_p\} - \{0.5 \times L_{c1} \times L_{c2} \times H_c\} \quad (5)$$

Where:
$L_{b1} = L_{b2}$ = length of the top shape of the hopper which is considered to be a square.
$L_{c1} = L_{c2}$ = length of the base shape of the hopper which is considered to be a square.
H_p = vertical height of the pyramid; and H_c = vertical height of the cut away pyramid
The water horse power (WHP) is the power output of the pump and it is stated as

$WHP = \omega Q H_m$ where H_m = manometric height (6)

$WHP = \rho g Q H_m$ [10] (7)

Where ρ ang g are the density of water and acceleration due to gravity respectively.
The efficiency of the pump is obtained as

$$\gamma_{pump} = \frac{WHP}{SHP} \quad [10] \quad (8)$$

Where SHP = Shaft horse power = The power input to the pump from the electric motor
The volume of the parboiling chamber V_{pc} was obtained as

$$V_{pc} = H_r.B_r L_r + 0.5\left(\frac{\pi B_r^{\,2} L_r}{4}\right) \quad (9)$$

Where:
H_r = Height of the rectangular section of the parboiling chamber
B_r = Breadth of the rectangular section of the parboiling chamber = diameter of the cylindrical section
L_r = Length of the rectangular section of the parboiling chamber = length of the cylindrical section
The internal pressure of the parboiling chamber 'P_{ch}' was obtained to from

$$P_{ch} = \rho(L_r - 0.3) \times 100 \quad (10)$$

Where ρ and L_r are the density of water and length of the rectangular section of the parboiling chamber.
The hot water reservoir used in the parboiling machine is made from plate material. The thickness of the plate material t_{hwr} was determined from:

$$t_{hwr} = \frac{P_{hwr} D \times 10^3}{2 f_{hwr} J} + C \qquad [10] \qquad (11)$$

Where:
P_{hwr} = The internal pressure of the hot water reservoir
D = Diameter of the hot water reservoir; f_{hwr} = Permissible stress in the hot water reservoir
J = Joint efficiency; and C = Corrosion allowance
The Euler's theory for crippling and buckling load 'W_{cr}' under various end conditions was used to determine the buckling load on the machine, and it is given as:

$$\mathrm{W_{cr}} = \frac{c\pi^2 EA}{\left(l/k\right)^2} \qquad (12)$$

Where C is the constant representing the end conditions of the column or end fixity coefficient of 4 for welded and bolted joints
E *and* A = Young's modulus of elasticity for the material of the column and cross sectional area respectively.
I and k are the length of column and least radius of gyration of the cross section respectively.

Where: $k = \sqrt{\frac{I}{A}}$ such that I is called polar moment of area.

The Schematic diagram of the designed dryer is shown in figure 3. The volume of the drying drum was derived from:

$$\mathrm{V_{dr}} = \frac{\pi D_{dr}{}^2 L_{dr}}{4} \qquad (13)$$

Where:
L_{dr} = length of the drying drum ; and D_{dr} =diameter of the drying drum
The number of holes 'n_h' on the metal plate was obtained as

$$n_h = \frac{\pi D_{dr} \times L_{dr}}{0.0004} \qquad (14)$$

The volume of each hole 'V_h ' is determined using :

$$\mathrm{V_h} = \frac{\pi D_h{}^2 t_{dr}}{4} \qquad (15)$$

Where D_h = diameter of the hole and t_{dr} = thickness of the metal plate from which the drying drum is made .
Hence the total volume of all the holes V_{Th} as obtained using

$$V_{Th} = n_h V_h \qquad (16)$$

$$V_{Th} = n_h \left\{ \frac{\pi D_h{}^2 t_{dr}}{4} \right\} \qquad (17)$$

The total volume of the materia 'V_{mT}' assuming there is no hole in it can be obtained from:

$$V_{mT} = \pi D_{dr} \times L_{dr} \times t_{dr} \qquad (18)$$

Hence the volume of the material 'V_m' when there are holes in it was obtained from

$$V_m = V_{mT} - V_{Th} \qquad (19)$$

The thermal energy input to the dryer in KJ/hr was obtained from

$$H_{in} = C_{h-in} \times \left(T_{in} - T_{amb}\right) \qquad [12] \qquad (20)$$

Where; H_{in} = the thermal energy input, $C_{h\text{-}in}$, the specific heat of humid air and T_{in} and T_{amb} are the input temperature and ambient temperature respectively.
The amount of moisture removed from the yam *(M_r)* during the drying operation was estimated using:

$$M_r = \frac{M_i(M_o - M_f)}{100 - M_f} \quad [12] \quad (21)$$

Where :
M_i = initial mass of the yam = mass of yam at maximum volume of drying drum = dryer capacity
M_o = initial moisture content of the yam
M_f = final moisture content of the yam.

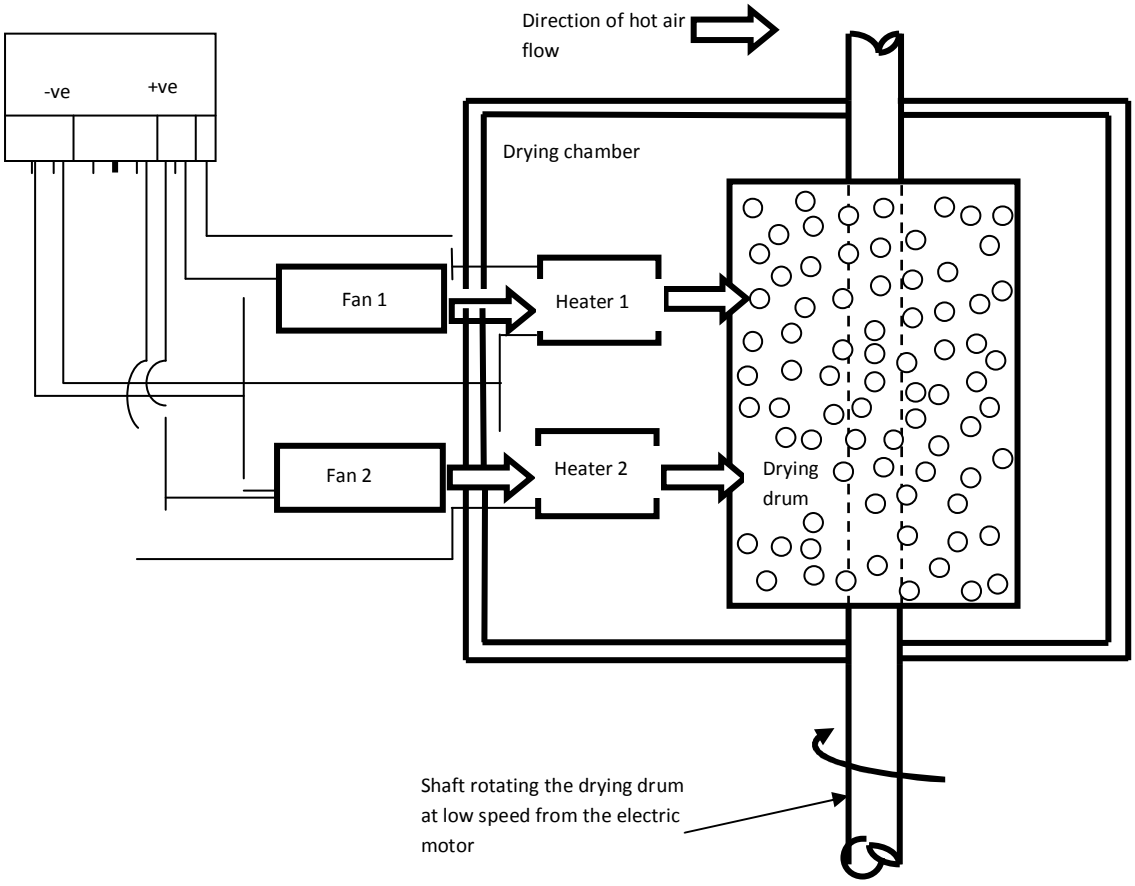

FIGURE 3: Schematic Diagram of the Dryer

Figure 4 shows the isometric view of the sieve frame made from wood. The volume of wood V_{wood} was obtained using

$$V_{wood} = 2L_{CD}^{\ 2}(L_{DE} + L_{AB}) \quad (22)$$

The sieves are two and they are of the same size, then the total volume of the wood can be obtained as $V_{Twood} = 2 \times V_{wood} = 4L_{CD}^{\ 2}(L_{DE} + L_{AB})$ (23)

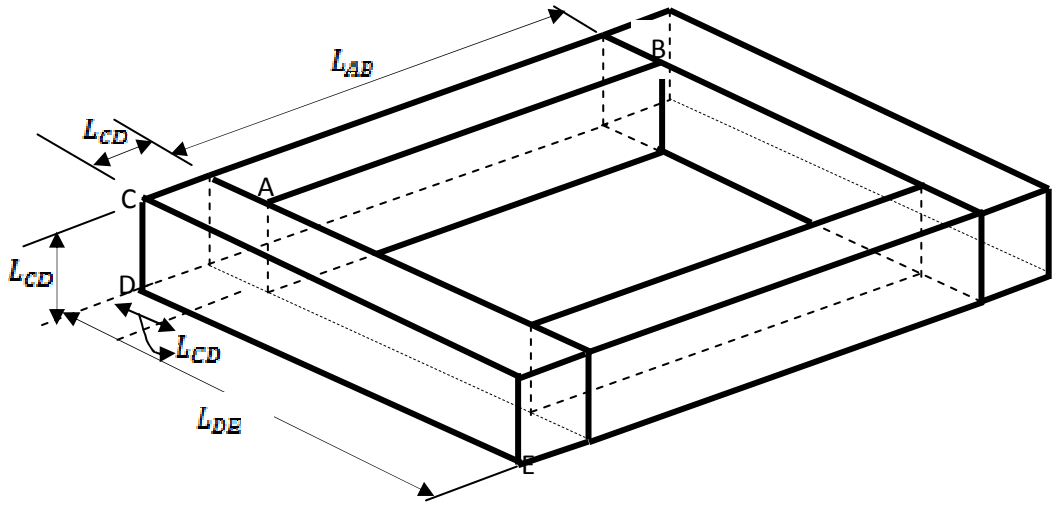

FIGURE 4: Sieve Frame

The volume of the sieving chamber V_{sc} was obtained from:

$$V_{sc} = 2\{(L_{DE} - 2L_{CD})\} \times L_{AB} \times L_{CD} \quad (24)$$

The time, velocity, and acceleration of the follower at return stroke and out-stroke are tabulated as follows

$$t = \frac{\theta}{\omega_{cam}} \quad (25)$$

$$V = \frac{\pi \omega_{cam} S}{2\theta} \quad (26)$$

$$a_o = \frac{\pi^2 \times \omega_{cam}{}^2 S}{2\theta^2} \quad [8] \quad (27)$$

Parameters/motion	Return stroke motion	Out- stroke motion
Time (s)	0.05	0.03
Velocity (m/s)	9.40	6.23
Acceleration (m/s^2)	884	395

TABLE 2: Values for Follower Motion

The rated life of the bearing supporting the auger shaft of the grinding machine was derived as

Rated life $L = \left(\frac{C}{p}\right)^3 \times 16^6$ *revolutions*

Where:
C = load rating; and P = dynamic equivalent load [8]
Figure (3) shows the schematic diagram of the conveyor used in the process plant.

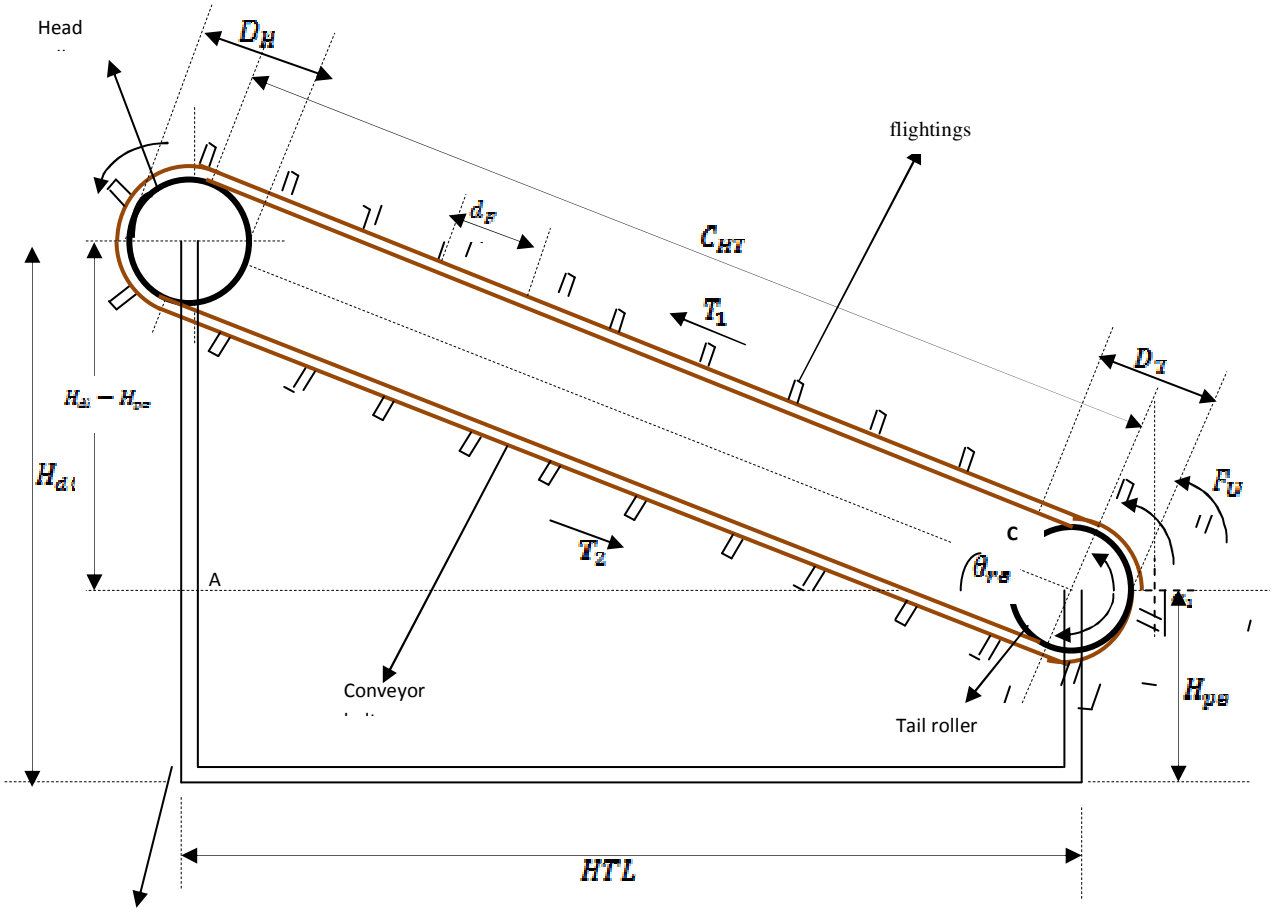

FIGURE 5: Diagram of the conveyor used in the poundo yam process plant

Where
D_H = Diameter of the head roller which is equal to the diameter of the tail roller
d_f = Distance between two flights on the belt
C_{HT}=Center distance between the head and tail roller = conveying length
θ_{re}= Angle of elevation of the rollers
H_{pe} = Height of the parboiling machine exit to the ground
HTL = Horizontal travel distance between the parboiling machine and the drying machine
H_{di} = Height of the drying machine exit to the ground
α= angle of wrap on the rollers
$T_1 = Tension$ in the tight side of the belt
T_2 = Tension in the slack side of the belt
The center distance between the head and tail roller (which is the conveying length) is obtained from:

$$C_{HT}^{\ 2} = HTL^2 + \left(H_{di} - H_{pe}\right)^2 \tag{28}$$

The length of the conveyor belt L_{CB} was obtained from:

$$L_{CB} = 2\left(CHT + \frac{\alpha}{360}\pi D_r\right) \tag{29}$$

The number of Flights on the belt was obtained from:

$$n_f = \left(\frac{L_{CB}}{d_f}\right) \tag{30}$$

The load stream volume Qv (which is defined as the conveying capacity of the conveyor) was obtained from

$$Qv = 3600\ Av\ (m^3/hr) \quad [13] \quad (31)$$

Where :

A and *v* are the cross sectional area of the load stream and the belt speed respectively.

The mass of load stream which the conveyor can move at a time is called the capacity of the conveyor and it was derived accordingly.

$$Q_{m} = \rho_m Q_v \ \text{(tons/hr)} \quad (32)$$

Where ρ_m is the density of the material conveyed. The bulk density of yam, $\rho_m = 1104$ Kg/m^3 [11]

The power required at the drive sprocket is the summation of the power for empty conveyor and load over the horizontal distance (p_1) and the power required for lift (p_2).

$$P_T = P_1 + P_2 \quad (33)$$

Where :

$$p_1 = \left(\frac{C_B v + \mathrm{Q_m}}{C_L + k_f} \right) \quad (34)$$

Where

C_L= length factor of the belt ; C_B= width factor of the belt; and k_f = working condition factor

Where: $$p_2 = \left(\frac{H_{di} - H_{pc}}{367} \right) \mathrm{Q_m} \quad (35)$$

The material selected for each component part of the machine in the process plant is analyzed in Tables 3 to 8.

S /n	Machine Component	Criteria for Selection	Material used for the Design	Suitable Material	Reasons for Selecting the Material
1	Machine Frame	Strength, firmness, and rigidity	Angle bar (Mild Steel)	H- Beam	It is cheap and readily available
2	Peeling Shaft	Strength, resistant to shock and torsional deflection	Galvanized steel.	Stainless steel	It is cheap and readily available
3	Auger Shaft	Strength, resistant to shock and torsional deflection	Galvanized steel.	Stainless steel	Cheaper and readily available
4	Electric Motor	optimal functionality	8.4 Hp and speed of 2000rpm	8 Hp and speed of 2000rpm	Most suitable
5.	Slicing Blades	strength and must be corrosion free	Stainless Steel	Stainless Steel	strong resistance to corrosion and cheaper

TABLE 3: The materials selected for the key component parts of the peeling and slicing machine

S/n	Machine Component	Criteria for Selection	Material used for the Design	Suitable Material	Reasons for Selecting the Material
1.	Auger spiral/coiled plate	Strength, resistant to shock, torsional deflection, and corossion free	Mild Steel	Stainless Steel, galvanized steel, and mild steel	Strong resistance to corrosion and cheaper
2.	Hot water reservoir (Tank)	Non corrosive, light weight and ability to hold hot water.	Tin sheet Ready made drum	Stainless Steel sheet	It is cheaper suitable, readily available and corrosion resistance
3.	Electric Motor	High efficient 20 Horsepower with medium range speed.	Continuous running electric motor; 20 hp with speed of 2000 rpm	Continuous running electric motor; 22 hp with speed of 2500 rpm	Most suitable
4.	Hot Water Pump	High efficiency, medium range speed with good and appreciable discharge rate.	Rotary pump with brass meshed gear.	Pump with stainless impeller.	It is suitable, cheap and resistance to corrosion
5.	Insulation	It must possess a very low thermal conductivity, light weight and durable.	Wood-saw dust.	Glass wool, Fibre glass and asbestos insulation wool.	It is suitable very cheap and readily available.

TABLE 4: The materials selected for the key component parts of the parboiling machine

S/n	Machine Component	Criteria for Selection	Material used for the Design	Suitable Material	Reasons for Selecting the Material
1.	Machine Frame	Strength, firmness, and rigidity	Angle Bar (Mild Steel)	H-Beam or U-Channel	It is suitable, cheaper and readily available.
2	Sprockets	strength and ability to avoid wobbling.	Mild Steel	Forged Steel	Most suitable and cheaper
3	Conveyor Belt	Strenght, corossion or contamination free material.	Rubber	Leather, cotton or fabric, balata	Most suitable and cheaper
4	Rollers	Strenght, smoothness and concentricity to avoid wobbling.	Mild Steel	Forged Steel	Most suitable and cheaper

TABLE 5: The materials selected for the key component parts of the conveyor

S/n	Machine Component	Criteria for Selection	Material used for the Design	Suitable Material	Reasons for Selecting the Material
1	Drying Drum	No contamination, strength	Galvanized steel	Stainless steel, Galvanized steel	Low cost, Availabil`ity, Durability
2	Drying chamber	Lightness	Mild steel	Stainless steel, Galvanized steel, Mild steel	Low cost, Availability
3	Heating box	Good conductivity	Aluminium	Steel, Aluminium, Teflon	Low cost, Availability
4	Insulator	Low thermal conductivity, stability at high temperature	Hardboard	Fiber glass, plywood, hardboard, sawdust, carton	Low cost, Availability
5	Heaters	Good electricity-heat conversion			Availability Suitability
6	Fan	Good air current, minimum power consumption			Average cost, no need for D.C – A.C conversion

TABLE 6: materials selected for the key component parts of the drying machine

S/n	Machine Component	Criteria for Selection	Material used for the Design	Suitable Material	Reasons for Selecting the Material
1	Hopper	The material must not contaminate the dried cubes of yam put into it.	Galvanized mild steel	Mild steel, aluminum stainless steel, Galvanized mild steel	Low cost, Availability Suitability
2	Grating Drum	Strenght, and ability to withstand the distributed vibration.	Mild steel sheet	Stainless steel sheet	It is cheaper suitable and readily available
3	Grating Disc	It must be strong enough to withstand shock without torsional deflection, shearing and bending. It must not contaminate the food substance	Mild Steel	Stainless Steel	It is cheaper suitable and readily available.
4	Delivery Chute	Contamination Free, strength	Galvanized mild steel	Mild steel, aluminum stain- less steel, galva-nized mild steel	Low cost, Availability Suitability

TABLE 7: Materials selected for the component parts of the grinding machine

S/n	Machine Component	Criteria for Selection	Material used for the Design	Suitable Material	Reasons for Selecting the Material
1	Sieve	Corrosion resistance, lightness, surface finish, cost	Wood	Wood, cast iron mild steel	Lightness corrosion resistance
2	Cam	Strength, machinability	Mild steel	Mild steel stainless steel	Strength cost
3	Delivery Chute	No contamination, strength	Galvanized mild steel	Mild steel, aluminum stainless steel, Galvanized mild steel	Low cost, Availability Suitability

TABLE 8: materials selected for the key component parts of the sieving machine

4. RESULTS AND DISCUSSION

To determine the time required for the grinding operation, let the grinding machine produce 10000mm^3 of grounded poundo yam for every revolution of its auger shaft. Then it is necessary to

determine the number of revolution of the auger shaft that will produce the total volume of dried cubes of yam put into its hopper.
The total volume of the dried cubes put into the grinding machine is $0.154m^3 = 154000000mm^3$.
Hence the auger requires $\left(\frac{154000000}{10000}\right) revolutions$ to completely grind the volume of dried cubes put into its hopper.
If the auger shaft of the grinding machine rotates at 342.86 *rpm* then the time required for the grinding operation (t_g) can be obtained as :

$$t_g = \left(\frac{154000000}{10000}\right) revolutions \div 342.86 rpm$$

t_g = 45 mins

Since the sieving operation and grinding operation are designed to operate simultaneously, then the total time required by the plant per batch is obtained as:

$$T_{batch} = t_{ps} + t_p + t_g \quad (38)$$

T_{batch} = 427.4 *mins* = 7.12 hrs = 7*hrs*

5. CONCLUSIONS

The critical role that mechanization of traditional food processing techniques plays in national development cannot be overemphasized in Nigeria, because high-post harvest food losses arise largely from limited food preservation capacity. In essence small scale food industries that involve lower capital investment and that rely on traditional food processing technologies are crucial to rural development in the country. By generating employment opportunity in the rural areas small scale food industries reduce rural-urban migration and the associated social problem. They are vital to reducing post harvest food losses and increasing food availability. hence a poundo yam process plant will serve as a means of reducing post harvest food loss of yam in the country.

6. REFERENCES

[1] J.H. Hulse (1983): Food Science for the Richer, Poorer, Sick and Healthy People. Proceedings Instant Food Science Technology, 16 (1); pp. 2-15.

[2] International Institute of Tropical Agriculture, (IITA) Root and Tuber Systems, Internet: *www.iita.org,* 2008 [May 25, 2010]

[3] Wikipedia,Yam Vegetable, Internet: *http://www.en.wikipedia .org /wiki/yam(vegetable)* 2010 [May 5, 2010]

[4] A. L. Ihekeronye, P.O. Ngoddy. Integrated Food Science and Technology for the Tropics, London England, Macmillan publishers limited,1985, pp. 4

[5] A. O. Odior and E. S. Orsarh. "Design and Construction of A Yam Pounding Machine", International Journal of Natural and Applied Sciences, 4(3): 319-323, 2008

[6] A.S. Hall, R. H. Alfred and G. L. Herman. Theory and Problems of Machine Design (S.I Metric Edition); New Delhi India, Tata McGraw-Hill Publishing Company Ltd; 1961, pp. 115-129

[7] E.S. Joseph and R.M. Charles. Mechanical Engineering Design (6th edition), New York Mc Graw-Hill, 2001; pp. 589-650, 831-897,965-986, 1050-1105.

[8] R.S. Khurmi and J.K. Gupta. Machine Design, 14th Edition, New Delhi Eurasia Publishing House (PVT) Ltd, 2009; pp. 520-545,608-612,735-748,763-770,828-840, 965-967,1088-1097.

[9] O.E. Olowofeso, F.I. Alao, O. Olotu, S.T. Oni, D.O. Awoyemi, R.A. Ademiluyi, S.J. Kayode, O. Olabode, T.T. Yussuf, T.O. Awodola, and J.A. Dada: Introductory Mathematics for Pre-Degree Science and University Diploma Science; The Federal University of Technology Akure, Ondo State, 2006, pp. 320-322.

[10] A.M. Michael. Irrigation Theory and Practice; 1985 Edition, Shahdara Delhi India Vani Educational Books, 1985. pp. 198-282

[11] M.V. Joshi. Process Equipment Design, 2nd Edition, Macmillan India Limited, 1976, pp. 180-188, 198-205, 360-371.

[12] G. Williams. A Textbook of Industrial Drying ; George Godwin Ltd United States. 1990, pp. 76

[13] D. Enerka. Belt Conveyor Design. Internet: http://www.scribd.com/doc/28383402/belt-conveyor-Design Dunlop 1994. [March 03, 2011].

[14] M.O. Oke, S.O. Awonorin, O.J. Oyelade, J.O. Olajide, G.O. Olaniyan and P.O. Sobukola, (2009). "Some Thermo-physical Properties of Yam cuts of Two Geometries." African Journal of Biotechnology, Vol. 8(7), pp. 1300-1304, April, 6th 2009.

[15] O.A. Aderoba. Development of a Yam Peeling and Slicing Machine for a Yam (Poundo Yam) Process Plant, B-Eng project report, The Federal University of Technology, Akure Ondo State, Nigeria. 2008.

Design Novel Lookup Table Changed Auto Tuning FSMC: Applied to Robot Manipulator

Farzin Piltan SSP.ROBOTIC@yahoo.com
Industrial Electrical and Electronic Engineering SanatkadeheSabze Pasargad. CO (S.S.P. Co), NO:16 ,PO.Code 71347-66773, Fourth floor Dena Apr , Seven Tir Ave , Shiraz , Iran

Mohammad Ali Dialame *SSP.ROBOTIC@yahoo.com*
Industrial Electrical and Electronic Engineering SanatkadeheSabze Pasargad. CO (S.S.P. Co), NO:16 ,PO.Code 71347-66773, Fourth floor Dena Apr , Seven Tir Ave , Shiraz , Iran

Abbas Zare S*SP.ROBOTIC@yahoo.com*
Industrial Electrical and Electronic Engineering SanatkadeheSabze Pasargad. CO (S.S.P. Co), NO:16 ,PO.Code 71347-66773, Fourth floor Dena Apr , Seven Tir Ave , Shiraz , Iran

Ali Badri *SSP.ROBOTIC@yahoo.com*
Industrial Electrical and Electronic Engineering SanatkadeheSabze Pasargad. CO (S.S.P. Co), NO:16 ,PO.Code 71347-66773, Fourth floor Dena Apr , Seven Tir Ave , Shiraz , Iran

Abstract

Refer to this paper, design lookup table changed adaptive fuzzy sliding mode controller with minimum rule base and good response in presence of structure and unstructured uncertainty is presented. However sliding mode controller is one of the robust nonlinear controllers but when this controller is applied to robot manipulator with highly nonlinear and uncertain dynamic function; caused to be challenged in control. Sliding mode controller in presence of uncertainty has two most important drawbacks; chattering and nonlinear equivalent part which proposed method is solved these challenges with look up table change methodology. This method is based on self tuning methodology therefore artificial intelligence (e.g., fuzzy logic method) is played important role to design proposed method. This controller has acceptable performance in presence of uncertainty (e.g., overshoot=0%, rise time=0.8 s, steady state error = 1e-9 and RMS error=0.00017).

Keywords: Sliding Mode Controller, Fuzzy Logic Methodology, Fuzzy Sliding Mode Controller, Adaptive Methodology, Fuzzy Lookup Table Changed Sliding Mode Controller.

1. INTRODUCTION, BACKGROUND and MOTIVATION

A robot system without any controllers does not to have any benefits, because controller is the main part in this sophisticated system. The main objectives to control of robot manipulators are stability, and robustness. Lots of researchers work on design the controller for robotic manipulators to have the best performance. Control of any systems divided in two main groups: linear and nonlinear controller [1].

However, one of the important challenging in control algorithms is design linear behavior controller to easier implementation for nonlinear systems but these algorithms have some limitation such as controller working area must to be near the system operating point and this adjustment is very difficult specially when the system dynamic parameters have large variations, and when the system has hard nonlinearities [1-3]. Most of robot manipulators which work in industry are usually controlled by linear PID controllers. But the robot manipulator dynamic functions are, nonlinear with strong coupling between joints (low gear ratio), structure and unstructured uncertainty, and multi- inputs multi-outputs (MIMO) which, design linear controller is very difficult especially if the velocity and acceleration of robot manipulator be high and also when the ratio between joints gear be small [4-5]. To eliminate above problems in physical systems most of control researcher go toward to select nonlinear robust controller.

One of the most important powerful nonlinear robust controllers is sliding mode controller (SMC). Sliding mode control methodology was first proposed in the 1950 [1-3]. This controller has been analyzed by many researchers in recent years. Many papers about the main theory of SMC are proposed such as references [1-44]. This controller now a day's used in wide range areas such as in robotics, in process control, in aerospace applications, and in power converters. The main reason to select this controller in wide range area is have an acceptable control performance and solve some main challenging topics in control such as resistivity to the external disturbance and uncertainty. However, this controller used in wide range area but, pure sliding mode controller has following disadvantages. Firstly, chattering problem; which can caused the high frequency oscillation of the controllers output. Secondly, sensitive; this controller is very sensitive to the noise when the input signals very close to the zero. Last but not the least, equivalent dynamic formulation; calculate the equivalent control formulation is difficult because it is depending on the nonlinear dynamic equation [6-9]. Many papers were presented to solve above problems such as references [21-44].

After the invention of fuzzy logic theory in 1965 by Zadeh [10], this theory was used in wide range area. Fuzzy logic controller (FLC) is one of the most important applications of fuzzy logic theory. This controller can be used to control of nonlinear, uncertain, and noisy systems. Fuzzy logic control systems, do not use complex mathematically models of plant for analysis. This method is free of some model-based techniques that used in classical controllers. It must be noted that application of fuzzy logic is not limited only to modeling of nonlinear systems [11-15, 20, 36] but also this method can help engineers to design easier controller. However pure FLC works in many engineering applications but, it cannot guarantee two most important challenges in control, namely, stability and acceptable performance [10-15].

Some researchers applied fuzzy logic methodology in sliding mode controllers (FSMC) to reduce the chattering and solve the nonlinear dynamic equivalent problems in pure sliding mode controller so called fuzzy sliding mode controller [23, 25-27] and the other researchers applied sliding mode methodology in fuzzy logic controller (SMFC) to improve the stability of systems [29, 32-35].

Adaptive control used in systems whose dynamic parameters are varying and need to be training on line. In general states adaptive control classified in two main groups: traditional adaptive method and fuzzy adaptive method, that traditional adaptive method need to have some information about dynamic plant and some dynamic parameters must be known but fuzzy adaptive method can training the variation of parameters by expert knowledge. Adaptive fuzzy inference system provide a good knowledge tools for adjust a complex uncertain nonlinear system with changing dynamics to have an acceptable performance [37-44]. Combined adaptive method to artificial sliding mode controllers can help to controllers to have a better performance by online tuning the nonlinear and time variant parameters [23-44].

In this research we will highlight a new auto adjust sliding surface slope derived in the Lyapunov sense. This algorithm will be analyzed and evaluated on robotic manipulators. Section 2, is

served as a problem statements, robot manipulator dynamics and introduction to the pure sliding mode controller with proof of stability and its application to robot manipulator. Part 3, introduces and describes the methodology algorithms and proves Lyapunov stability. Section 4 presents the simulation results of this algorithm applied to a 3 degree-of-freedom robot manipulator and the final section is describe the conclusion.

2. ROBOT MANIPULATOR DYNAMICS, PROBLEM STATEMENTS and SLIDING MODE CONTROLLER FORMULATION

Robot Manipulator Dynamic Formulation: The equation of an *n-DOF* robot manipulator governed by the following equation [1, 3, 16-28, 30, 38-40]:

$$M(q)\ddot{q} + N(q,\dot{q}) = \tau \quad (1)$$

Where τ is actuation torque, M (q) is a symmetric and positive define inertia matrix, $N(q,\dot{q})$ is the vector of nonlinearity term. This robot manipulator dynamic equation can also be written in a following form:

$$\tau = M(q)\ddot{q} + B(q)[\dot{q}\ \dot{q}] + C(q)[\dot{q}]^2 + G(q) \quad (2)$$

Where B(q) is the matrix of coriolios torques, C(q) is the matrix of centrifugal torques, and G(q) is the vector of gravity force. The dynamic terms in equation (2) are only manipulator position. This is a decoupled system with simple second order linear differential dynamics. In other words, the component $\ddot{q}$ influences, with a double integrator relationship, only the joint variableq_i, independently of the motion of the other joints. Therefore, the angular acceleration is found as to be [3, 16-28]:

$$\ddot{q} = M^{-1}(q).\{\tau - N(q,\dot{q})\} \quad (3)$$

Sliding Mode Control: This technique is very attractive from a control point of view. The central idea of sliding mode control (SMC) is based on nonlinear dynamic equivalent. It has assumed that the desired motion trajectory for the manipulator $q_d(t)$, as determined, by a path planner. Defines the tracking error as [4-9, 18, 21, 31-44]:

$$e(t) = q_d(t) - q_a(t) \quad (4)$$

Where e(t) is error of the plant, $q_d(t)$ is desired input variable, that in our system is desired displacement, $q_a(t)$ is actual displacement. Consider a nonlinear single input dynamic system of the form [6]:

$$x^{(n)} = f(\vec{x}) + b(\vec{x})u \quad (5)$$

Where u is the vector of control input, $x^{(n)}$ is the n^{th} derivation of$x$, $x = [x, \dot{x}, \ddot{x}, \ldots, x^{(n-1)}]^T$ is the state vector, $f(x)$ is unknown or uncertainty, and $b(x)$ is of known *sign* function. The control problem is truck to the desired state; $x_d = [x_d, \dot{x}_d, \ddot{x}_d, \ldots, x_d{}^{(n-1)}]^T$, and have an acceptable error which is given by:

$$\tilde{x} = x - x_d = [\tilde{x}, \ldots, \tilde{x}^{(n-1)}]^T \quad (6)$$

A time-varying sliding surface $s(x,t)$ is given by the following equation:

$$s(x,t) = (\frac{d}{dt} + \lambda)^{n-1}\tilde{x} = 0 \quad (7)$$

where λ is the positive constant. To further penalize tracking error integral part can be used in sliding surface part as follows:

$$s(x,t) = (\frac{d}{dt} + \lambda)^{n-1}\left(\int_0^\tau \tilde{x}\,dt\right) = 0 \quad (8)$$

The main target in this methodology is kept the sliding surface slope $s(x,t)$ near to the zero. Therefore, one of the common strategies is to find input U outside of $s(x,t)$.

$$\frac{1}{2}\frac{d}{dt}s^2(x,t) \le -\zeta|s(x,t)| \quad (9)$$

where ζ is positive constant.

$$\text{If } S(0)>0 \rightarrow \frac{d}{dt}S(t) \le -\zeta \quad (10)$$

To eliminate the derivative term, it is used an integral term from t=0 to t=t_{reach}

$$\int_{t=0}^{t=t_{reach}} \frac{d}{dt}S(t) \leq -\int_{t=0}^{t=t_{reach}} \eta \rightarrow S(t_{reach}) - S(0) \leq -\zeta(t_{reach} - 0) \quad (11)$$

Where t_{reach} is the time that trajectories reach to the sliding surface so, suppose S($t_{reach} = 0$) defined as

$$0 - S(0) \leq -\eta(t_{reach}) \rightarrow t_{reach} \leq \frac{S(0)}{\zeta} \quad (12)$$

and

$$if\ S(0) < 0 \rightarrow 0 - S(0) \leq -\eta(t_{reach}) \rightarrow S(0) \leq -\zeta(t_{reach}) \rightarrow t_{reach} \leq \frac{|S(0)|}{\eta} \quad (13)$$

Equation (13) guarantees time to reach the sliding surface is smaller than $\frac{|S(0)|}{\zeta}$ since the trajectories are outside of $S(t)$.

$$if\ S_{t_{reach}} = S(0) \rightarrow error(x - x_d) = 0 \quad (14)$$

suppose S is defined as

$$s(x,t) = (\frac{d}{dt} + \lambda) \quad \tilde{x} = (\dot{x} - \dot{x}_d) + \lambda(x - x_d) \quad (15)$$

The derivation of S, namely, $\dot{S}$ can be calculated as the following;

$$\dot{S} = (\ddot{x} - \ddot{x}_d) + \lambda(\dot{x} - \dot{x}_d) \quad (16)$$

suppose the second order system is defined as;

$$\ddot{x} = f + u \rightarrow \dot{S} = f + U - \ddot{x}_d + \lambda(\dot{x} - \dot{x}_d) \quad (17)$$

Where f is the dynamic uncertain, and also since $S = 0\ and\ \dot{S} = 0$, to have the best approximation ,$\hat{U}$ is defined as

$$\hat{U} = -\hat{f} + \ddot{x}_d - \lambda(\dot{x} - \dot{x}_d) \quad (18)$$

A simple solution to get the sliding condition when the dynamic parameters have uncertainty is the switching control law:

$$U_{dis} = \hat{U} - K(\vec{x}, t) \cdot sgn(s) \quad (19)$$

where the switching function $sgn(S)$ is defined as

$$sgn(s) = \begin{cases} 1 & s > 0 \\ -1 & s < 0 \\ 0 & s = 0 \end{cases} \quad (20)$$

and the $K(\vec{x}, t)$ is the positive constant. Suppose by (9) the following equation can be written as,

$$\frac{1}{2}\frac{d}{dt}s^2(x,t) = \dot{S} \cdot S = [f - \hat{f} - Ksgn(s)] \cdot S = (f - \hat{f}) \cdot S - K|S| \quad (21)$$

and if the equation (13) instead of (12) the sliding surface can be calculated as

$$s(x,t) = (\frac{d}{dt} + \lambda)^2 \left(\int_0^t \tilde{x}\, dt\right) = (\dot{x} - \dot{x}_d) + 2\lambda(\dot{x} - \dot{x}_d) - \lambda^2(x - x_d) \quad (22)$$

in this method the approximation of U is computed as

$$\hat{U} = -\hat{f} + \ddot{x}_d - 2\lambda(\dot{x} - \dot{x}_d) + \lambda^2(x - x_d) \quad (23)$$

Based on above discussion, the control law for a multi degrees of freedom robot manipulator is written as:

$$\tau = \tau_{eq} + \tau_{dis} \quad (24)$$

Where, the model-based component τ_{eq} is the nominal dynamics of systems and τ_{eq} can be calculate as follows:

$$\tau_{eq} = [M^{-1}(B + C + G) + \dot{S}]M \quad (25)$$

Where [15-44]

$$\tau_{eq}=\begin{bmatrix}\tau_{eq1}\\ \tau_{eq2}\\ \tau_{eq3}\\ \tau_{eq4}\\ \tau_{eq5}\\ \tau_{eq6}\end{bmatrix},M^{-1}=\begin{bmatrix}M_{11}&M_{12}&M_{13}&0&0&0\\ M_{21}&M_{22}&M_{23}&0&0&0\\ M_{31}&M_{32}&M_{33}&0&M_{35}&0\\ 0&0&0&M_{44}&0&0\\ 0&0&0&0&M_{55}&0\\ 0&0&0&0&0&M_{66}\end{bmatrix}^{-1}$$

$$B+C+G=\begin{bmatrix}b_{112}\dot{q}_1\dot{q}_2+b_{113}\dot{q}_1\dot{q}_3+0+b_{123}\dot{q}_2\dot{q}_3\\ 0+b_{223}\dot{q}_2\dot{q}_3+0+0\\ 0\\ b_{412}\dot{q}_1\dot{q}_2+b_{413}\dot{q}_1\dot{q}_3+0+0\\ 0\\ 0\end{bmatrix}+\begin{bmatrix}C_{12}\dot{q}_2{}^2+C_{13}\dot{q}_3{}^2\\ C_{21}\dot{q}_1{}^2+C_{23}\dot{q}_3{}^2\\ C_{31}\dot{q}_1{}^2+C_{32}\dot{q}_2{}^2\\ 0\\ C_{51}\dot{q}_1{}^2+C_{52}\dot{q}_2{}^2\\ 0\end{bmatrix}+\begin{bmatrix}0\\ g_2\\ g_3\\ 0\\ g_5\\ 0\end{bmatrix}$$

$$\dot{S}=\begin{bmatrix}\dot{S}_1\\ \dot{S}_2\\ \dot{S}_3\\ \dot{S}_4\\ \dot{S}_5\\ \dot{S}_6\end{bmatrix}\text{ and }M=\begin{bmatrix}M_{11}&M_{12}&M_{13}&0&0&0\\ M_{21}&M_{22}&M_{23}&0&0&0\\ M_{31}&M_{32}&M_{33}&0&M_{35}&0\\ 0&0&0&M_{44}&0&0\\ 0&0&0&0&M_{55}&0\\ 0&0&0&0&0&M_{66}\end{bmatrix}$$

and τ_{dis} is computed as;

$$\tau_{dis}=K\cdot \mathrm{sgn}(S) \quad (26)$$

where

$$\tau_{dis}=\begin{bmatrix}\tau_{dis1}\\ \tau_{dis2}\\ \tau_{dis3}\\ \tau_{dis4}\\ \tau_{dis5}\\ \tau_{dis6}\end{bmatrix},K=\begin{bmatrix}K_1\\ K_2\\ K_3\\ K_4\\ K_5\\ K_6\end{bmatrix},(S)=\begin{bmatrix}S_1\\ S_2\\ S_3\\ S_4\\ S_5\\ S_6\end{bmatrix}\ and\ \ S=\lambda e+\dot{e}$$

The result scheme is shown in Figure 1.

Problem Statement: Even though, SMC is used in wide range areas but, pure SMC has the chattering phenomenon disadvantages to reduce or eliminate the chattering this paper focuses on applied fuzzy logic methodology in sliding mode controller with minimum rule base after that sliding surface slope which has play important role in remove the chattering is auto adjusted.

Proof of Stability in Pure Sliding Mode Controller: The proof of Lyapunov function can be determined by the following equations. The dynamic formulation of robot manipulate can be written by the following equation

$$\tau=M(q)\ddot{q}+V(q,\dot{q})\dot{q}+G(q) \quad (27)$$

the lyapunov formulation can be written as follows,

$$V=\frac{1}{2}S^T.M.S \quad (28)$$

the derivation of V can be determined as,

$$\dot{V}=\frac{1}{2}S^T.\dot{M}.S+S^T M\dot{S} \quad (29)$$

the dynamic equation of robot manipulator can be written based on the sliding surface as

$$M\dot{S}=-VS+M\dot{S}+VS+G-\tau \quad (30)$$

it is assumed that

$$S^T(\dot{M} - 2V)S = 0 \quad (31)$$

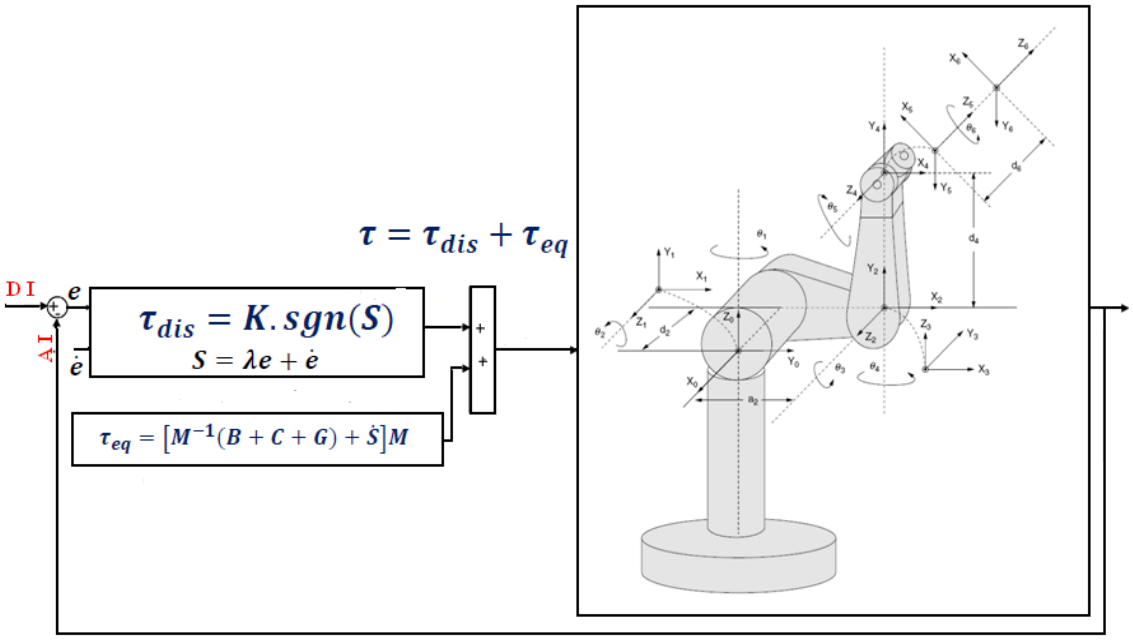

FIGURE 1: Block diagram of Sliding Mode Controller (SMC)

by substituting (30) in (29)

$$\dot{V} = \frac{1}{2}S^T\dot{M}S - S^TVS + S^T(M\dot{S} + VS + G - \tau) = S^T(M\dot{S} + VS + G - \tau) \quad (32)$$

suppose the control input is written as follows

$$\hat{\tau} = \widehat{\tau_{eq}} + \widehat{\tau_{dis}} = [\widehat{M^{-1}}(\hat{V} + \hat{G}) + \dot{S}]\hat{M} + K.sgn(S) + K_vS \quad (33)$$

by replacing the equation (33) in (32)

$$\dot{V} = S^T(M\dot{S} + VS + G - \hat{M}\dot{S} - \hat{V}S - \hat{G} - K_vS - Ksgn(S) = S^T\left(\tilde{M}\dot{S} + \tilde{V}S + \tilde{G} - K\right. \quad (34)$$

it is obvious that

$$|\tilde{M}\dot{S} + \tilde{V}S + \tilde{G} - K_vS| \leq |\tilde{M}\dot{S}| + |\tilde{V}S| + |\tilde{G}| + |K_vS| \quad (35)$$

the Lemma equation in robot manipulator system can be written as follows

$$K_u = \left[|\tilde{M}\dot{S}| + |VS| + |G| + |K_vS| + \eta\right]_i, i = 1, 2, 3, 4, \ldots \quad (36)$$

the equation (31) can be written as

$$K_u \geq \left|\left[\tilde{M}\dot{S} + VS + G - K_vS\right]_i\right| + \eta_i \quad (37)$$

therefore, it can be shown that

$$\dot{V} \leq -\sum_{i=1}^{n} \eta_i |S_i| \quad (38)$$

Consequently the equation (38) guaranties the stability of the Lyapunov equation.

Improve the Chattering: To remove the chattering boundary layer method; in boundary layer method is used [32-44]. This method is based on the replace discontinuous method by saturation (linear) method with small neighborhood of the switching surface.

$$H(t) = \{x, |S(t)| \leq \emptyset\}; \emptyset > 0 \quad (39)$$

Where $\emptyset$ is the boundary layer thickness. Therefore the saturation function $\mathbf{Sat}(S/\emptyset)$ is added to the control law as

$$\tau_{sat} = K(\vec{x}, t) \cdot \mathbf{Sat}\left(S/\emptyset\right) \quad (40)$$

Where $\mathbf{Sat}\left(S/\emptyset\right)$ can be defined as

$$\mathbf{sat}\left(S/\emptyset\right) = \begin{cases} 1 & (S/\emptyset > 1) \\ -1 & (S/\emptyset < 1) \\ S/\emptyset & (-1 < S/\emptyset < 1) \end{cases} \quad (41)$$

Based on above discussion, the control law for a multi degrees of freedom robot manipulator is written as:

$$\tau = \tau_{eq} + \tau_{sat} \quad (42)$$

Where, the model-based component τ_{eq} is the nominal dynamics of systems and τ_{eq} can be calculate as follows:

$$\tau_{eq} = [M^{-1}(B + C + G) + \dot{S}]M \quad (43)$$

and τ_{sat} is computed as;

$$\tau_{sat} = K \cdot \mathbf{sat}\left(S/\emptyset\right) \quad (44)$$

By replace the formulation (44) in (42) the control output can be written as;

$$\tau = \tau_{eq} + K.\mathbf{sat}\left(S/\emptyset\right) = \begin{cases} \tau_{eq} + K.\mathbf{sgn}(S) & ,|S| \geq \emptyset \\ \tau_{eq} + K.S/\emptyset & ,|S| < \emptyset \end{cases} \quad (45)$$

Figure 2 shows the chattering free sliding mode control for robot manipulator. By (45) and (43) the sliding mode control of PUMA 560 robot manipulator is calculated as;

$$\tau = [M^{-1}(B + C + G) + \dot{S}]M + K \cdot \mathbf{sat}\left(S/\emptyset\right) \quad (46)$$

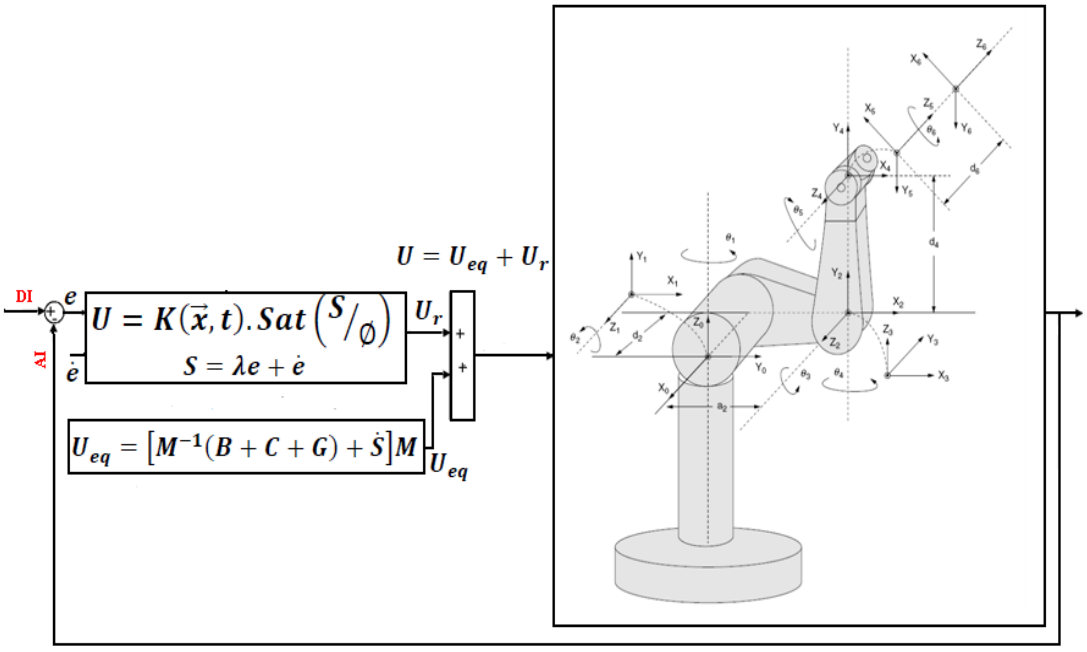

FIGURE 2: Block diagram of chattering free Sliding Mode Controller (SMC)

Second Step, Design Sliding Mode Fuzzy Controller: As shown in Figure 1, sliding mode controller divided into two main parts: equivalent controller, based on dynamics formulation of robot manipulators and sliding surface saturation part based on saturation continuous function to reduce the chattering. Boundary layer method (saturation function) is used to reduce the chattering. Reduce or eliminate the chattering regarding to reduce the error is play important role in this research therefore boundary layer method is used beside the equivalent part to solve the chattering problem besides reduce the error.

Combinations of fuzzy logic systems with sliding mode method have been proposed by several researchers. SMFC is fuzzy controller based on sliding mode method for easy implementation, stability, and robustness. Control rules for SMFC can be described as:

IF S is<ling.var> THEN U is<ling.var> **(47)**

Table 1 is shown the fuzzy rule table for SMFC, respectively:

S	NB	NM	NS	Z	PS	PM	PB
T	NB	NM	NS	Z	PS	PM	PB

TABLE 1: Rule table (SMFC)

A block diagram for sliding mode fuzzy controller is shown in Figure 3.

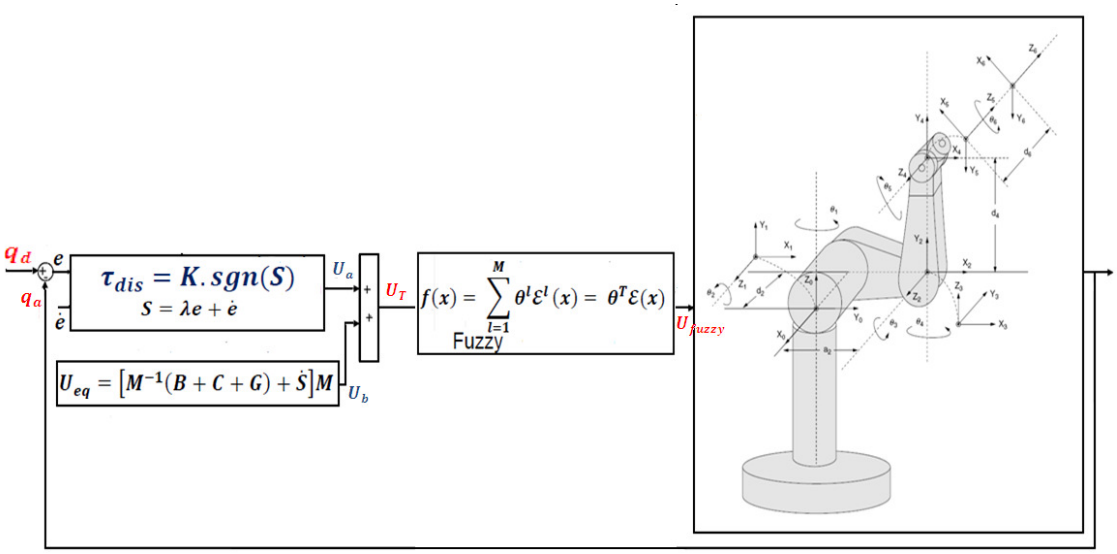

FIGURE3: Block Diagram of sliding mode Fuzzy Controller with Minimum Rule Base

It is basic that the system performance is sensitive to the sliding surface slope λ for sliding mode fuzzy controller. For instance, if large value of λ are chosen the response is very fast but the system is very unstable and conversely, if small value of λ considered the response of system is very slow but the system is very stable. Therefore, calculate the optimum value of λ for a system is one of the most important challenging works. SMFC has two most important advantages i.e. the number of rule base is smaller and Increase the robustness and stability.
In this method the control output can be calculated by

$$U_T = U_{dis} + U_{eq} \quad \textbf{(48)}$$

Where U_{eq} the nominal compensation is term and U_{dis} is the output of sliding function [9].

Third Step; Auto Tuning Sliding Surface Slope: All conventional controller have common difficulty, they need to find and estimate several nonlinear parameters. Tuning sliding surface slope can tune by mathematical automatically the scale parameters using mathematical model free method. To keep the structure of the controller as simple as possible and to avoid heavy computation, in this design model free mathematical supervisor tuner is selected. For nonlinear, uncertain, and time-variant plants (e.g., robot manipulators) adaptive method can be used to self adjusting the surface slope and gain updating factors. Research on adaptive sliding mode fuzzy controller is significantly growing, for instance, the different ASMFC have been reported in [5]; [10-12]. It is a basic fact that the system performance in SMFC is sensitive to sliding surface slope, λ. Thus, determination of an optimum λ value for a system is an important problem. If the system parameters are unknown or uncertain, the problem becomes more highlighted. This problem may be solved by adjusting the surface slope and boundary layer thickness of the sliding mode controller continuously in real-time. To keep the structure of the controller as simple as possible and to avoid heavy computation, a new supervisor tuner based on updated by a new coefficient factor kn is presented. In this method the supervisor part tunes the output scaling factors using gain online updating factors. The inputs of the supervisor term are error and change of error $(e, \dot{e})$ and the output of this controller is U, which it can be used to tune sliding surface slope, λ.

$$k_n = e^2 - \frac{(r_v - r_{vmin})^5}{1+|e|} + r_{vmin} \quad (49)$$

$$r_v = \frac{(de(k) - de(k-1))}{de(.)} = \frac{\ddot{e}(t)}{\dot{e}(.)} \quad (50)$$

$$de(.) = \begin{cases} de(k): & if\ de(k) \geq de(k-1) \\ de(k-1) & if\ de(k) < de(k-1) \end{cases}$$

$$S_{new} = \lambda_{new} \times e_{new} + \dot{e}_{new}$$

$$e_{new} = e \times \lambda_{new}$$

$$\lambda_{new} = \lambda \times K_n$$

In this way, the performance of the system is improved with respect to the SMFC controller.
In this method the tunable part tunes the sliding surface slope. However pure sliding mode controller has satisfactory performance in a limit uncertainty but tune the performance of this controller in highly nonlinear and uncertain parameters (e.g., robot manipulator) is a difficult work which proposed methodology can solve above challenge by applied adaptive. The lyapunov candidate formulation for our design is defined by:

$$V = \frac{1}{2}S^T MS + \frac{1}{2}\sum_{j=1}^{M}\frac{1}{\gamma_{sj}}\phi^T.\phi_j \quad (51)$$

Where γ_{sj} is positive coefficient, $\phi = \theta^* - \theta$; θ^* *is mintmum error* & θ *is adjustable parameter*
Since $\dot{M} - 2V$ is skew-symetric matrix, we can get

$$S^T M\dot{S} + \frac{1}{2}S^T \dot{M}S = S^T(M\dot{S} + VS) \quad (52)$$

From following two functions:

$$\tau = M(q)\ddot{q} + V(q,\dot{q})\dot{q} + G(q) \quad (53)$$

And

$$\tau = \hat{M}\ddot{q}_r + \hat{V}\dot{q}_r + \hat{G} - AS - K \quad (54)$$

We can get:

$$M(q)\ddot{q} + V(q,\dot{q})\dot{q} + G(q) = \hat{M}\ddot{q}_r + \hat{V}\dot{q}_r + \hat{G} - AS - K \quad (55)$$

Since; $\dot{q}_r = \dot{q} - S$ & $\ddot{q}_r = \ddot{q} - \dot{S}$ then

$$M\dot{S} + (V+A)S = \Delta f - K \quad (56)$$

$$M\dot{S} = \Delta f - K - VS - AS$$

The derivative of V defined by;

$$\dot{V} = S^T M\dot{S} + \frac{1}{2}S^T \dot{M}S + \sum_{j=1}^{M}\frac{1}{\gamma_{sj}}\phi^T.\dot{\phi}_j \quad (57)$$

$$\dot{V} = S^T(M\dot{S} + VS) + \sum_{j=1}^{M}\frac{1}{\gamma_{sj}}\phi^T.\dot{\phi}_j \quad (58)$$

$$\dot{V} = S^T(\Delta f - K - VS - AS + VS) + \sum_{j=1}^{M}\frac{1}{\gamma_{sj}}\phi^T.\dot{\phi}_j \quad (59)$$

$$\dot{V} = \sum_{j=1}^{M}[S_j(\Delta f_j - K_j)] - S^T AS + \sum_{j=1}^{M}\frac{1}{\gamma_{sj}}\phi^T.\dot{\phi}_j \quad (60)$$

suppose K_n is defined as follows

$$k_n = e^2 - \frac{(r_v - r_{vmin})^5}{1+|e|} + r_{vmin} \quad (61)$$

Based on $\phi = \theta^* - \theta \rightarrow \theta = \theta^* - \phi$

$$\dot{V} = \sum_{j=1}^{M} [S_j(\Delta f_j - (\theta^*)^T \zeta(S_j) k_n] - S^T A S + \sum_{j=1}^{M} \frac{1}{\gamma_{sj}} \phi_j^T [\gamma_{sj}, S_j, \zeta_j(S_j) + \dot{\phi}_j]) \quad (62)$$

where $\dot{\theta}_j = \gamma_{sj} S_j \zeta_j(S_j)$ is adaption law, $\dot{\phi}_j = -\dot{\theta}_j = -\gamma_{sj} S_j \zeta_j(S_j)$
consequently $\dot{V}$ can be considered by

$$\dot{V} = \sum_{j=1}^{m} [S_j \Delta f_j - ((\theta_j^*)^T \zeta_j(S_j) k_n)] - S^T A S \quad (63)$$

If the minimum error can be defined by

$$e_{mj} = \Delta f_j - \left((\theta_j^*)^T \zeta_j(S_j)\right) \quad (64)$$

$\dot{V}$ is intended as follows

$$\begin{aligned} \dot{V} &= \sum_{j=1}^{m} [S_j e_{mj}] - S^T A S \\ &\leq \sum_{j=1}^{m} |S_j| |e_{mj}| - S^T A S \\ &= \sum_{j=1}^{m} |S_j| |e_{mj}| - \alpha_j S_j^2 \\ &= \sum_{j=1}^{m} |S_j| (|e_{mj}| - \alpha_j S_j) \end{aligned} \quad (65)$$

For continuous function $g(x)$, and suppose $\varepsilon > 0$ it is defined mathematical model free in form of

$$Sup_{x \in U} |f(x) - g(x)| < \epsilon \quad (66)$$

the minimum approximation error (e_{mj}) is very small.

$$if\ \alpha_j = \alpha \quad that \quad \alpha |S_j| > e_{mj}\ (S_j \neq 0) \quad then \quad \dot{V} < 0\ for\ (S_j \neq 0) \quad (67)$$

3. SIMULATION RESULTS

Classical sliding mode control (SMC) and adaptive sliding mode fuzzy control (ASMFC) are implemented in Matlab/Simulink environment. In theses controllers changing updating factor performance, tracking performance, error, and robustness are compared.

Changing Sliding Surface Slope performance: For various value of sliding surface slope (λ) in SMC and ASMFC the trajectory performances have shown in Figures 4 and 5.

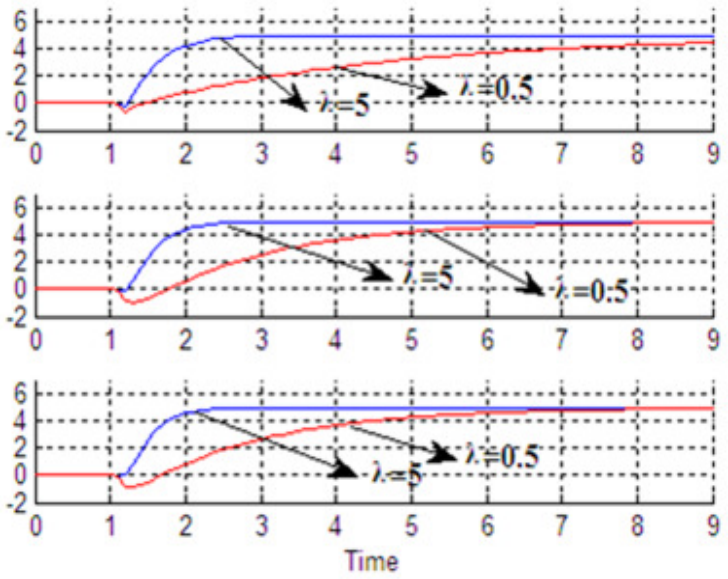

FIGURE 4: Sliding surface slope in SMC: applied to 3DOF's robot manipulator

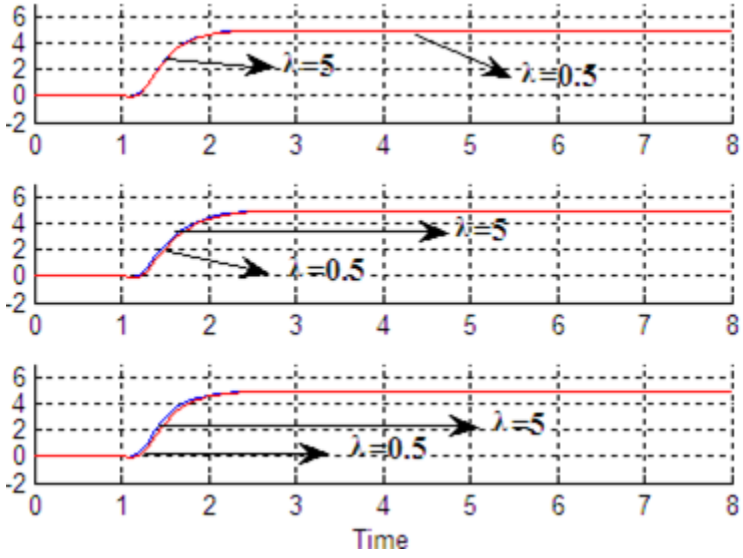

FIGURE 5: Sliding surface slope in ASMFC: applied to 3DOF's robot manipulator

Figures 4 and 5 are shown trajectory performance with different sliding surface slope; it is seen that AFSMC has the better performance in comparison with classical SMC.

Tracking Performances

From the simulation for first, second and third trajectory without any disturbance, it was seen that SMC and ASMFC have the about the same performance because this system is worked on certain environment and in sliding mode controller also is a robust nonlinear controller with acceptable performance. Figure 6 shows tracking performance without any disturbance for SMC and ASMFC.

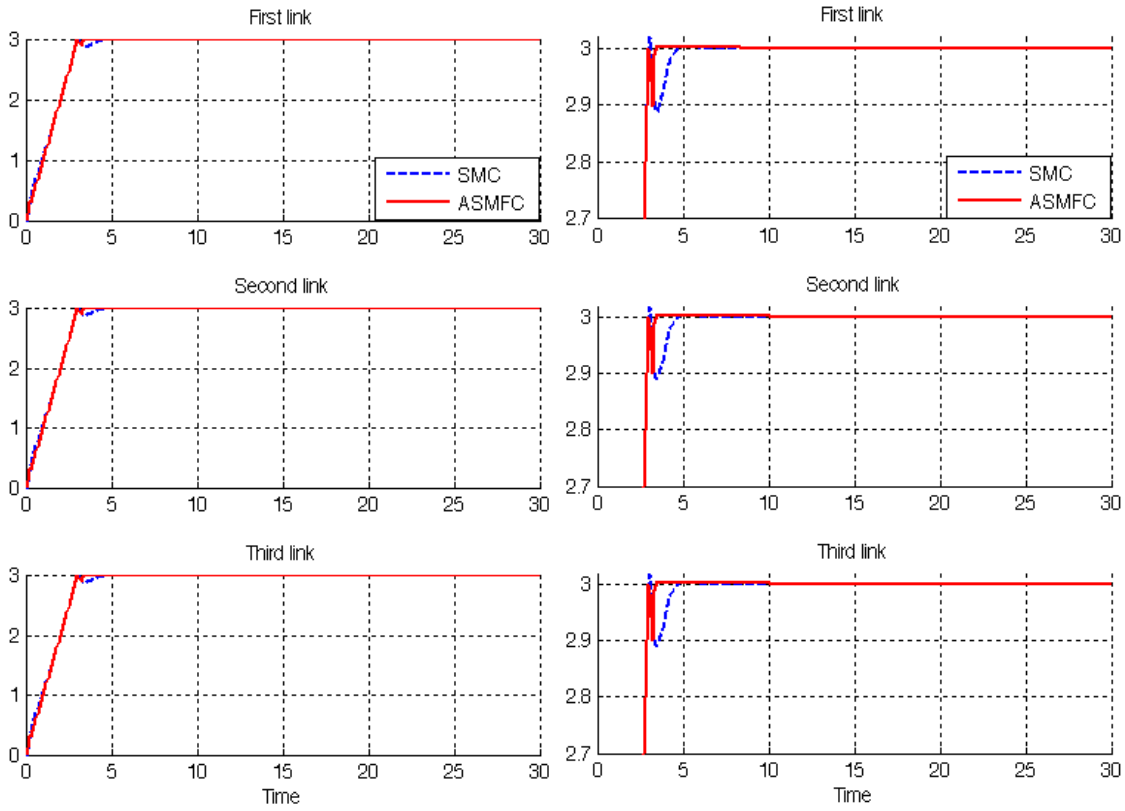

FIGURE 6: SMC Vs. ASMFC: applied to 3DOF's robot manipulator

By comparing trajectory response trajectory without disturbance in SMC and ASMFC, it is found that the SMFC's overshoot **(0%)** is lower than IDC's **(3.33%)** and the rise time in both of controllers are the same.

Disturbance Rejection

Figure 7 has shown the power disturbance elimination in SMC and ASMFC. The main targets in these controllers are disturbance rejection as well as the remove the chattering phenomenon. A band limited white noise with predefined of 40% the power of input signal is applied to the SMC and SMFC. It found fairly fluctuations in SMC trajectory responses.

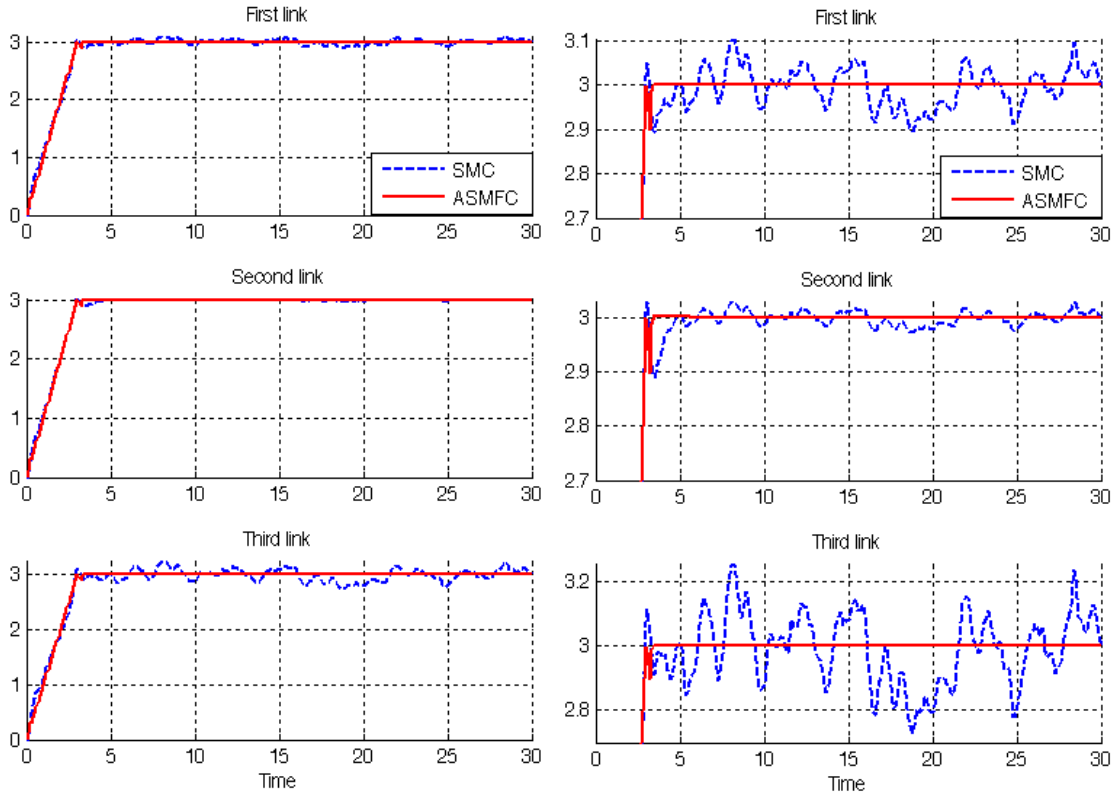

FIGURE 7: SMC Vs. ASMFC in presence of uncertainty: applied to robot manipulator.

Among above graph relating to trajectory following with external disturbance, SMC has fairly fluctuations. By comparing some control parameters such as overshoot and rise time it found that the ASMFC's overshoot **(0%)** is lower than SMC's **(12.4%)**, although both of them have about the same rise time**.**

4. CONCLUSIONS

This research presents a design auto adjust sliding surface slope in sliding mode fuzzy controller (ASMFC) with improved in sliding mode controller which offers a model-free sliding mode controller. The sliding mode fuzzy controller is designed as 7 rules Mamdani's error-based to estimate the uncertainties in nonlinear equivalent part. To eliminate the chattering with regard to the uncertainty and external disturbance applied mathematical self tuning method to sliding mode fuzzy controller for adjusting the sliding surface slope coefficient (λ). In this research new λ is obtained by the previous λ multiple gains updating factor (K_n) which it also is based on error and change of error and also the second derivation of error. The proof of stability in this method is discussed. As a result auto adjust sliding surface slope in sliding mode fuzzy controller has superior performance in presence of structure and unstructured uncertainty (e.g., overshoot=0%, rise time=0.9 s, steady state error = 1e-7 and RMS error=0.00016) and eliminate the chattering.

REFERENCES

[1] Thomas R. Kurfess, Robotics and Automation Handbook: CRC press, 2005.

[2] Bruno Siciliano and Oussama Khatib, Handbook of Robotics: Springer, 2007.

[3] Slotine J. J. E., and W. Li., Applied nonlinear control: Prentice-Hall Inc, 1991.

[4] Piltan Farzin, et al., “Artificial Chattering Free on-line Fuzzy Sliding Mode Algorithm for Uncertain System: Applied in Robot Manipulator,” International Journal of Engineering, 5 (5):220-238, 2011.

[5] L.X.Wang, “stable adaptive fuzzy control of nonlinear systems”, IEEE transactions on fuzzy systems, 1(2): 146-154, 1993.

[6] Frank L.Lewis, Robot dynamics and control, in robot Handbook: CRC press, 1999.

[7] Piltan, F., et al., “Evolutionary Design on-line Sliding Fuzzy Gain Scheduling Sliding Mode Algorithm: Applied to Internal Combustion Engine,” International journal of Engineering Science and Technology, 3 (10): 7301-7308, 2011.

[8] Soltani Samira and Piltan, F. “Design artificial control based on computed torque like controller with tunable gain,” World Applied Science Journal, 14 (9): 1306-1312, 2011.

[9] Piltan, F., et al., “Designing on-line Tunable Gain Fuzzy Sliding Mode Controller using Sliding Mode Fuzzy Algorithm: Applied to Internal Combustion Engine,” World Applied Sciences Journal, 14 (9): 1299-1305, 2011.

[10] Lotfi A. Zadeh” Toward a theory of fuzzy information granulation and its centrality in human easoning and fuzzy logic” Fuzzy Sets and Systems 90 (1997) 111-127

[11] Reznik L., Fuzzy Controllers, First edition: BH NewNes, 1997.

[12] Zhou, J., Coiffet, P,” Fuzzy Control of Robots,” Proceedings IEEE International Conference on Fuzzy Systems, pp: 1357 – 1364, 1992.

[13] Banerjee, S., Peng Yung Woo, “Fuzzy logic control of robot manipulator,” Proceedings Second IEEE Conference on Control Applications, pp: 87 – 88, 1993.

[14] Akbarzadeh-T A. R., K.Kumbla, E. Tunstel, M. Jamshidi. ,”Soft Computing for autonomous Robotic Systems,” IEEE International Conference on Systems, Man and Cybernatics, pp: 5252-5258, 2000.

[15] Lee C.C.,” Fuzzy logic in control systems: Fuzzy logic controller-Part 1,” IEEE International Conference on Systems, Man and Cybernetics, 20(2), P.P: 404-418, 1990.

[16] F. Piltan*, et al.*, "Artificial Control of Nonlinear Second Order Systems Based on AFGSMC," Australian Journal of Basic and Applied Sciences, 5(6*)*, pp. 509-522, 2011.

[17] Piltan, F., et al., “Design sliding mode controller for robot manipulator with artificial tunable gain,” Canadian Journal of pure and applied science, 5 (2): 1573-1579, 2011.

[18] Piltan, F., et al., “Design Artificial Nonlinear Robust Controller Based on CTLC and FSMC with Tunable Gain,” International Journal of Robotic and Automation, 2 (3): 205-220, 2011.

[19] Piltan, F., et al., “Design of FPGA based sliding mode controller for robot manipulator,” International Journal of Robotic and Automation, 2 (3): 183-204, 2011.

[20] Piltan Farzin, et al., “Design PID-Like Fuzzy Controller With Minimum Rule Base and Mathematical Proposed On-line Tunable Gain: Applied to Robot Manipulator,” International Journal of Artificial intelligence and expert system, 2 (4):184-195, 2011.

[21] Farzin Piltan, A. R. Salehi and Nasri B Sulaiman.," Design artificial robust control of second order system based on adaptive fuzzy gain scheduling," world applied science journal (WASJ), 13 (5): 1085-1092, 2011.

[22] Piltan, F., et al., "Design On-Line Tunable Gain Artificial Nonlinear Controller," Journal of Advances In Computer Research, 2 (4): 19-28, 2011.

[23] Piltan, F., et al., "Design Mathematical Tunable Gain PID-Like Sliding Mode Fuzzy Controller with Minimum Rule Base," International Journal of Robotic and Automation, 2 (3): 146-156, 2011.

[24] Piltan Farzin, et al., "Design of PC-based sliding mode controller and normalized sliding surface slope using PSO method for robot manipulator," International Journal of Robotics and Automation, 2 (4):245-260, 2011.

[25] Piltan, F., et al., "A Model Free Robust Sliding Surface Slope Adjustment in Sliding Mode Control for Robot Manipulator," World Applied Science Journal, 12 (12): 2330-2336, 2011.

[26] Piltan, F., et al., "Design Adaptive Fuzzy Robust Controllers for Robot Manipulator," World Applied Science Journal, 12 (12): 2317-2329, 2011.

[27] Piltan Farzin, et al., "Design Model Free Fuzzy Sliding Mode Control: Applied to Internal Combustion Engine," International Journal of Engineering, 5 (4):302-312, 2011.

[28] Piltan Farzin, et al., "Design of PC-based sliding mode controller and normalized sliding surface slope using PSO method for robot manipulator," International Journal of Robotics and Automation, 2 (4):245-260, 2011.

[29] Piltan, F., et al., "Design a New Sliding Mode Adaptive Hybrid Fuzzy Controller," Journal of Advanced Science & Engineering Research, 1 (1): 115-123, 2011.

[30] Piltan, F., et al., "Novel Sliding Mode Controller for robot manipulator using FPGA," Journal of Advanced Science & Engineering Research, 1 (1): 1-22, 2011.

[31] Piltan Farzin, et al., "Design of Model Free Adaptive Fuzzy Computed Torque Controller: Applied to Nonlinear Second Order System," International Journal of Robotics and Automation, 2 (4):232-244, 2011.

[32] Piltan Farzin, et al., "Control of IC Engine: Design a Novel MIMO Fuzzy Backstepping Adaptive Based Fuzzy Estimator Variable Structure Control ," International Journal of Robotics and Automation, 2 (5):357-370, 2011.

[33] Piltan, F., et al., "Adaptive MIMO Fuzzy Compensate Fuzzy Sliding Mode Algorithm: Applied to Second Order Nonlinear System," International Journal of Engineering, 5 (5): 249-263, 2011.

[34] Piltan, F., et al., "Novel Robot Manipulator Adaptive Artificial Control: Design a Novel SISO Adaptive Fuzzy Sliding Algorithm Inverse Dynamic Like Method," International Journal of Engineering, 5 (5): 264-279, 2011.

[35] Piltan Farzin, et al., "Position Control of Robot Manipulator: Design a Novel SISO Adaptive Sliding Mode Fuzzy PD Fuzzy Sliding Mode Control," International Journal of Artificial intelligence and Expert System, 2 (5):184-198, 2011.

[36] Piltan Farzin, et al., "Artificial Control of PUMA Robot Manipulator: A-Review of Fuzzy Inference Engine And Application to Classical Controller," International Journal of Robotics and Automation, 2 (5):387-403, 2011.

[37] Piltan, F., et al., “Design Adaptive Fuzzy Inference Sliding Mode Algorithm: Applied to Robot Arm,” International Journal of Robotics and Automation, 2 (5): 275-295, 2011.

[38] Piltan, F., et al., “Novel Artificial Control of Nonlinear Uncertain System: Design a Novel Modified PSO SISO Lyapunov Based Fuzzy Sliding Mode Algorithm,” International Journal of Robotics and Automation, 2 (5): 310-325, 2011.

[39] Piltan Farzin, et al., “Evolutionary Design of Mathematical tunable FPGA Based MIMO Fuzzy Estimator Sliding Mode Based Lyapunov Algorithm: Applied to Robot Manipulator,” International Journal of Robotics and Automation, 2 (5):340-356, 2011.

[40] Piltan Farzin, et al., “Evolutionary Design of Backstepping Artificial Sliding Mode Based Position Algorithm: Applied to Robot Manipulator,” International Journal of Engineering, 5 (5):239-248, 2011.

[41] Piltan, F., et al., “An Adaptive sliding surface slope adjustment in PD Sliding Mode Fuzzy Control for Robot Manipulator,” International Journal of Control and Automation, 4 (3): 65-76, 2011.

[42] Piltan, F., et al., “Design PID-Like Fuzzy Controller with Minimum Rule base and Mathematical proposed On-line Tunable Gain: applied to Robot manipulator,” International Journal of Artificial Intelligence and Expert System, 2 (5): 195-210, 2011.

[43] Piltan Farzin, et al., “Design and Implementation of Sliding Mode Algorithm: Applied to Robot Manipulator-A Review,” International Journal of Robotics and Automation, 2 (5):371-386, 2011.

[44] Piltan Farzin, et al., “Control of Robot Manipulator: Design a Novel Tuning MIMO Fuzzy Backstepping Adaptive Based Fuzzy Estimator Variable Structure Control,” International Journal of Control and Automation, 4 (4):25-36, 2011.

Heat Transfer in Porous Media With Slurry of Phase Change Materials

Manali Shukla *manali.shukla@utdallas.edu*
Graduate Student, Department of Mechanical Engineering, University of Texas at Dallas Richardson, 75080, USA

Fatemeh Hassanipour *fatemeh@utdallas.edu*
Assistant Professor, Department of Mechanical Engineering, University of Texas at Dallas Richardson, 75080, USA

Abstract

3-D laminar model of a rectangular porous channel with high thermal conductivity and constant wall heat flux is chosen to investigate the enhancement of heat transfer when used in conjunction with the phase change material slurry. Numerical simulations for various wall heat fluxes and inlet velocities are carried out. The slurry consists of microencapsulated octadecane (C18H38) and water. The heat transfer coefficient of the porous channel with pure water and with micro-encapsulated phase change material are calculated and compared. The effect of porosity and permeability of the porous medium on the heat transfer coefficient while using slurry of phase change material are studied. The results show that the heat transfer coefficient of the porous channel can improve by introducing phase change material slurry, but only under certain heat fluxes, inlet velocities, and porous media properties.

Keywords: Porous Media, Phase Change Material, Forced Convection Heat Transfer

1. INTRODUCTION

There is a growing need to develop systems with high rate of heat dissipation in many industrial products, including electronic cooling packages, air conditioning and refrigeration systems. Recently, particulate flow of phase-change materials has attracted attention for enhancing the heat transfer rate. Encapsulated phase-change materials are attractive due to their high energy storage density and small temperature variation during the heat transfer. There are various phase-change materials, e.g. paraffin, fibers, foams and composites which are developed to enhance thermal efficiency as coolants, when used in conjunction with other fluids [1–4].

Forced convective heat transfer enhancement with micro-encapsulated phase change material (MCPCM) slurries have been investigated experimentally and numerically [5–11]. These studies show that the heat transfer coefficients measured for MCPCM slurry are significantly higher than for those of single-phase fluid flow in laminar flow conditions. However, slurries of phase change materials carry two main disadvantages: their low thermal conductivity hinders heat transfer and the slurry form does not strongly take advantage of mixing effect. Therefore the use of PCM slurry is limited to high heat fluxes as the particles in the slurry melt away very quickly and the advantage of small temperature variation characteristic of phase change materials is lost.

Another approach for enhancing the heat transfer rate is using porous media. Porous media increase the rate of heat transfer by their high thermal conductivity and by agitating the flow which improves local convection. Both numerical and experimental results show that the convective heat transfer is considerably enhanced by inserting porous medium in the flow channel [12–15]. The presence of the porous matrix has significant effect on the heat transfer and melting rate of the phase change

FIGURE 1: Schematic of domain for numerical simulations.

2.1 Phase Change Material Slurry

A mixture of water and octadecane paraffin ($C_{18}H_{38}$) is used as the micro-encapsulated PCM slurry. The inlet fluid temperature T_{in} *is* 298*K* which is below the melting range of octadecane 298 – 308 *K*. Mass and energy balance equations [23] are used to calculate the density and specific heat of micro-encapsulated phase change material slurry.

$$\rho_b = \xi\rho_p + (1-\xi)\rho_f \tag{1}$$

$$c_b = \frac{\xi\rho_p c_p + (1-\xi)\rho_f c_f}{\rho_f} \tag{2}$$

Here, the properties for the shell are neglected since the encapsulation layer is assumed to be very thin and can be neglected in modeling. For calculating the suspension conductivity, Maxwell's [25] relation for the bulk thermal conductivity is used.

$$k_b = k_f \frac{2 + \frac{k_p}{k_f} + 2\xi\left(\frac{k_p}{k_f} - 1\right)}{2 + \frac{k_p}{k_f} - \xi\left(\frac{k_p}{k_f} - 1\right)} \tag{3}$$

Representative values of the slurry properties obtained using the above equations for 15% microencapsulated octadecane paraffin are shown in Table 1.

	T<298°K	298°K<T<308°K	T>308°K
ρ_p (kg/m3)	850	-7T-2936	780
C_p (kJ/kgK)	1800	40T-10120	2200
K_p(W/mK)	0.31	-0.017+5.376	0.14
H (kJ/kg)		270	

TABLE 1: Properties of Octadecane Paraffin $C_{18}H_{38}$

The heat transfer process inside the phased-change filled particles is modeled using the following enthalpy based energy balance equation:

$$\frac{\partial}{\partial t}\left(\rho_p H\right) + \nabla \cdot \left(\rho_p u H\right) = \nabla \cdot \left(k_p \nabla T\right) \tag{4}$$

where the enthalpy H of the material is computed as the sum of the sensible enthalpy, E , and the latent heat, ΔH , where

$$\Delta H = \alpha L \tag{5}$$

α is a parameter to track the phase-change process inside the particle is the liquid fraction defined as:

$$\begin{aligned} &\alpha = 0 && T < T_{sol} \\ &\alpha = 1 && T > T_{liq} \\ &\alpha = \frac{T - T_{sol}}{T_{sol} - T_{liq}} && T_{sol} \le T \le T_{liq} \end{aligned} \tag{6}$$

The solution for the heat transfer process inside the particles is obtained using the energy balance Eq. 4 and the liquid fraction Eq. 5.

2.2 Porous Media

Porous Media is modeled using the local volume average of the mass, momentum and energy equations for an incompressible fluid flow through an isotropic, rigid, homogeneous porous medium confined within an impermeable wall by Brinkman-extended Darcy model [22]. In this model the thermo physical properties of the fluid and porous medium are constant. The volume average process is done by relating every point in the porous medium as a tiny volume V surrounded by a closed surface area of A. V_f *is* the fraction of volume V containing the fluid (10). When flow through a porous medium is involved, these equations are valid inside the pores in which some form of the macroscopic balance equations based on the volumetric element are employed.

The governing continuity, momentum and energy equations (7), (8), (9) for present work are:

$$\nabla \cdot \langle u \rangle = 0 \tag{7}$$

$$0 = -\nabla\left(\phi \cdot \langle P \rangle\right) + \mu_{eff} \cdot \nabla^2 \langle u \rangle - \frac{\mu_b}{K}\phi\langle u \rangle - C\rho_b \phi^2 \langle u \rangle \langle u \rangle \tag{8}$$

$$\langle u \rangle \cdot \nabla \langle \rho_b c_b T \rangle = \frac{1}{\phi}\nabla \cdot \left(k_{eff} \cdot \nabla \langle T \rangle\right) \tag{9}$$

Where:

$$\langle P \rangle = \frac{1}{V}\int P.dV \tag{10}$$

$$\langle u \rangle = \frac{1}{V}\int u.dV \tag{11}$$

$$k_{eff} = \phi k_b + (1-\phi)k_s \tag{12}$$

$$\phi = \frac{A_f}{A_t} \tag{13}$$

A_f is the area occupied by the fluid and A is the total volume of the material. Parameters p, ρ, μ can be measured independently. However, μe, K and C depend on the geometry or the permeable medium and cannot be measured directly, nor calculated analytically, because there is no model relating them to more basic (measurable) quantities valid for all porous media. The Brinkman-Hazen-Dupuit-Darcy equation has an alternative form where C is replaced by C_f/K. The constant C_f *is* often takes the value 0.55 ($1/m$).

$$C = \frac{C_f}{\sqrt{K}} \tag{14}$$

In this study the value of C is calculated by considering $10^{-8}m^2 < K < 10^{-2}m^2$.

To determine the heat transfer rate, a local heat transfer coefficient h_{loc} is defined as,

$$h_{loc} = \frac{q''}{T_s - T_{in}} \tag{15}$$

where T_s is the temperature along the heated surface and can be obtained by solving the above energy equations using the finite volume method. Therefore, an averaged heat transfer coefficient along the heated surface, is defined as

$$h = \frac{1}{A}\int h_{loc} dA \tag{16}$$

The mathematical formulation for the convection heat transfer problem considered here is solved by the finite-volume method with successive over-relaxation. The solver method is segregated and second-order accurate in space and time. An unstructured grid technique was adopted for

accelerating the convergence. Grid and time-step accuracies are established by varying the grid size and the time-step utilized in the simulations, considering the most stringent configuration considered here, namely maximum heat flux of 30*kW/m*2 and inlet flow velocity 0.03*m/s*, see Figures 2 and 3. As shown the data appear to be almost equivalent for the grid size of 0.25*mm* and 0.5*mm* and also for 0.25*s* and 0.5*s*. Based on this successive refinement, the time interval Δt = 0.5*s* and grid size ΔG = 0.5*mm* were chosen for the solution.

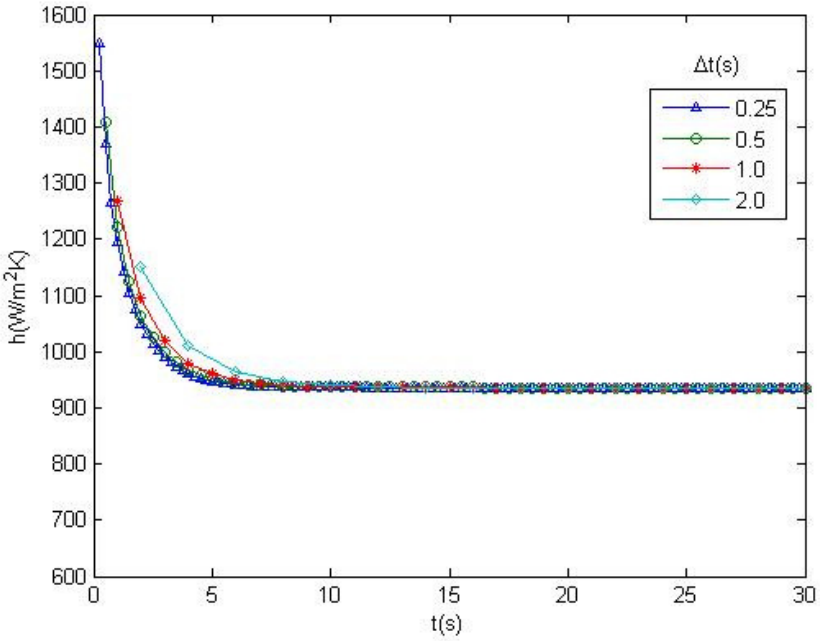

FIGURE 2: Representative of time interval size accuracy test.

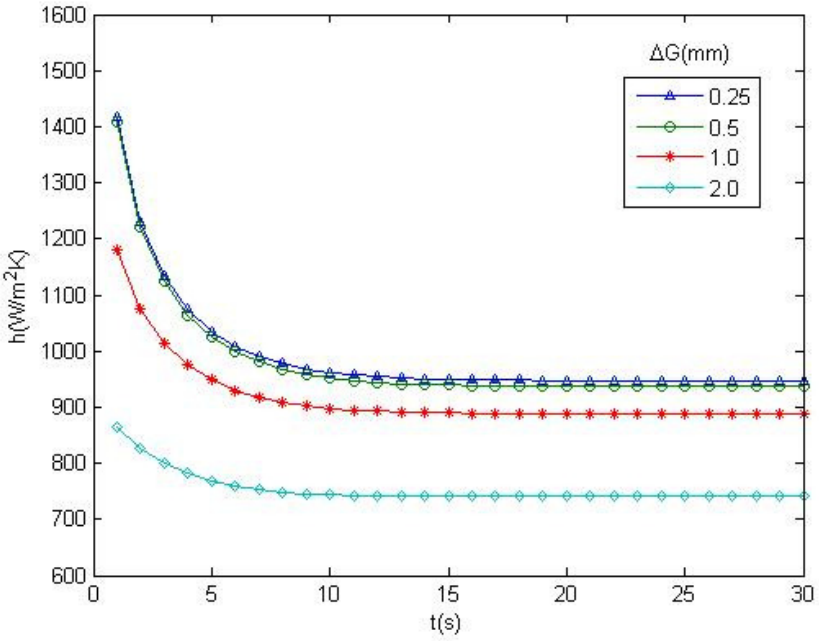

FIGURE 3: Representative of grid size accuracy test.

3. RESULTS

Heat transfer coefficients are compared for three cases: (1) pure water flow in a porous channel (h_p), (2) PCM slurry flow in non-porous channel (h_S), and finally (3) PCM slurry flow in a porous channel (h_{PS}). The values of heat transfer coefficients are obtained for three different heat fluxes of q'' = 10$kW/m2$, 30$kW/m2$ and 50$Kw/m2$ and three different velocities ranging from u = 0.01m/s to u = 0.05m/s.

Figure 4 shows that between cases (1) water in porous media and (2) PCM slurry in non-porous media, the higher heat transfer coefficient occurs when pure water flows through a porous channel. To illustrate how the addition of PCM particles affects the heat transfer rate, we define a new parameter known as Δh that shows the difference between both heat transfer coefficients in porous media, that is, case (1) water in porous media, and case (3) PCM slurry through porous media:

$$\Delta h = h_{ps} - h_p \tag{17}$$

The variation in Δh over time is depicted for different heat fluxes and flow velocity values in Figures 5, 6, 7. Non-linear behavior of the heat transfer coefficient for PCM slurry in the first 30 seconds is caused by the phase change process inside the particles. For the remaining graphs, the results are shown exclusively for just the phase change intervals.

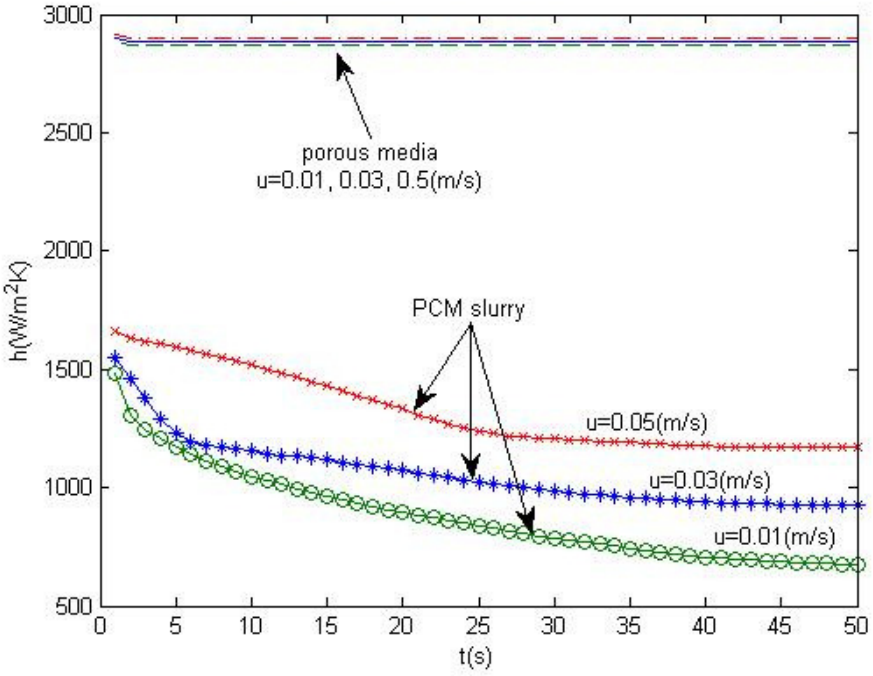

FIGURE 4: Heat transfer coefficient, water in porous media versus PCM slurry through porous media.

Figure 5 shows that for a low heat flux such as q'' = 10$kW/m2$, the heat transfer coefficient of phase change material slurry through porous channel is almost identical to that of pure water through porous channel because the slurry of phase change material has not fully melted. Effect of the velocity change for the same heat flux, is shown in Figure 5 and suggests no significant change in Δh even when the inlet flow velocity is increased. This result indicates the need of higher heat flux and inlet flow velocity to gain the advantage of slurry flow through porous media.

Figure 6 shows the variation of Δh over time for heat flux 30$kW/m2$ at various flow velocities. Here, the heat transfer is more affected by the PCM particles due to the advantage of the melting process and the latent heat release. The heat transfer coefficients are better at high velocities which increases

the mixing effect in porous media. When velocity increases, the effect of latent heat and mixing effect become comparable.

To further illustrate the effect of PCM slurry through porous media in higher heat fluxes, the results are plotted at 50*kW/m*2 at various velocities in Figure 7. The results show significant increase in Δh, suggesting complete melting of PCM slurry in porous media. When velocity is low, particles have more time to melt completely and give up all their latent heat. By increasing the velocity, both mixing affects and latent heat of solid particles cause the enhancement of heat transfer rate (Figure7).

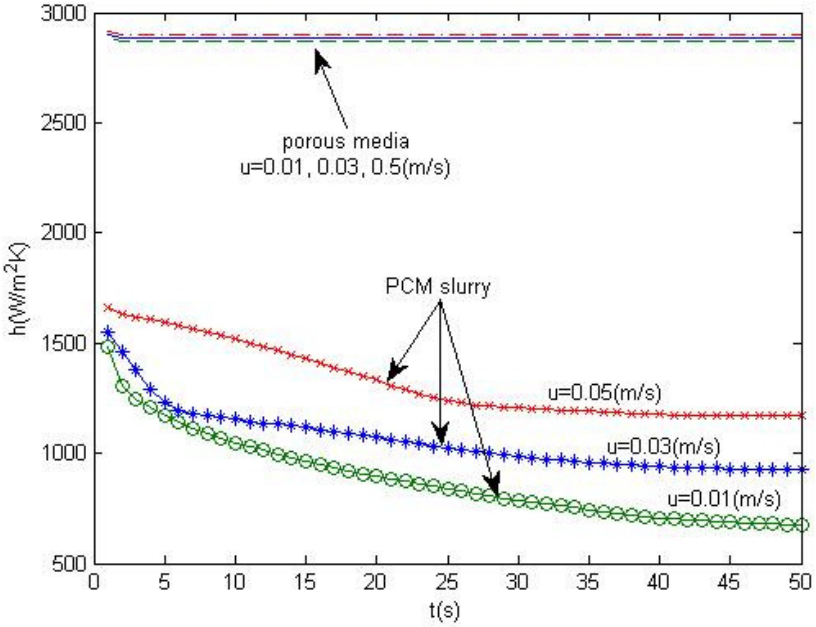

FIGURE 5: Effect of PCM addition to the flow in porous media on the heat transfer coefficient enhancement q"=10kW/m^2.

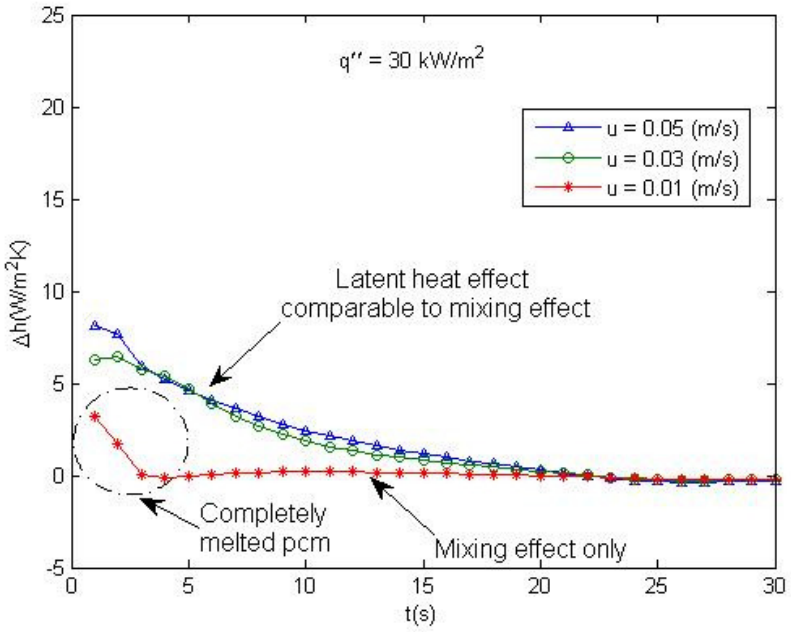

FIGURE 6: Effect of PCM addition to the flow in porous media on the heat transfer coefficient enhancement q"=30kW/m^2.

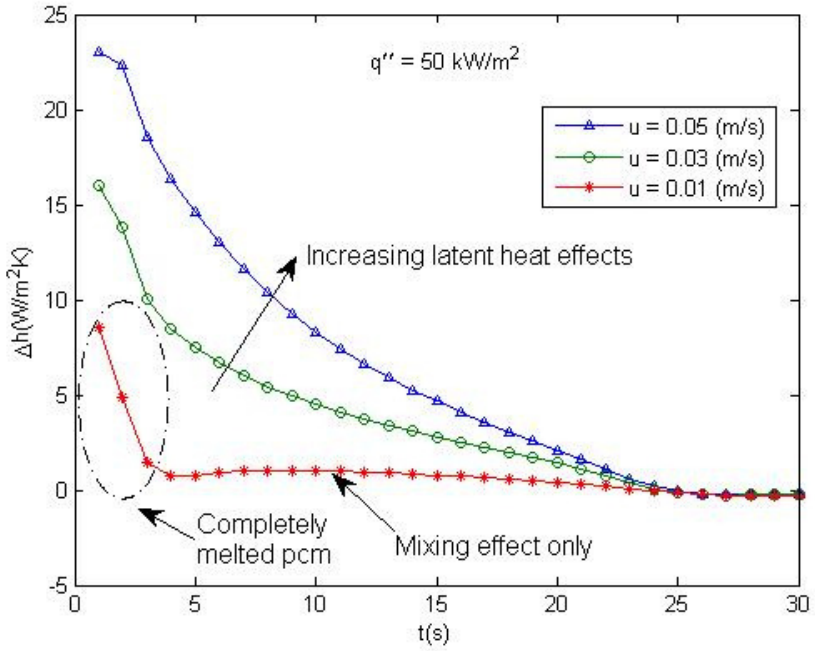

FIGURE 7: Effect of PCM addition to the flow in porous media on the heat transfer coefficient enhancement q"=50kW/m^2.

All the above results suggest that encapsulated phase-change material slurry flow through porous channel increases the heat transfer coefficient for specific ranges of heat flux and velocity.

The effect of porosity and permeability of the porous media on the heat transfer coefficient is also investigated. In this study, porosity is changed between 0.2 and 0.8 and the permeability from $10^{-2}m^2$ to $10^{-8}m^2$. Effect of porosity on the heat transfer coefficient can be seen in Figure 8. The results show that the heat transfer coefficient increases as the porosity decreases for the case of PCM slurry flowing through porous media. Although the coolant flow passes through the high pores channels more easily but the effect of high conductivity porous media structure is dominant in enhancing the heat transfer.

Figure 9 shows the heat transfer coefficient versus time for maximum and minimum porosity and permeability. The results indicate that porosity changes have the dominant effect on enhance- ment of heat transfer coefficient compared to the permeability. For the maximum porosity of 0.8, the initial values of heat transfer coefficients are higher for more permeable media. The reason is that for high porosity media, presence of more PCM slurry while flowing easily through porous media causes the heat transfer enhancement. After melting completion around 15 seconds, the heat transfer increases for lower permeability. The results for porosity of □ = 0.2 show very small changes in heat transfer coefficient, indicating less effect of PCM slurry at higher porosities, Figure 9.

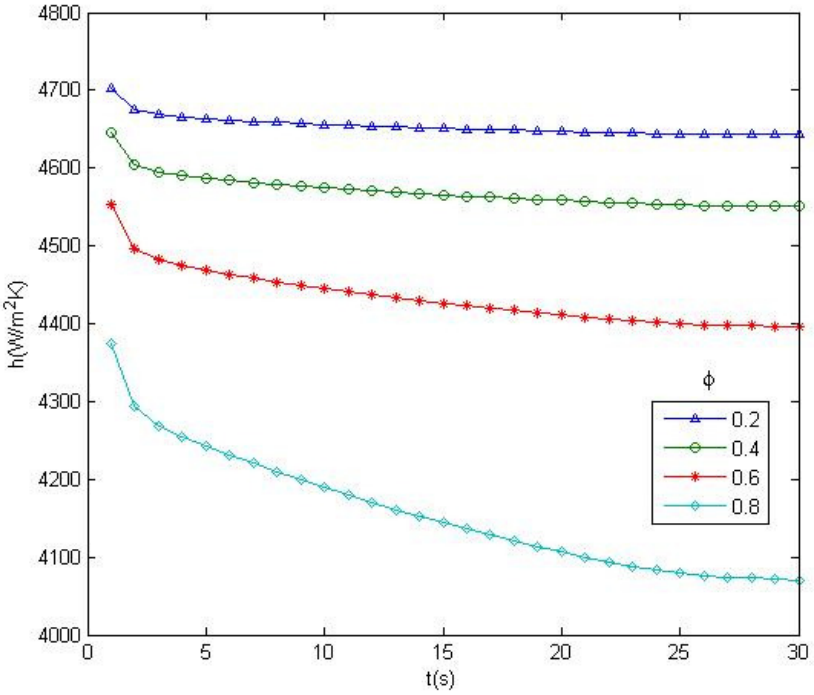

FIGUR 8: Effect of porosity on heat transfer coefficient at q"=50kW/m^2, u=0.05m/s and K=10^{-2}(m^2).

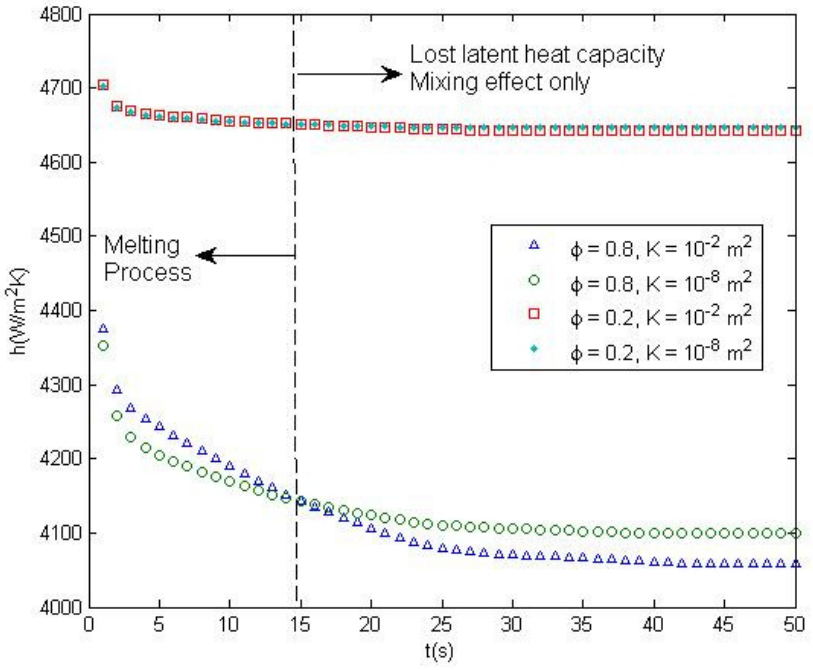

FIGURE 9: Effect of permeability on heat transfer coefficient at q"=50kW/m^2, u=0.05m/s and Φ=0.8.

4. CONCLUSION

A brief summary of the present study is given below. When using phase change material slurry carrier through porous media:

1. At low heat fluxes, mixing effect by porous media has dominant effect on heat transfer rate compared to the latent heat affects of phase change materials.
2. At high heat fluxes, addition of phase change material particles to the flow in porous media is more beneficial for enhancing heat transfer rate.
3. PCM slurry through porous media with low porosity has the maximum heat transfer coefficient.
4. For low porosity media, the effect of permeability is negligible in term of contribution to the heat transfer rate.
5. For high porosity media, permeability affect on the enhancement of heat transfer rate.
6. Before melting process, higher permeable media enhances heat transfer coefficient. However, after melting process, low permeability media have better heat transfer rate.

REFERENCES

[1] Huang, L., Petermann, M., and Doetsch, C., 2009. "Evaluation of paraffin/water emulsion as a phase change slurry for cooling applications". *Energy,* 34(9), Sept., pp. 1145–1155.

[2] Gschwander, S., Schossig,P., and Henning, H.-M., 2005. "Micro-encapsulated paraffin in phase-change slurries". *Solar Energy Materials and Solar Cells,* 89(2-3), Nov., pp. 307–315.

[3] Himran, S., Suwono, A., and Mansoori, G. A., 1994. "Characterization of alkanes and paraffin waxes for application as phase change energy storage medium". *Energy Sources, Part A: Recovery, Utilization, and Environmental Effects,* 16(1), pp. 117–128.

[4] Peng,S.,Fuchs,A.,andWirtz,R.A.,2004. "Polymeric phase change composites for thermal energy storage". *J. Appl. Polym. Sci.,* 93(3), pp. 1240–1251.

[5] Wang,X.,Niu,J.,Li,Y.,Wang,X.,Chen,B.,Zeng,R.,Song,Q.,andZhang,Y., 2007. "Flow and heat transfer behaviors of phase change material slurries in a horizontal circular tube". *International Journal of Heat and Mass Transfer,* 50(13-14), July, pp. 2480–2491.

[6] Zeng, R.,Wang, X., Chen, B., Zhang,Y., Niu, J.,Wang, X., and Di, H., 2009. "Heat transfer characteristics of microencapsulated phase change material slurry in laminar flow under constant heat flux". *Applied Energy,* 86(12), Dec., pp. 2661–2670.

[7] Hu, X., and Zhang, Y., 2002. "Novel insight and numerical analysis of convective heat transfer enhancement with microencapsulated phase change material slurries: laminar flow in a circular tube with constant heat flux". *International Journal of Heat and Mass Transfer,* 45(15), July, pp. 3163–3172.

[8] Charunyakorn,P., Sengupta, S., and Roy, S., 1991. "Forced convection heat transfer in microencapsulated phase change material slurries: flow in circular ducts". *International Journal of Heat and Mass Transfer,* 34(3), Mar., pp. 819–833.

[9] Roy, S., and Avanic, B., 1997. "Laminar forced convection heat transfer with phase change material emulsions". *International Communications in Heat and Mass Transfer,* 24(5), Sept., pp. 653–662.

[10] Ho, C., 2005. "A continuum model for transport phenomena in convective flow of solid-liquid phase change material suspensions". *Applied Mathematical Modeling,* 29(9), Sept., pp. 805–817.

[11] XinW., Y.Z., andH.,X., 2003."Turbulent heat transfer enhancement of micro-encapsulated phase change material slurries with constant wall heat flux". *Journal of Enhanced Heat Transfer,* 11(1), pp. 13–2.

[12] Huang, Z., Nakayama, A., Yang, K., Yang, C., and Liu,W., 2010. “Enhancing heat transfer in the core flow by using porous medium insertina tube”. *International Journal of Heat and Mass Transfer,* 53(5-6), Feb., pp. 1164–1174.

[13] Szen, M., and Kuzay, T. M., 1996. “Enhanced heat transfer in round tubes with porous inserts”. *International Journal of Heat and Fluid Flow,* 17(2), Apr., pp. 124–129.

[14] Sung, H. J., Kim, S.Y., and Hyun, J. M., 1995. “Forced convection from an isolated heat source in a channel with porous medium”. *International Journal of Heat and Fluid Flow,* 16(6), Dec., pp. 527–535.

[15] Jiang,P.-X.,andRen,Z.-P.,2001. “Numerical investigation of forced convection heat transfer in porous media using a thermal non-equilibrium model”. *International Journal of Heat and Fluid Flow,* 22(1), Feb., pp. 102–110.

[16] Mesalhy, O., Lafdi, K., Elgafy, A., and Bowman, K., 2005. “Numerical study for enhancing the thermal conductivity of phase change material (pcm) storage using high thermal conductivity porous matrix”. *Energy Conversion and Management,* 46(6), Apr., pp. 847–867.

[17] Liu,W., Shen, S., and Riffat, S. B., 2002. “Heat transfer and phase change of liquid in an inclined enclosure packed with unsaturated porous media”. *International Journal of Heat and Mass Transfer,* 45(26), Dec., pp. 5209–5219.

[18] Rubin, A., and Schweitzer, S., 1972. “Heat transfer in porous media with phase change”. *International Journal of Heat and Mass Transfer,* 15(1), Jan., pp. 43–60.

[19] Beckermann, C., and Viskanta, R., 1988. “Natural convection solid/liquid phase change in porous media”. *International Journal of Heat and Mass Transfer,* 31(1), Jan., pp. 35–46.

[20] Goel M, Roy SK, S. S., 1994. “Laminar forced convection heat transfer in microencapsulated phase change material suspensions”. *International Journal Heat Mass Transfer,* 37(4), pp. 593–604.

[21] Maxell, J., 1954. *A treatise on electricity and magnetism*. NewYork: Dover.

[22] Nield, D., Junqueria, S., and Lage, J., 1996. “Forced convection in a fluid saturated porous medium channel with isothermal or isoflux boundaries”. *Journal of Fluid Mechanics,* 322, pp. 201–214.

A Study to Predict the Effects of Tyres Vibration to Sound Quality in Passenger Car Cabin

Ahmad Kadri Junoh *kadri@unimap.edu.my*
Industrial Mathematics Research Group (IMRG),
Institute of Engineering Mathematics,
Universiti Malaysia Perlis,
02000, Kuala Perlis, Perlis, Malaysia

Zulkifli Mohd Nopiah *zmn1993@gmail.com*
Department of Mechanical and Materials Engineering,
Universiti Kebangsaan Malaysia,
43600, Bangi, Selangor, Malaysia

Abdull Halim Abdul *abdhalim@unimap.edu.my*
Industrial Mathematics Research Group (IMRG),
Institute of Engineering Mathematics,
Universiti Malaysia Perlis,
02000, Kuala Perlis, Perlis, Malaysia

Mohd. Jailani Mohd Nor *jai@mohe.gov.my*
Department of Mechanical and Materials Engineering,
Universiti Kebangsaan Malaysia,
43600, Bangi, Selangor, Malaysia

Ahmad Kamal Ariffin Mohd. Ihsan *kamal@eng.ukm.my*
Department of Mechanical and Materials Engineering,
Universiti Kebangsaan Malaysia,
43600, Bangi, Selangor, Malaysia

Mohammad Hosseini Fouladi *mfoolady@gmail.com*
Taylor's University College,
47500, Subang Jaya, Selangor, Malaysia

Abstract

Vehicle acoustical comfort and vibration in passenger car cabin are the factors which attract the buyers to a vehicle in order to have a comfortable driving environment. The amount of discomfort depends on the magnitude, frequency, direction and also the duration of exposed vibration in the cabin. Generally the vibration is caused by two main sources, which are engine transmission and interaction between tyres and the road surface. The comfort of the driving will affect the drivers by influencing their performance by bothering vision, and at the same time giving stress to the driver due to generated noise. In this study an approach has been carried out to find the amount of noise which influenced by the vibration due to interaction between tyres and road surface. The sound quality study has focused on the estimation of the noise changes through the generated sound quality depending on engine speeds. From the results, the amount of sound quality followed the increase and decrease of the engine speeds. Through the study, a technical method is provided to show the correlation between generated noise sound quality and the exposed vibration caused by the interaction between tyres and road surface.

Keywords: Vibration, Sound Quality, Vibration Dos Value

1. INTRODUCTION

Generally noise which is generated by the vehicle system vibration will affect driver's emotions and decrease the level of driving focus. Vibration exposure may cause relative movement between the viewed object and the retina, resulting in a blurred image. This will decrease the visual performance and at the same time affect the driving comfort and will alter the driving focus, which could potentially cause an accident. This noise may also be described as a source of annoyance for humans where unwanted noise may interfere with speech communication between passengers, affect driving concentration and also can cause sleep disturbance during the night. In this study both the noise (sound quality) and vibration trends against engine speeds will be compared in order to determine the correlation between exposed vibration and produced noise level in passenger car cabin.

1.1 Evaluation of Vibration

Basically, vibration or noise is directly related to engine speed due to changes in direct proportion to engine rpm [1-6]. A vibration that comes from engine surface will generate noise where the sources of the vibration are combustion vibration and mechanical vibration. Based on previous research, generally the main sources of vehicle interior vibrations in vehicle systems can be influenced by two sources: engine transmission during acceleration or deceleration of the car and tyre interaction with the road surface.

At certain speeds, the vibration is mainly caused by the interaction between rolling tyres and road surface [7,8]. The generated vibration is not only caused by the rolling tyres, but also radiated by structure-borne vibration which spread to the rim and other parts of the vehicle body.

The vibration is dependent on the roughness of the road surface where the tyres are rolling on, with the rougher the surface of the road causing more vibration to be generated. Here, the vibration sources that act at the tyres caused by the up–and-down of the road surface. In this case, Kindt et al [9] has conducted study to do measurement and do analysis to the vibration of rolling tyres. Their findings show that for the velocity more than 40 km/h the main source of the noise to passenger cars is the interaction between tyre and road surface. The results also show the important fact about the tyre resonance frequencies at the onset of rolling. Here, the excitation amplitude dependency showed to be restricted to the tyre sidewall stiffness. Basically the stiffness vibration is determined by mass, stiffness and dumping forces which are contained in their component parts. Meanwhile the vibration source to the vehicle body due to change of the engine speeds. The generated vibration depends on vehicle speed and may be felt in the steering wheel, seats or floor board.

In this study, BS6841 (British Standards Institution 1997) refers to the use of the vibration magnitude evaluation method using r.m.s acceleration *a(t)* . The reason why BS6841 is used is the standard is simple, less ambiguous, internally consistent and quite familiar with assessment of whole body vibration. Due to car motion by shocks or impulsive velocity changes, the use of the time integrated fourth power of an acceleration, known as vibration dose value (*VDV*) is considered more suitable for vibration assessment. Here, the value of *VDV* shows the total amount vibration received by the human over a period of time. Generally, *VDV* ($ms^{-1.75}$) is the measure of total exposure to vibration which considers the magnitude, frequency and exposure duration and can be defined as

$$VDV = \left(\int_0^T a(t)^4 dt \right)^{1/4} \quad (1)$$

Where VDV : Vibration dose value ($ms^{-1.75}$)

$a(t)$: Frequency- weighted acceleration

T : Total period in seconds that the vibration occurred

1.2 Evaluation of Noise

A lot of researches have been done by automotive researchers to determine and predict the generated noise and exposed vibration in internal vehicle at moving conditions [10, 11]. Generally, noise transmission into vehicle can be divided to sources: airborne noise and vehicle structure borne. For the vehicle manufacturing company, they may take the results into account to optimize or improve the structure of the parts which are believed may reduce the generated vibration and at the same time may decrease the noise in passenger car cabin [12-15]. D.J. O'Boy et al (2008) in their study have investigated the effect of vibration of tyre belt (tread rubber) to the interior noise in passenger car cabin. The results show that the characteristics of the tread rubber will produce different level of sound.

By using a Proton Perdana V6 as a tested vehicle, the generated sound quality is measured at two conditions which are stationary and moving condition, where the types of road are highway and pavement road (Table 1, Figure 1). In order to evaluate the noise level, sound quality metrics are measured depending on engine speeds (rpm). The parameters of sound quality which considered are four types which are Zwicker loudness [sone], sharpness [acum], roughness [asper] and fluctuation strength [vacil]. The measurement results will be summarized and correlation between generated sound quality parameters and engine speeds will be obtained in order to look the trends of noise over the generated vibration in passenger car cabin. Then, formulas will be formed to let the future automotive researchers be able to predict the effects of the vibration due to the noise which caused by interaction between tyres and road surface.

Road Type	Location	Characteristic
Highway	Kajang – Bangi Highway	Two lanes each side highway with smooth road surface
Pavement	Putrajaya	Broad pavement road surface

TABLE 1: Locations of Tested Road

FIGURE 1: Two different roughness of road surface (a) Highway and (b) Pavement road

2. METHODOLOGY

The sound quality measured at two condition which are stationary condition and moving condition.

Measured sound quality will be analyzed to obtain sound quality parameters which are loudness, sharpness, roughness and fluctuation strength [17]. Sound quality is measured by the binaural Head and Torso (HAT) equipment based on its frequencies and amplitudes.

Vibration is normally evaluated by measuring the level of vibration at certain parts that are identified as dominant source of vibration for the driver in the car interior. Here, the car floor next to the drive side was chosen as the location for vibration measurement.

The noise and vibration are measured by depending on engine speeds [rpm]. The reasons why this study choose to measure the noise and vibration by depending on engine speeds is, vehicle speed measurement (velocity [km/h]) only can be done while the car is moving and not at the stationary condition. However, in this case, the study assumes that:-

i. both of the noise that produced due to the engine transmission during at stationary and moving condition are equal.
ii. the noise that produced due to interaction between tyre and road surface at stationary condition is '0'.

Thus, the reason why both of the condition (stationary and moving) dependent to engine speeds is the engine transmission noise are considered only will give minor effect to the measurements of noise and the major contributor of the noise is assumed came from the effect of vibration caused by the interaction between tyres and road surface.

2.1 Test Method

In this test, a Proton Perdana V6 Automatic car was used as the vehicle in measurements of sound quality. The sound quality will be conducted using Bruel & Kjaer portable and multi-channel PULSE type 3560D. B&K Head & Torso (HAT) type 4100 (Figure 2) was placed at the front seat next to the driver side area. Measured noise from only the right channel is recorded due to HAT being a binaural device (choose either right or left channel to standardize the measurement). In this study four metrics are analyzed and considered to find the correlation between the sound quality and engine speeds. They are Zwicker loudness (*L*), sharpness(*S*), roughness (*R*) and fluctuation strength (*F*) (Table 2). B&K type 7698 sound quality software is used to analyze and find the metrics for sound quality.

FIGURE 2: The B&K head and torso used to measure the sound quality during the test

Metric	Right	Left	Unit
Inst . Loudness	10.5	10.4	sone
Sharpness (Mean)	1.21	1.17	acum (Z)
Roughness	1.89	1.46	asper
Fluctuation Strength	1.03	1.21	Vacil

TABLE 2: Example of Measured Sound Quality

The vibration level measured only at moving condition since we assuming that no vibration occur due to the interaction between tyre and the road surface. Vibration detector was B&K isotron accelerometer model 751-100 installed at the front floor next to the driver side (Figure 3). The measurement software is B&K Pulse Labshop. By using formula (1), vibration dose value was obtained in order to evaluate the level of exposed vibration at the car floor.

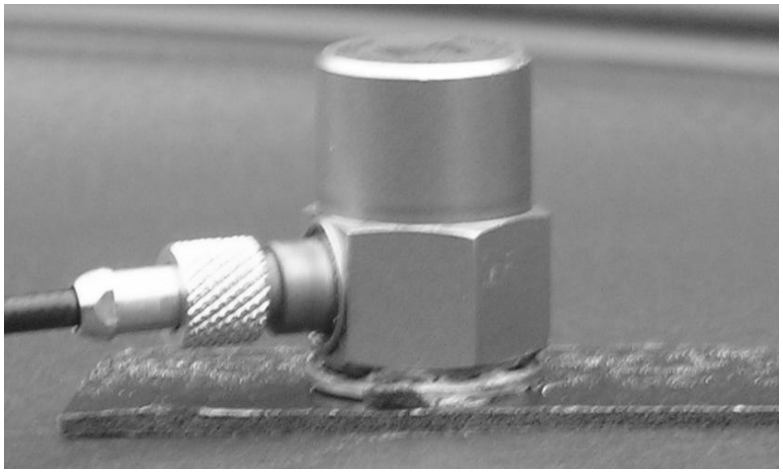

FIGURE 3. B&K Accelerometermodel 751-100 and installed location

The sound quality measurement will be carried out at two conditions, stationary and moving condition. At stationary condition, sound quality is measured five times depending on the engine speeds. That engine speeds are 1500rpm, 2000 rpm, 2500 rpm, 3000 rpm and 3500 rpm. Since the type of road influences the generated noise in passenger car cabin at moving condition, the sound quality was measured on two types of road which are highway road and pavement road. Since different tyre surface pattern (tread) will produce different level of noise, Figure 4 and Table 3 shows the tyre tread pattern and specification of the tested tyres on the Perdana V6.

The duration for each measurement is 10 seconds, with the test being conducted by two members, including the driver. The driver's task is to drive the car while maintaining specific engine speeds (rpm) according to the testing plan. One test assistant is compulsory to handle the laptop computer and at the same time record the sound quality of noise and vibration measurements. For highway road the measurements are taken for 4 times only due to velocity constraints. However, for pavement road and at stationary condition, the sound quality and vibration measurement will be taken for 5 times depending on the engine speeds. That engine speeds are shown in Table 4. To get reliable data, the measurement for each engine speed is repeated for 4 times. The details about

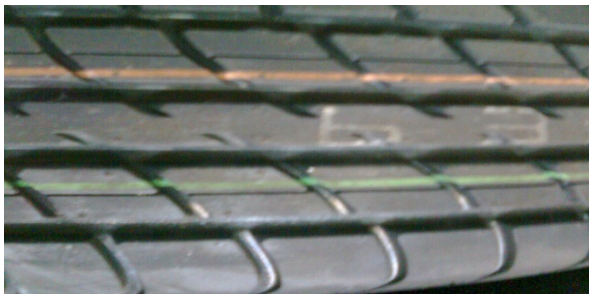

FIGURE 4: Two different tyre surface patterns (treads)(a) Tyre A and (b) Tyre B

Specification	Front portion	Back portion
Type	A	B
Model	P205/55R	P205/55R
Nominal section width	205 [mm]	205 [mm]
Aspect ratio	55%	55%
Radius	16 " (inch)	16 " (inch)
Load index	91V (615kg)	89V (580kg)

TABLE 3 : Specifications of tested tyres

the research procedure can be referred in Figure 5.

Stationary	Moving	
	Highway	Pavement
1500	1600 rpm	1200 rpm
2000	1900 rpm	1500 rpm
2500	2500 rpm	1600 rpm
3000	2800 rpm	1800 rpm
3500	-	1900 rpm

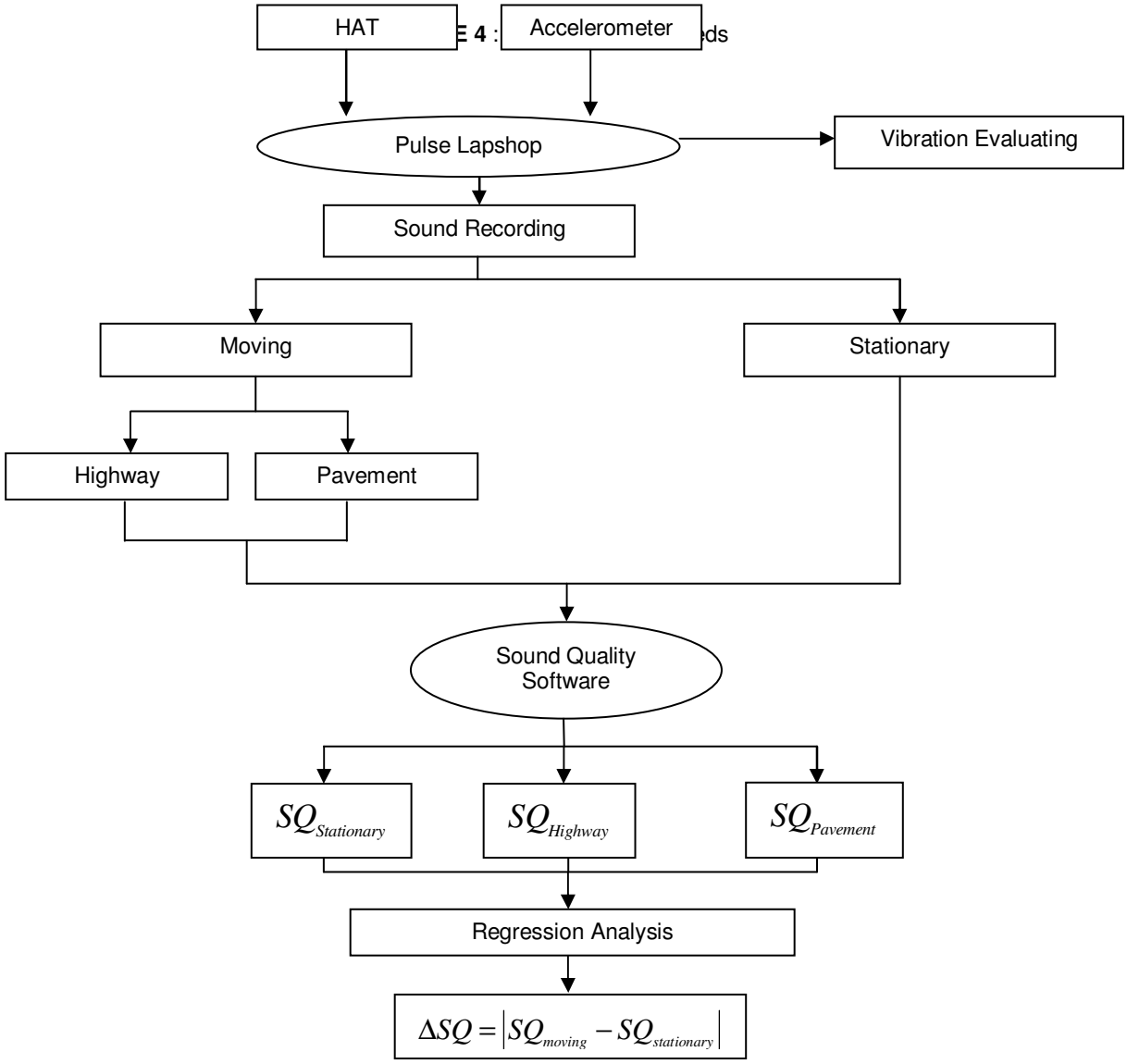

FIGURE 5: Research procedures process flow

3. RESULTS AND DISCUSSION

Figure 6 and Table 5 illustrates the results for measurement of the sound quality metrics for Zwicker loudness, sharpness, roughness and fluctuation strength. For both of the highway and pavement road, the parameter of loudness increase with the increase of engine speed. Meanwhile, for sharpness metrics, the values decrease with the increase of engine speeds. However there is no particular trend for fluctuation strength metric values with the increase of engine speeds.Table 6 shows the vibration level in VDV unit that exposed at the car floor depending on engine speeds and to show the correlation ship between the vibration level and generated noise, Table 7 is formed to illustrate the measured sound quality depending on the vibration level exposed at the car floor. Figure 7-9 are plotted look the changes trend of sound quality corresponding to engine speeds for both condition either stationary or moving condition,

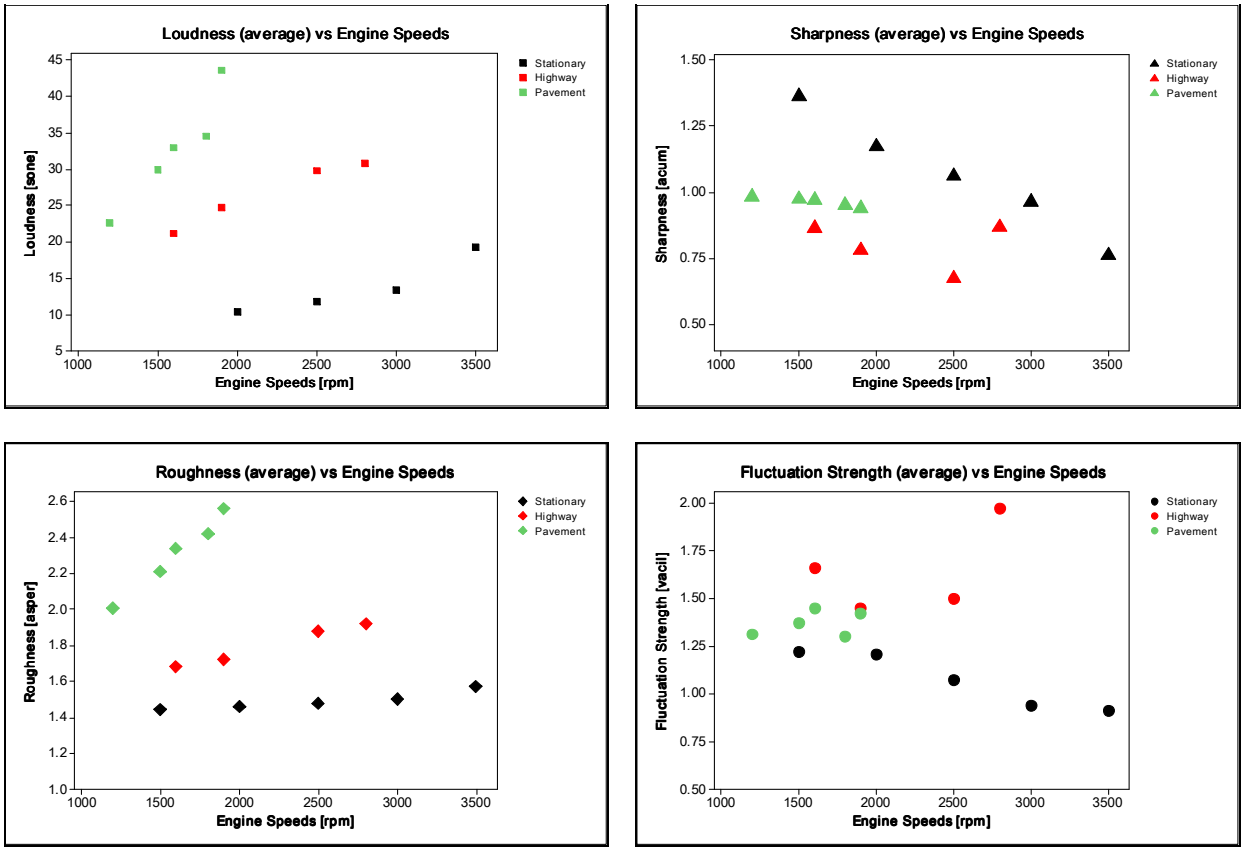

FIGURE 6 : Measured sound quality (average)

Engine Speed (rpm)	Stationary				Moving								
					Highway				Pavement Road				
			R	*F*			*R*				*R*		
2000									2.6	0.9811	2.01	.31	
2500	.8	1.3622	.44	.22					9.9	0.9773	2.21	.37	
3000					**1.1**	**0.8661**	**1.68**	**.66**	3.0	0.9699	2.34	.45	
3500									4.5	0.9488	2.42	.30	
4000					**4.8**	**0.7811**	**1.72**	**.45**	3.6	0.9377	2.56	.42	
4500	0.4	1.1773	1.46	.21						-	-		
5000	1.8	1.1061	1.48	.07	**9.8**	**0.6744**	**1.88**	**.50**		-	-		
5300			-		**0.8**	**0.8667**	**1.92**	**.97**		-	-		
6000	3.4	0.9	1.50	.94						-	-		

500		64					
	9.3	0.7626	1.57	.91		-	-

L: Loudness[Sone] , S: Sharpness [Acum] , Roughness [Asper] and F: Fluctuation Strength [Vacil]

TABLE 5: The values of sound quality metrics (average)

Condition	Engine Speed [rpm]	Read 1	Read 2	Read 3	Read 4	Average [ms$^{-1.75}$]
Stationary	1600	0.0	0	0.0	0.0	0.01
	2000	0.0	0	0.0	0.0	0.02
	2500	0.0	0	0.0	0.0	0.03
	3000	0.0	0	0.0	0.0	0.02
	3500	0.0	0	0.0	0.0	0.02
Highway	**1600**	**0.0**	**0**	**0.0**	**0.0**	**0.36**
	1900	**0.0**	**0**	**0.0**	**0.0**	**0.41**
	2500	**0.5**	**0**	**0.5**	**0.0**	**0.44**
	2800	**0.5**	**0**	**0.5**	**0.0**	**0.43**
Pavement	1200	0.6	0	0.7	0.6	0.69
	1500	0.8	0	0.8	0.8	0.83
	1600	0.7	0	0.8	0.7	0.90
	1800	1.0	1	1.0	0.0	0.91
	1900	1.0	1	1.0	1.4	1.16

TABLE 6: The average values of vibration dos value [ms$^{-1.75}$] versus engine speed

Condition	VDV [ms$^{-1.75}$]	Average Loudness	Sharpness	Roughness	Fluct. Str.
Stationary	0.011	4.8	1.362	1.44	1.22
	0.024	10.4	1.173	1.46	1.21
	0.034	11.8	1.061	1.48	1.07
	0.022	13.4	0.964	1.50	0.94
	0.078	19.3	0.762	1.57	0.91
Highway	**0.3657**	**21.1**	**0.861**	**1.68**	**1.66**
	0.4115	**24.8**	**0.781**	**1.72**	**1.45**
	0.4400	**29.8**	**0.674**	**1.88**	**1.50**
	0.4267	**30.8**	**0.867**	**1.92**	**1.97**
Pavement	0.6006	22.6	0.981	2.01	1.31
	0.8277	29.8	0.973	2.21	1.37

0.9	33.0	0.969	2.34	1.45
0.9	34.5	0.948	2.42	1.30
1.1	43.6	0.937	2.56	1.42

Loudness[Sone] , S: Sharpness [Acum] , Roughness [Asper] and F: Fluctuation Strength

TABLE 7: The average values of vibration dos value versus engine speed

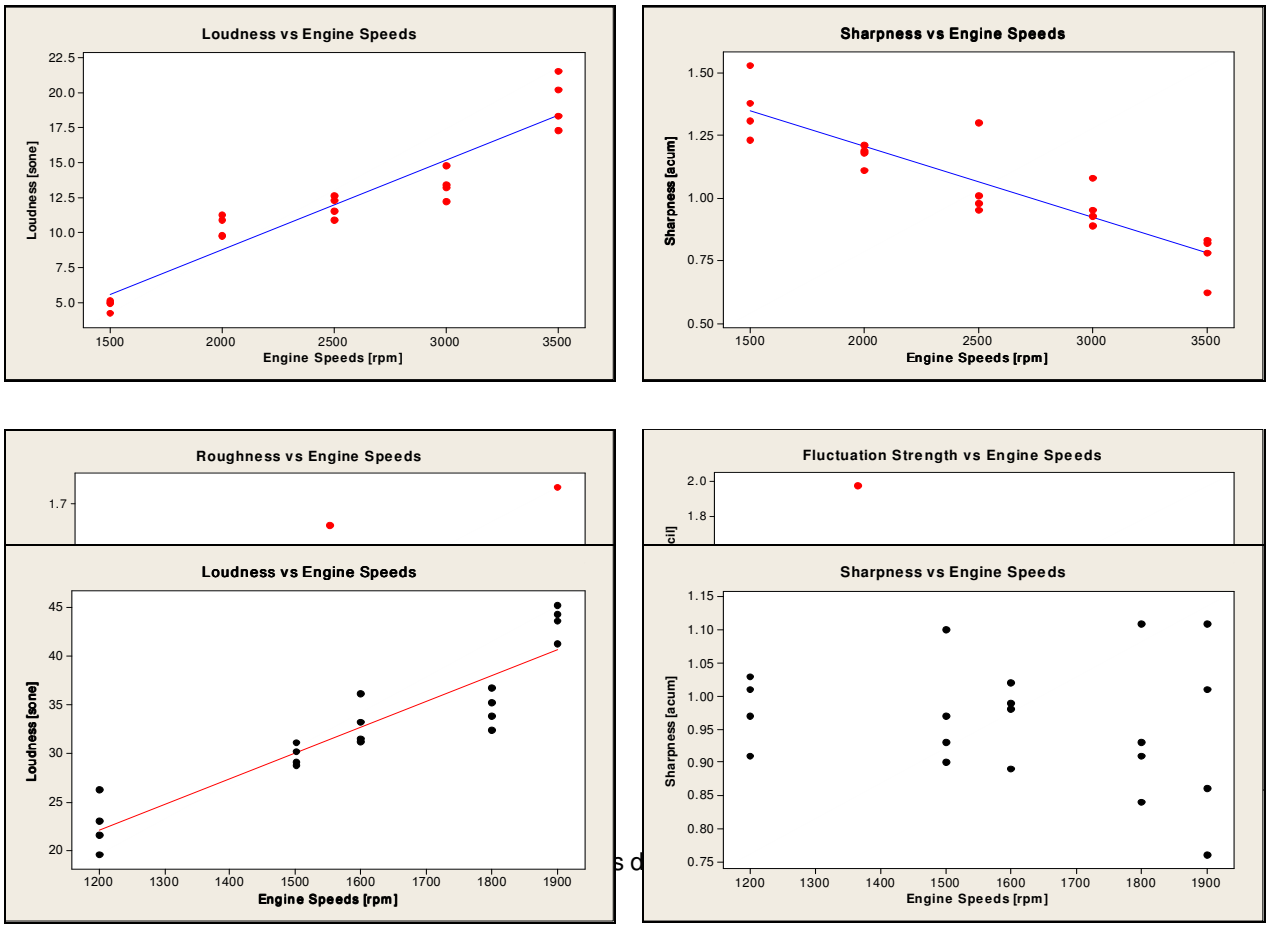

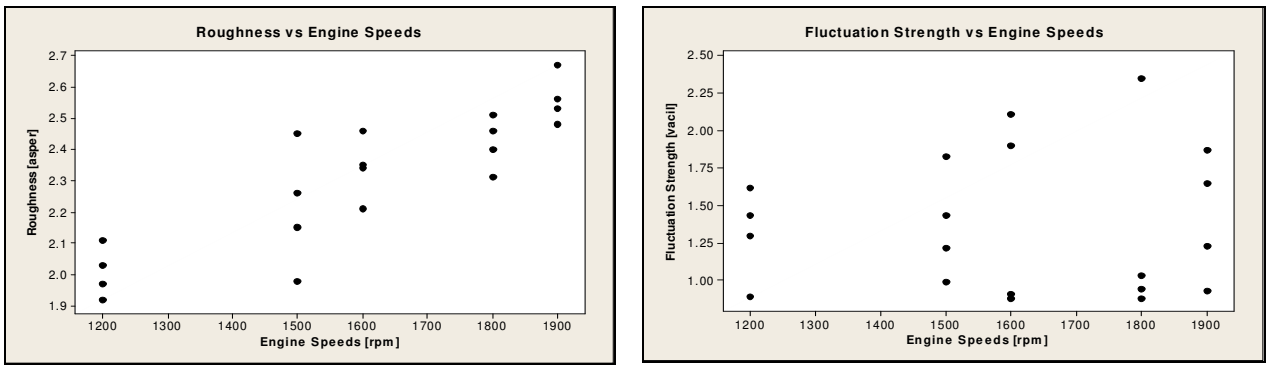

FIGURE 9 : Sound quality trends at moving condition on the pavement road

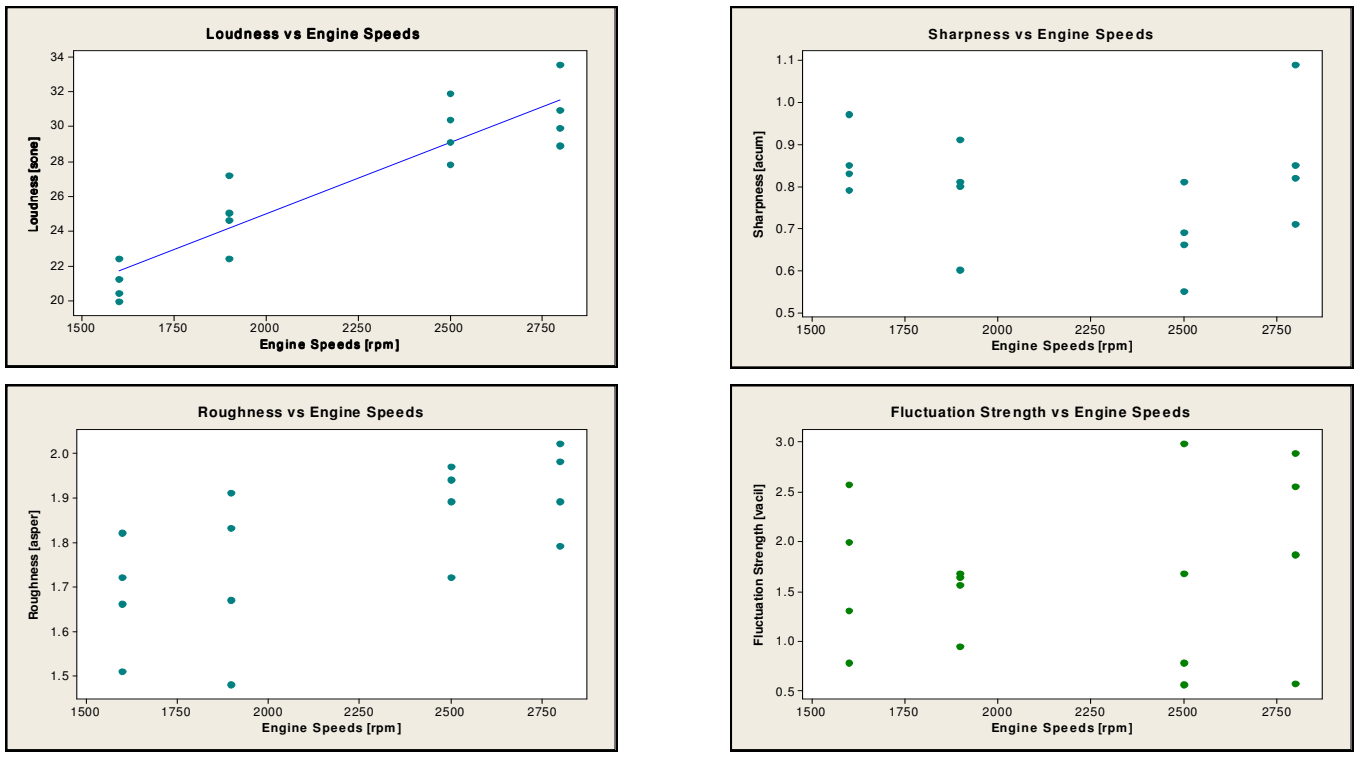

FIGURE 8 : Sound quality trends during moving condition on the highway road

Each parameter must fulfill 2 criteria below in order to be chose which metric of sound quality is significant and truly corresponds with the engine speeds

(i) Regression value R^2 for correlation between each sound quality parameter and engine speeds
must be greater than 50%

(ii) p-value must be smaller than 0.05

After regression analysis is performed, each sound quality trend is observed and we only chose which sound quality that fulfilled above criteria for both condition stationary and moving condition. In this case we successfully found that only loudness parameter is significant and linearly corresponds with engine speeds for both of condition. The regression equations are obtained in order to predict the generated sound quality depending on engine speeds in the future (Table 8). The obtained equations for loudness parameters are shown below.

Stationary	**Highway**	**Pavement**
$L = 0.00641 \times V_{engine} - 4.07$	$L = 0.00821 \times V_{engine} + 8.54$	$L = 0.0265 \times V_{engine} - 9.77$

Condition	**Metrics**	**Regression (R^2)**	**Multiple R**	**p-value**
Stationary	Loudness	0.897	0.947	0.00678
	Sharpness	0.803	0.896	5.5E-14
	Roughness	0.178	0.422	1.6E-12
	Fluctuation Strength	0.423	0.179	4.4E-06
Highway	***Loudness***	***0.846***	***0.920***	***0.00117***
	Sharpness	***0.011***	***0.106***	***0.00013***
	Roughness	***0.647***	***0.418***	***4.8E-07***
	Fluctuation Strength	***0.018***	***0.136***	***0.25484***
Pavement	Loudness	0.854	0.924	5.7E-05
	Sharpness	0.032	0.178	3.6E-07
	Roughness	0.755	0.869	3.3E-06
	Fluctuation Strength	0.002	0.046	0.093

TABLE 8 : Results of Regression Analysis

By assuming more vibration will produce more noise, thus we look the changes trend of the loudness parameter with the increase of vibration level. The objective is to verify that the loudness parameter is exactly parameter that we supposed to consider. Figure 10 is plotted to recognize the trend pattern of the loudness parameters corresponding with the exposed vibration dose value at the car floor. The regression analysis result shows that loudness parameter linearly corresponds with the increase value of vibration dose value where regression (R^2) is 84.7% and adjusted R is 84.4% (Figure 11).

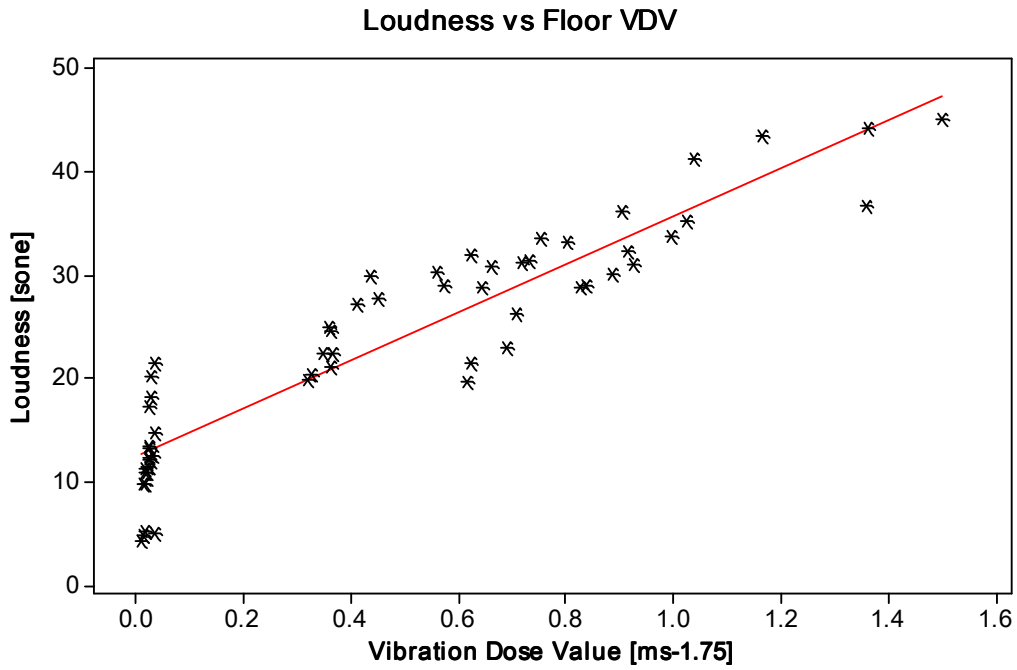

FIGURE 10 : Changes trend of loudness parameter with increase of vibration dose value

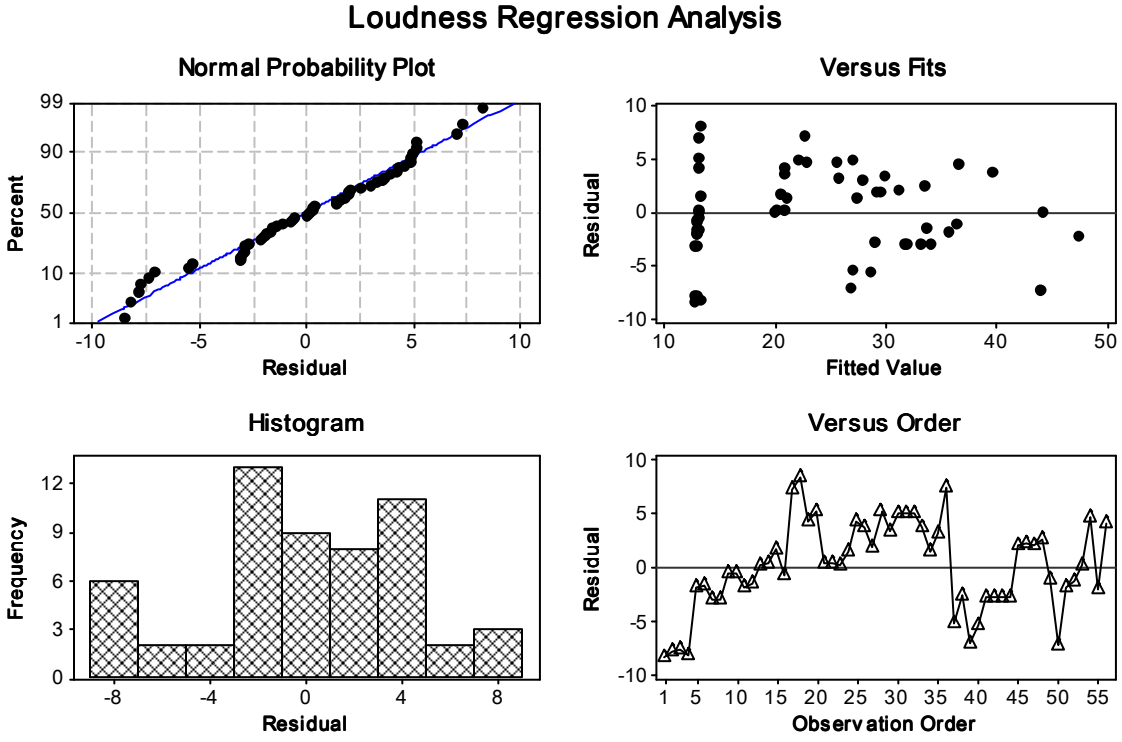

FIGURE 11 : Regreesion analysis for loudness vs vibration dose value

Table 9 shows the noise which is considered the noise contributed by interaction between tyres and road surfaces. From Table 9, there are two sources of noise that can be separated by dividing the values of annoyance levels to SQ and ΔSQ. In this case we assume that ΔSQ is the annoyance of noise produced by tyres, With this technical method, we belive that to reduce the noise in passenger car cabin, we can cluster the source of the noise into two types. These two noises are the noise produced by the engine and the noise produced by the vibration due to interaction between tyres and road surface. By using this technical method, automotive researchers able to predict the noise produced by the tyres (ΔSQ) by using the proposed equation (9).

$$\Delta SQ = \left| SQ_{moving} - SQ_{stationary} \right| \tag{2}$$

Engine Speeds [rpm]	Stationary	Highway		Pavement	
	L	***L***	ΔL	***L***	ΔL
1200	3.62	18.39	**14.77**	22.03	**18.41**
1300	4.26	19.21	**14.95**	24.68	**20.42**
1400	4.90	20.03	**15.13**	27.33	**22.43**
1500	5.55	20.86	**15.31**	29.98	**24.44**
1600	6.19	21.68	**15.49**	32.63	**26.44**
1700	6.83	22.50	**15.67**	35.28	**28.45**
1800	7.47	23.32	**15.85**	37.93	**30.46**
1900	8.11	24.14	**16.03**	40.58	**32.47**
2000	8.75	24.96	**16.21**	43.23	**34.48**
2100	9.39	25.78	**16.39**	45.88	**36.49**
2200	10.03	26.60	**16.57**	48.53	**38.50**
2300	10.67	27.42	**16.75**	51.18	**40.51**
2400	11.31	28.24	**16.93**	53.83	**42.52**
2500	11.96	29.07	**17.11**	56.48	**44.53**
2600	12.60	29.89	**17.29**	59.13	**46.53**
2700	13.24	30.71	**17.47**	61.78	**48.54**
2800	13.88	31.53	**17.65**	64.43	**50.55**
2900	14.52	32.35	**17.83**	67.08	**52.56**
3000	15.16	33.17	**18.01**	69.73	**54.57**

TABLE 8 : Amount of noise contributed by the vibration due to interaction between tyres and road surface

4. CONCLUSION

From the results, the studies successfully clustering the noise into two sources: Noise due to engine transmission and noise due to interaction between tyres and road surface. The results also show that main contributor of the noise in passenger car cabin is the noise which produced due to the vibration that generated by the interaction between tyres and the road surface.

The results of the study are displayed in Table 8. The results show that the increase in the engine speed values corresponds to an increase in the level of vibration. The table shows that the value of loudness parameter increases with the increase of the engine speed values. From the observation of the results also we understood that with the increase of the engine speeds will increase level of exposed vibration to the car body either at stationary or moving condition. Thus, we may conclude that the higher the vibration, the higher the annoyance factor of the noise. From Table 6-7, it can be concluded that the increase of engine speed can influence the noise level by increasing the value of the loudness parameter; in other words, with the increase of engine speeds it may cause more noise due to the vibration from the engine combustion and vibration due to interaction between tyre and the road surface.

The purpose of this study is to obtain the amount of noise level which produced by the interactions between tyres and road surface. Thus, the equations that proposed in this study cannot be applied or used directly by the researcher. In order to obtain the noise produced by the tyre vibration, researcher has to conduct the testing on the vehicle started from the first until the last step in order to predict the amount of noise. Since the type of road influences the generated noise in passenger car cabin, it is important to the automotive researchers to ensure that during the testing, the road surface must having similar characteristics and specifications in order to obtain the read of measurements for noise and vibration more precise and accurate. Furthermore, different tyre surface pattern (tread) will produce different level of noise.

REFERENCES

[1] Ih, J.-G., Kim, H.-J., Lee, S.-H., & Shinoda, K. (2009). Prediction of Intake noise of an automotive engine in run-up condition. *Applied Acoustics, 70*(2), 347-355.

[2] Leopoldo P.R. de Oliveira, K. J., Peter Gajdatsy, Herman Van der Auweraer, Paulo S. Varoto, Paul Sas, Wim Desmet. (2009). Active sound quality control of engine induced cavity noise. *Mechanical Systems and Signal Processing, 23*(2), 476-488.

[3] M. Ferrer, A. G., M. de Diego, G. Piñero, J. J. Garcia-Bonito. (2003). Sound quality of low-frequency and car engine noises after active noise control *Journal of Sound and Vibration, 265*(3), 663-679.

[4] Shin, S.-H., Ih, J.-G., Hashimoto, T., & Hatano, S. (2009). Sound quality evaluation of the booming sensation for passenger cars *Applied Acoustics, 70*(2), 309-320.

[5] Daruis, D. D. I., Nor, M. J. M., Deros, B. M., & Fouladi, M. H. (2008). *Whole –body Vibration and Sound Quality of Malayisan Cars*. Paper presented at the 9th Asia Pacific Industrial Engineering & Management Systems Conference.

[6] H. Nahvi, M. H. F., M.J. Mohd Nor. (2009). Evaluation of Whole-Body Vibration and Ride Comfort in a Passenger Car. *International Journal of Acoustics and Vibration, 14*(3), 143-149.

[7] D.J. O'Boy, A. P. D. (2009). Tyre/road interaction noise—A 3D viscoelastic multilayer model of a tyre belt. *Journal of Sound and Vibration, 322*(4-5), 829-850.

[8] D.J. O'Boy, A. P. D. (2009). Tyre/road interaction noise—Numerical noise prediction of a patterned tyre on a rough road surface. *Journal of Sound and Vibration, 323*(1-2), 270-291.

[9] P.Kindt, P.Sas, & W.Desmet. (2009). Measurement and analysis of rolling tire vibrations. *Optics and Lasers in Engineering, 47*, 443-453.

[10] Wang, Y. S., Lee, C.-M., Kim, D.-G., & Xu, Y. (2007). Sound-quality prediction for nonstationary vehicle interior noise based on wavelet pre-processing neural network model.

[11] Wang, Y. S. (2009). Sound quality estimation for nonstationary vehicle noises based on discrete wavelet transform. *Journal of Sound and Vibration, 324*(3-5), 1124-1140.

[12] Maria B. Dühring, J. S. J., Ole Sigmund. (2008). Acoustic design by topology optimization. *Journal of Sound and Vibration, 317*(3-5), 557-575.

[13] Ricardo Penna Leite, S. P., Samir N.Y. Gerges. A sound quality-based investigation of the HVAC system noise of an automobile model. *Applied Acoustics, 70*(4), 636-645.

[14] Şahin Yıldırım, İ. E. (2008). Sound quality analysis of cars using hybrid neural networks. *Simulation Modelling Practice and Theory, 16*(4), 410-418.

[15] Shin, S.-H., Ih, J.-G., Hashimoto, T., & Hatano, S. (2009). Sound quality evaluation of the booming sensation for passenger cars *Applied Acoustics, 70*(2), 309-320.

[16] Genuit, K. (2004). The sound quality of vehicle interior noise: a challenge for the NVH-engineers. *International Journal of Vehicle Noise and Vibration, 1*(1/2), 158-168.

[17] Nor, M. J. M., Fouladi, M. H., Nahvi, H., & Ariffin, A. K. (2008). Index for vehicle acoustical comfort inside a passenger car. *Applied Acoustics, 69*, 343-353.

INSTRUCTIONS TO CONTRIBUTORS

The *International Journal of Engineering (IJE)* is devoted in assimilating publications that document development and research results within the broad spectrum of subfields in the engineering sciences. The journal intends to disseminate knowledge in the various disciplines of the engineering field from theoretical, practical and analytical research to physical implications and theoretical or quantitative discussion intended for both academic and industrial progress.

Our intended audiences comprises of scientists, researchers, mathematicians, practicing engineers, among others working in Engineering and welcome them to exchange and share their expertise in their particular disciplines. We also encourage articles, interdisciplinary in nature. The realm of International Journal of Engineering (IJE) extends, but not limited, to the following:

To build its International reputation, we are disseminating the publication information through Google Books, Google Scholar, Directory of Open Access Journals (DOAJ), Open J Gate, ScientificCommons, Docstoc and many more. Our International Editors are working on establishing ISI listing and a good impact factor for IJE.

The initial efforts helped to shape the editorial policy and to sharpen the focus of the journal. Starting with volume 6, 2012, IJE appears in more focused issues. Besides normal publications, IJE intend to organized special issues on more focused topics. Each special issue will have a designated editor (editors) – either member of the editorial board or another recognized specialist in the respective field.

We are open to contributions, proposals for any topic as well as for editors and reviewers. We understand that it is through the effort of volunteers that CSC Journals continues to grow and flourish.

IJE LIST OF TOPICS

The realm of International Journal of Engineering (IJE) extends, but not limited, to the following:

- Aerospace Engineering
- Biomedical Engineering
- Civil & Structural Engineering
- Control Systems Engineering
- Electrical Engineering
- Engineering Mathematics
- Environmental Engineering
- Geotechnical Engineering
- Manufacturing Engineering
- Mechanical Engineering
- Nuclear Engineering
- Petroleum Engineering
- Telecommunications Engineering
- Agricultural Engineering
- Chemical Engineering
- Computer Engineering
- Education Engineering
- Electronic Engineering
- Engineering Science
- Fluid Engineering
- Industrial Engineering
- Materials & Technology Engineering
- Mineral & Mining Engineering
- Optical Engineering
- Robotics & Automation Engineering

CALL FOR PAPERS

Volume: 6 - **Issue:** 3 - June 2012

i. Paper Submission: March 31, 2012 **ii. Author Notification:** May 15, 2012

iii. Issue Publication: June 2012

CONTACT INFORMATION

Computer Science Journals Sdn BhD
B-5-8 Plaza Mont Kiara, Mont Kiara
50480, Kuala Lumpur, MALAYSIA

Phone: 006 03 6207 1607
006 03 2782 6991

Fax: 006 03 6207 1697

Email: cscpress@cscjournals.org

COMPUTER SCIENCE JOURNALS SDN BHD
M-3-19, PLAZA DAMAS
SRI HARTAMAS
50480, KUALA LUMPUR
MALAYSIA

PHONE: 006 03 6207 1607
006 03 2782 6991

FAX: 006 03 6207 1697
EMAIL: cscpress@cscjournals.org